The Pennsylvania State University

The Graduate School

Department of Chemistry

INORGANIC-ORGANIC ELECTROLYTE MATERIALS FOR ENERGY APPLICATIONS

A Dissertation in

Chemistry

by

Shih-To Fei

Submitted in Partial Fulfillment
of the Requirements
for the Degree of

Doctor of Philosophy

May 2010

The dissertation of Shih-to Fei was reviewed and approved* by the following:

Harry R. Allcock
Evan Pugh Professor of Chemistry
Dissertation Advisor
Chair of Committee

Tom Mallouk
DuPont Professor of Materials Chemistry and Physics

Mary Beth Williams
Associate Professor of Chemistry
Acting Associate Dean, Eberly College of Science

Mark Horn
Associate Professor of Engineering Science and Mechanics

Barbara J. Garrison
Shapiro Professor of Chemistry
Head of the Department of Chemistry

*Signatures are on file in the Graduate School

ABSTRACT

This thesis research is devoted to the development of phosphazene-based electrolyte materials for use in various energy applications. Phosphazenes are inorganic-organic materials that provide unusal synthetic advantages and unique process features that make them useful in energy research. This particular thesis consists of six chapters and is focused on four specific aspects: lithium battery, solar cell, and fuel cell electrolytes, and artificial muscles.

Chapter 1 is written as an introduction and review of phosphazene electrolytes used in energy applications. In this introduction the basic history and characteristics of the phosphazenes are discussed briefly, followed by examples of current and future applications of phosphazene electrolytes related to energy. Notes are included on how the rest of the chapters relate to previous work.

Chapters 2 and 3 discuss the conductivity and fire safety of ethyleneoxy phosphazene gel electrolytes. The current highly flammable configurations for rechargeable lithium batteries generate serious safety concerns. Although commercial fire retardant additives have been investigated, they tend to decrease the overall efficiency of the battery. In these two chapters the discussion is focused on ionically conductive, non-halogenated lithium battery additives based on a methoxyethoxyethoxyphosphazene oligomer and the corresponding high polymer, both of which can increase the fire

resistance of a battery while retaining a high energy efficiency. Conductivities in the range of 10^{-4} Scm^{-1} have been obtained for self-extinguishing, ion-conductive methoxyethoxyethoxyphosphazene oligomers. The addition of 25 wt% high polymeric poly[bis(methoxyethoxyethoxy)phosphazene] to propylene carbonate electrolytes lowers the flammability by 90% while maintaining a good ionic conductivity of 2.5×10^{-3} Scm^{-1}. Chapter 2 is focused more on the electrochemical properties of the electrolytes and how they compare to other similar materials, while Chapter 3 emphasizes the flammability studies.

Chapter 4 expands the application of the ethyleneoxy phosphazene system to dye sensitized solar cell systems, and uses this material as a model for the study of electrode-electrolyte interfaces. We report here the results of our study on polymer electrolyte infiltration and its effect on dye-sensitized solar cells. In-depth studies have been made to compare the effects of different cell assembly procedures on the electrochemical properties as well as infiltration of electrolytes into various electrode designs. The first part of the study is based on the use of thermoplastic phosphazene electrolytes and how the overall fabrication procedure affects electrochemical performance, and the second is the use of cross-section microscopy to characterize the degree of electrolyte infiltration into various nanostructured titanium dioxide electrode surfaces. The results of this study should eventually improve the efficiency and longevity of thermally stable polymer dye solar cell systems.

In Chapter 5 the effect of pendant polymer design on methanol fuel cell membrane performance was investigated. A synthetic method is described to produce a proton conductive polymer membrane with a polynorbornane backbone and inorganic – organic cyclic phosphazene pendent groups that bear sulfonic acid units. This hybrid polymer combines the inherent hydrophobicity and flexibility of the organic polymer with the tuning advantages of the cyclic phosphazene to produce a membrane with high proton conductivity and low methanol crossover at room temperature. The ion exchange capacity (IEC), the water swelling behavior of the polymer, and the effect of gamma radiation crosslinking were studied, together with the proton conductivity and methanol permeability of these materials. A typical membrane had an IEC of 0.329 $mmolg^{-1}$ and had water swelling of 50 wt%. The maximum proton conductivity of 1.13×10^{-4} Scm^{-1} at room temperature is less than values reported for some commercially available materials such as Nafion. However the average methanol permeability was around 10^{-9} cms^{-1}, which is one hundred times smaller than the value for Nafion. Thus, the new polymers are candidates for low-temperature direct methanol fuel cell membranes.

Finally, Chapter 6 focuses on the electroactivity of a mixed-substituent phosphazene electrolyte and its viability as an actuator material. We report here an electrochemically responsive polymer hydrogel based on ionic crosslinking. The crosslinking by metal cations and anionic carboxylic acid side groups can be controlled by redox reactions. The crosslinks dissociate when the cation crosslinker is reduced to a lower oxidation state and reform following oxidation, which leads to a reversible and

localized swelling–contraction. By choosing biocompatible components and miniaturization designs, the system has potential in microrobotic and biomedical applications.

TABLE OF CONTENTS

LIST OF FIGURES

LIST OF TABLES

PREFACE

Portions of this thesis have been adapted for publication. Chapters 2 and 3 were adapted for publication in *Material Research Society Symposium Proceedings* and *Journal of Power Sources* and were coauthored by H.R. Allcock. Chapter 4 will be adapted for publication and was coauthored by H.R. Allcock, T.E. Mallouk, M.W. Horn, C.A. Grimes, S.-H.A. Lee, S.M. Pursel, P. Hoertz, and J. Basham, Chapter 5 has been adapted for publication in *Journal of Membrane Science* and was coauthored by H.R. Allcock, H.-L. Chang, R.M. Wood, D.K. Lee, and D.A. Stone. Chapter 6 has been adapted for publication in *Soft Matters* and was coauthored by H.R. Allcock, F. Gandhi, M.V.B. Phelps, Y. Wang, and E. Barrett.

ACKNOWLEDGEMENTS

Someone once told me that the purpose of higher education is not to teach you what mankind knows, but to teach you what mankind doesn't know. And indeed, my Ph.D. program was a humbling experience on the sheer amount of knowledge Nature can provide, as well as the fact that much effort must be made before she rewards us with those insights. Through the past few years on my quest for knowledge I have received tremendous support from mentors, teammates, friends and family, and it was only through their help that this thesis could be completed. I thank them from the bottom of my heart.

First of all, I would like to thank my Ph.D. advisor Professor Harry R. Allcock. It is through his knowledge and wisdom that these research projects are possible in the first place. His scientific insights in his field of specialty was amazing, but even more admirable was his ability to develop interdisciplinary solutions to practical problems. The fact that he taught me all he can with skill and passion was most appreciated. He also showed me the importance of communicating with those outside our field, as well as demonstrating how to maintain a professional lifestyle. He was also a fatherly figure to me, supporting me during the most difficult times and being flexible to allow me working on my own research interests. I own him so much.

I would also like to thank my thesis committee for their most helpful advice: Professor Thomas E. Mallouk, Professor Mary Beth Williams, Professor T.C. Mike Chung and Professor Mark W. Horn are all experts in their field, and their feedback was

one of the main reasons that I was exposed to a much wider range of knowledge than I possibly could otherwise. Especially for Professor Mallouk and Professor Horn who were also our collaborators, working with and learning from them was truly the most educational experience. Professor Mallouk was also crucial in his help with DOE proposal writing, where he introduced me to various collaborators and led me to approach the projects in a unique scientific manner with his incredible intellect.

I would like to thank all my co-workers and collaborators, those in the Allcock group and those outside the group, for what I would consider the best lessons in teamwork. A few of those were directly involved in the various projects and I would like to mention in name here: I would like to thank Dr. Daniel T. Welna, Dr. David A. Stone, Dr. Richard M. Wood, Dr. Eric Barrett, and Dr. Mwita V. B. Phelps who have all been great mentors on my various projects, and I would like to thank Dr. Song-Yun Cho, David K. Lee, and Andrew Hess for their help and efforts in the various projects. I would like to thank our various collaborators for their assistance, including Professor Thomas E. Mallouk, Professor Mark W. Horn, Professor Craig A. Grimes, Professor Farhan Gandhi, Dr. Hwei-Liang Chang, Dr. D. T. Shieh, Dr. Dmitry Belov, Anna H.-S. Lee, Sean Pursal, and James Bashamen.

I would also like to thank all the funding agencies that provided support fro our research projects, which includes DOE Golden Office, DARPA, INER Taiwan and ITRI Taiwan. It is through the continuous support of both governmental and industrial sources that science can be truly advanced.

Finally for my family members: I would like to thank my parents for their love and care throughout my life, and their continuous support and understanding even when

half a world away. I would like to thank my wife Yang Wang, who remained by my side the whole time and supported me through with endless love and devotion.

Chapter 1

Introduction: Phosphazene-based electrolytes in energy applications

1.1. Overview

Electrolytes have long been essential components for a wide range of energy applications since the invention of the first battery by Volta [1-5]. As the technology progressed, so has the development of more advanced electrolyte components, ranging from polymeric systems to ionic liquids. One consequence of this sustained push for better electrolytes, as with the advance of many other materials, is that the line has blurred between “inorganic” and “organic” compounds. Originally reserved for blends and composites, the field of inorganic-organic systems has been growing steadily with the introduction of ingenious chemistry discoveries such as organometallics and organosiloxanes. [6-14] These materials combined the desirable properties of both organic and inorganic compounds and thus open up a wide range of possibilities in the world of energy-related technologies. Among these exciting developments, one family of molecules that are among the most interesting is the group called organophosphazenes [15-22]. The fact that phosphazenes have high stability – especially in the electrochemical sense – and a wide range of synthetic variability makes this family of molecules a highly valuable platform for the development of all types of materials,

especially in the field of electrolytes for energy applications. In this introduction the basic history and characteristics of the phosphazenes will be discussed briefly, followed by examples of current and future applications of phosphazene electrolytes related to energy issues. Notes will also be included on how the other chapters relate to the earlier work mentioned here.

1.2. Definition and history of phosphazenes

Organophosphazenes, sometimes also referred as phosphonitriles, are defined by the general structure of an alternating phosphorus-nitrogen ring or chain bearing organic functionalities, as shown in Figure 1-1 [21, 23-26]. The history of organophosphazene chemistry dates back to 1834, when Liebig and Wohler first synthesized what is now known as the hexachlorocyclotriphosphazene [27]. However, it was not until over one hundred years later, in the 1950s, that the methods were developed for the substitution of chloride on these molecules with organic substituents [28]. The discovery of such a versatile reaction opportunity led to a large number of related breakthroughs, which eventually extended to other phosphazene ring systems.

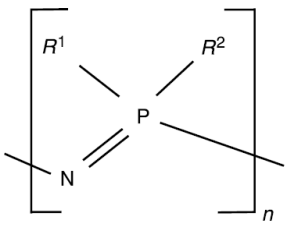

Figure **1-1**: Generic representation of phosphazene structure [21].

Another notable point in the history of organophosphazene compounds was the discovery of a polymerization reaction for cyclophosphazenes. First introduced in the 1960s [25, 26, 29], the process led to a macromolecular intermediate that can undergo the same types of substitution reactions as the small-molecule cyclic counterparts. The combination of substition and polymerization resulted in a system that provides unusual synthetic opportunities: More than a thousand organophosphazene compounds have been synthesized since then, including a wide range of structures and properties developed around the world [16, 17, 18, 20, 30]. Examples of possible structural variations are shown in Figure 1-2.

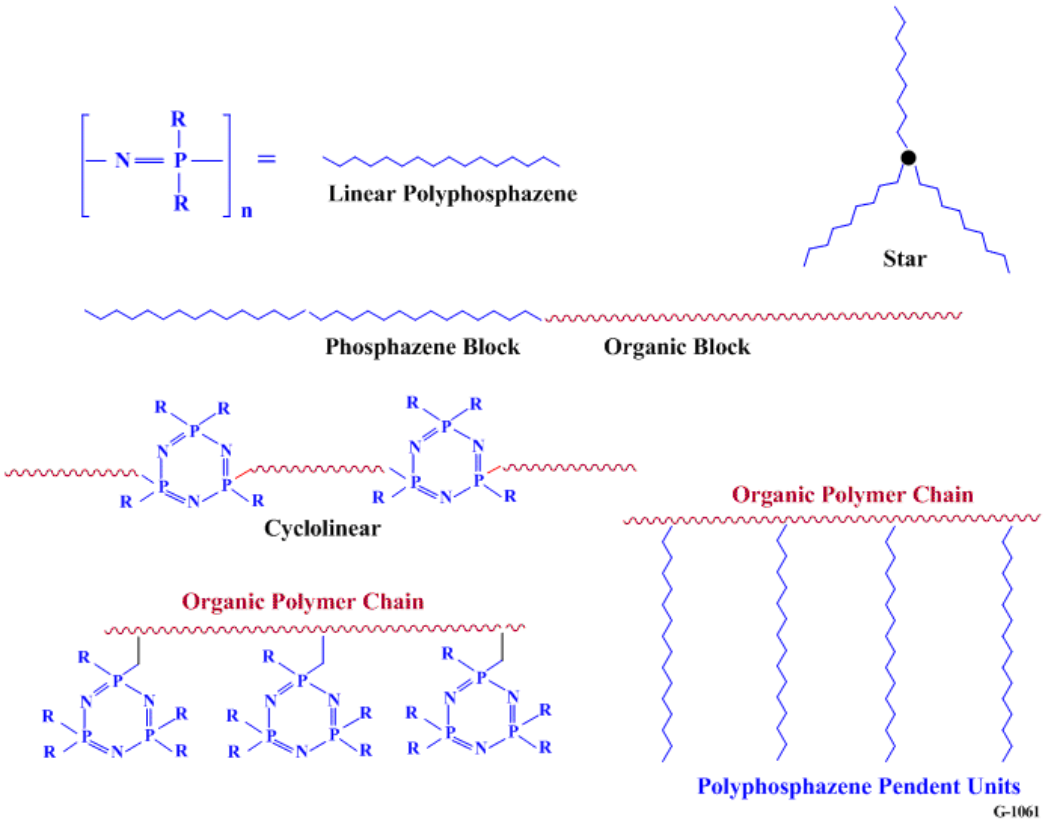

Figure **1-2**: Various molecular structures derived from phosphazene chemistry [20].

1.3. Characteristics of phosphazenes

In addition to the variety of synthetic options available, organophosphazenes possess other unique features that make them useful for energy applications. The ability to carry out substitution reactions after building a core structure means that it is possible to predict the final structure and often, from structure-property relationships, the properties of the final compound. This allows for the design and synthesis of electrolytes used in very specific applications through synthetic fine-tuning processes. Also, the

phosphrous-nitrogen core structure is inherently tough, stable to thermal / oxidative dedragation, electrochemically stable, transparent over a wide range of wavelengths and, in the case of polymeric structures, highly flexible. [31]

1.4. Phosphazene synthesis

The syntheses of small-molecular phosphazene structures are generally through the reaction of ammonium chloride with phosphorus pentachloride, which evolves hydrochloric acid as a side product [27] (**Equation 1-1**).

$$n\mathrm{NH_4Cl} + n\mathrm{PCl_5} \longrightarrow (\mathrm{NPCl_2})_{3\ \mathrm{to}\ >10} + 4n\mathrm{HCl}\uparrow \quad \textbf{(Equation 1-1)}$$

By changing the conditions and starting materials [32, 33], these small-molecule processes can produce a number of structurally different cyclic and linear products, although the cyclic trimer is generally the most common and most stable product. The polymer can be then produced through a cationic ring opening reaction (Figure 1-3) [25, 26, 29, 34], usually under high temperature melt conditions, although a number of other procedures are possible [35-43]. Linear compounds can also be synthesized via a living cationic polycondensation reaction, using monomers such as trichloro(trimethylsilyl)phosphoranimine[44-46]. This procedure, in addition to the fine control in molecular weight typical of a living polymerization, also allows for the formation of more interesting structures such as block copolymers. [45-52].

Conversion of halogenophosphazenes to organophosphazenes involved a replacement reaction of chlorine atoms by nucleophiles. The reactivity of the P-Cl bonds are so high that chlorophosphazenes are generally water-sensitive (Figure 1-3) [53-55]. The most common of these reactions involves either one of the following two reactions: One ultilizes the hydroxyl functionality on the substitution candidate, usually activated by sodium or sodium hydride to form active NaOR species, which then attacks the phosphous-chlorine bond to form a P-OR linkage and release sodium chloride as a side product. Similar alternative procedures involving hydrochloride acceptors such as cesium carbonate also exist [56-81]. The other common reaction involves a primary or secondary amine activated using a strong base such as triethylamine. Here the hydrogen chloride released by the interaction is neutralized by the acid sponge [82-88]. A number of other approaches, while less common, are of equal importance. These include substitution by thiol compounds [89-91] and the direct formation of P-C bonds[92-94], among others.

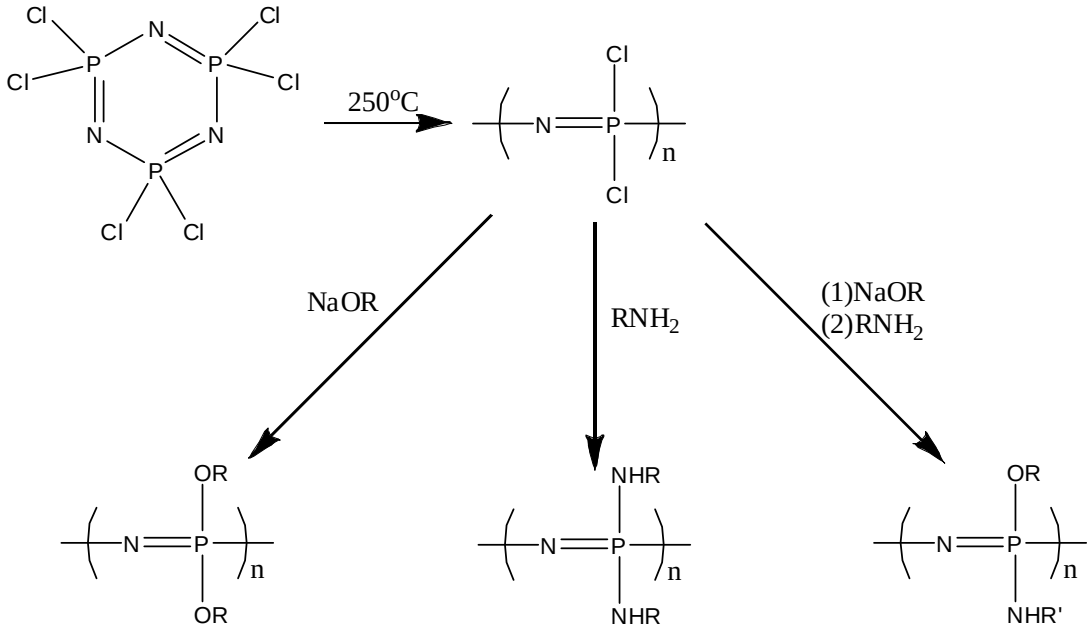

Figure **1-3**: Example of phosphazene thermal ring-opening polymerization followed by alkoxy or amino substitution.

One notable exception in the process described above is the polymerization of organo-substituted precursors, including some phosphoranimines and cyclic phosphazenes. These reactions allow for designs different from substitution via the chlorophosphazene core. However, only a selected number of organophosphazenes have been successfully synthesized through these routes. [17, 95] Especially in the case of substituted ring phosphazenes, the number of chlorine atoms remaining on the ring seem affect the reactivity. It is also possible to attach an oligomeric phosphazene unit to an organic polymer precursor, in which case the polymerization is less dependent on the availability of chlorine atoms. This approach, while providing yet another way of developing various unique structures, also sacrifices some of the properties of the

phosphazene for those of the common organic species [96]. Nevertheless, between the various synthetic methods a wide variety of organophosphazene electrolytes can be made, and many of the most successful discoveries are described below.

1.5. Applications

1.5.1. Battery materials

One area where the phosphazene electrolytes have received much attention is in lithium battery applications. [97, 98] The word “lithium battery” covers a wide range of chemical energy storage devices, ranging from lithium metal single-use batteries to intercalated lithium-ion rechargeable devices. For the most part, new research has mainly focused on the lithium ion polymer batteries, as this direction promises better safety and stability in high-performance rechargeable secondary battery systems. The challenges for electrolytes in these systems mainly involve the improvement of ionic conductivity. Mass transport issues are one of the major concerns for polymeric electrolyte systems compared to traditional small-molecule electrolyte designs.

A large number of organophosphazene compounds have been developed for this application over the years, but the most iconic among contain side groups based on ethyleneoxy sidechains. The most well-known example, poly[bis(methoxyethoxyethoxy)polyphosphazene] (MEEP, Figure 1-4), was first developed in 1984 [99] as the first phosphazene polymer electrolyte. As a low Tg (-84^{o}C) amorphous polymer, it is a good solvent for a large number of salts commonly used in

battery applications [100], This material has shown much better ionic conductivities than similar polymeric electrolytes such as those based on poly (ethylene oxide) (PEO) [17, 100]. Further improvements have been attempted to bring about better electrochemical performance as well as structural integrity. The most common approaches involved changing the geometry of the side groups, including use of linear and branched variations [101-102] as well as crown-ether type ring structures [103-105].Utilizing the freedom of multiple-substitution chemistry in phosphazenes, progress had also been made by using mixed side group substitutions [106-108]. A number of studies have been made to determine the conduction mechanism in these materials [109,110], and working battery cells have been fabricated for the study of practical feasibility [111, 112]

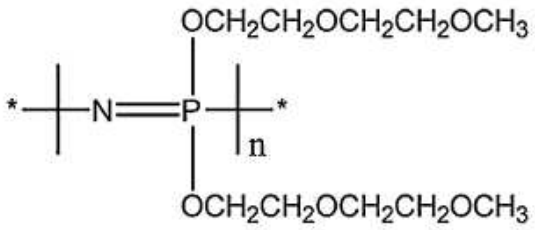

Figure **1-4**: Example of ethyleneoxy phosphazene electrolyte: The methoxy – ethoxy – ethoxy – polyphosphazene (MEEP).

It is also possible to change the properties of the ethyleneoxyphosphazene electrolytes through other means. For example, a number of studies have been carried out on the effects of crosslinking of the material: approaches included chemical crosslinking [113], radiation crosslinking [114-116], and ultraviolet crosslinking [117]. These

materials generally showed ionic conductivities comparable to their uncrosslinked counterparts under similar conditions, while improving the physical stability. Similarly, the formation of composites with materials such as aluminum oxide [118], PEO [119-121] or silanes/siloxides [122,123] also induces dimensional stability. On the other hand, the addition of liquid additives led to formation of gel electrolytes that increased the ionic conductivity [124, 125]. Finally, changes in the polymer structure from linear and cyclic phosphazenes to pendent or block copolymer systems also led to interesting results [126-135]. In fact, with the combination of side group substitution and backbone design (Figure 1-5), phosphazene electrolytes with unique properties can be made for very specific applications, such as the lithium sea-water battery [136, 137]. The most recent progress in improving these ethyleneoxy electrolytes will be described in Chapter 2.

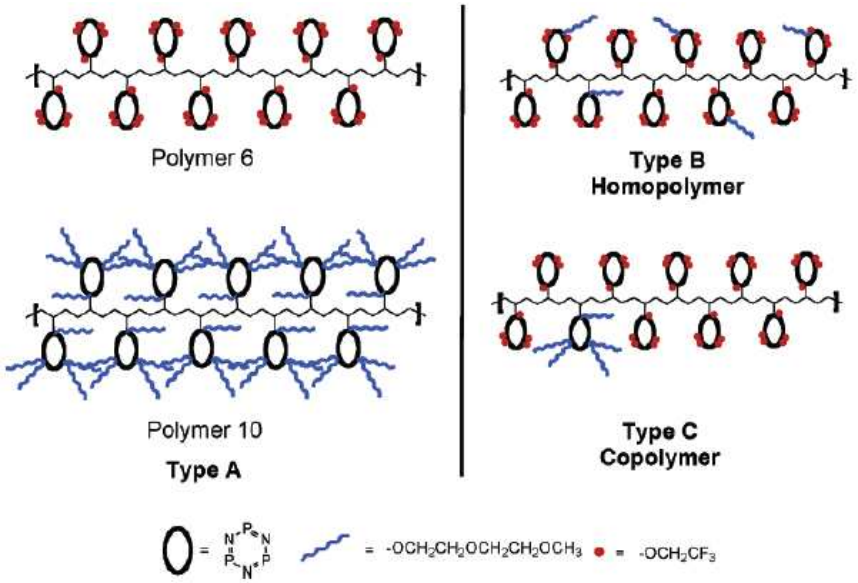

Figure **1-5**: Example of combination mixed group substitution – backbone design in phosphazene lithium battery electrolytes [137].

The other major class of phosphazene electrolytes used in lithium battery systems are single-ion conducting phosphazenes. [17, 138-140]. Although neutral electrolytes such as ethyleneoxy phosphazenes can induce highly effective ion-conduction through the high solubility of selected salt species, the fact that a non-contributing free counter-ion exists in the electrolyte raises concern about unnecessary polarization at the electrodes as well as ion pairing. As such, an anionic solvent in which only the ion that contributes to the electrochemical reaction – the lithium cation in this case – has been a focus of various electrolyte developments. However, the immobilized counter-ion tends to reduce the overall ion mobility by trapping mobile species in ionic crosslinks. Thus, recent research has focused on highly-dissociating species such as lithium sulfonamide

attached to the polymer backbone to produce materials with better conductivity, with some degree of success. [141].

Another important property of phosphazene electrolytes is fire retardancy [142-147]. As mentioned, one important driving force in the development of new electrolyte materials is the improvement of overall safety. Batteries made with phosphazene electrolytes can be non-flammable [148] and thus be used in heat-sensitive applications. This is probably due to the high organophosphorus content of the material, which is known to reduce flammability [149, 150]. More information on how the phosphazene electrolytes can improve the fire safety in battery systems is provided in Chapter 3.

1.5.2 Fuel cell materials

The other major direction in energy applications for phosphazene electrolytes is their use in fuel cell membrane systems [151, 152]. Fuel cells are devices that convert an external feed of chemicals into electrical energy (Figure 1-6). Common fuel components include hydrogen, methanol, or gaseous hydrocarbons such as methane. [153, 154] The major area in which organophosphazene electrolyte systems can contribute to fuel cell systems is the polymer memberene fuel cell. Here, a proton conducting membrane not only functions as an ionic conductor like that in a battery system, but also acts as a separator between the cathode and anode to prevent fuel crossover and thus undesirable

side reactions. [155-159] As such, the selectivity of the membrane is just as important as the rate of mass transfer in such an application.

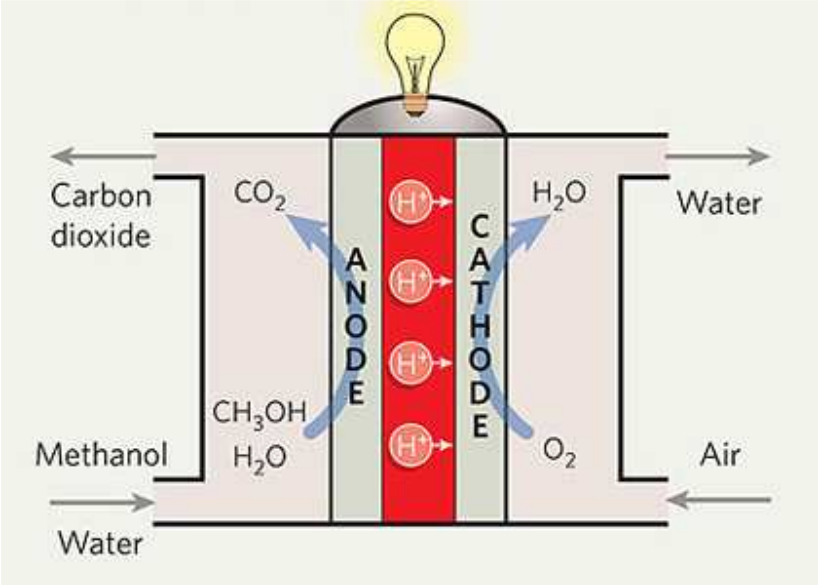

Figure **1-6**: Operation scheme of direct methanol fuel cell. The electrolyte membrane is shown in red [152].

The best known phosphazene system used in such applications is the sulfonated ayrloxy phosphazene system [160]. Especially in the methanol fuel cell field, sulfonated phosphazene membranes have been known to prevent crossover [161-163]. Studies have been made to explain the behavior of these materials through examination of their microstructures [164], and working cells have been fabricated to gain insight into their real-world performance [165]. The direct use of sulfonated precursors in the synthesis of

sulfonated phosphazenes generally leads to unfavorable side reactions [166]. Therefore, most of the materials in this class are based on the post-substitution sulfonation treatment by reagents such as SO_3 (Figure 1-7) [167-171]. This usually requires the use of aryloxy side groups due to their reactivity to electrophilic substitution. As in the case of battery electrolytes, crosslinking of these materials improves the physical properties of the resulting membranes without having a significant impact on their electrochemical performance [172-174]

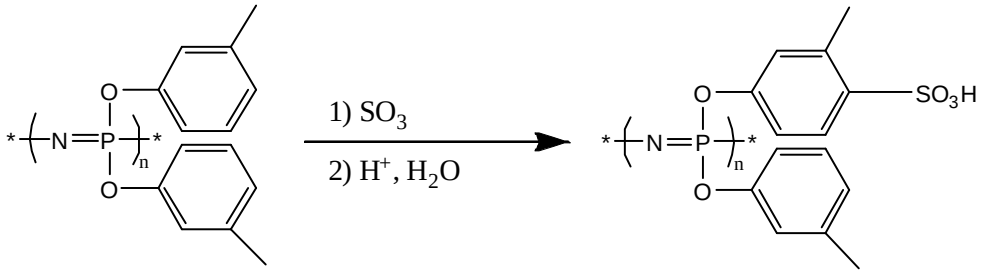

Figure **1-7**: Typical sulfonation reaction for phosphazene fuel cell membrane materials [171].

Other phosphazene systems for fuel cell membranes also exist, such as phosphonic acid (Figure 1-8) [175, 176] and sulfonimide substituted species [177, 178]. Also changes in backbone design have induced changes in behavior as in the case for battery electrolytes [179]. Recent reviews go into detail on this subject [180], but much potential exists for development of better phosphazene electrolytes for fuel cell

applications. The recent developments in this field is described in further detail in Chapter 5 of this thesis.

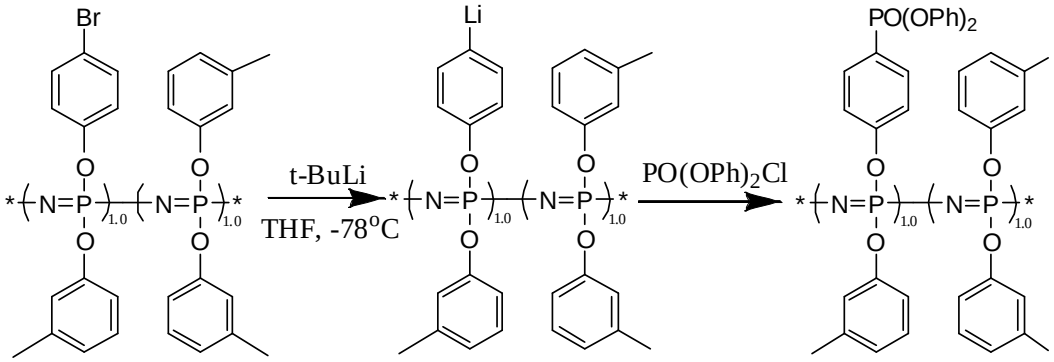

Figure **1-8**: Typical phosphonation reaction for phosphazene fuel cell membrane materials [176].

1.5.3. Further developments

While most of the energy-related phosphazene electrolyte research has been focused on the above directions, there are a number of future opportunities that can be explored. One of the possibilities is in chemical capacitors, sometimes called the super capacitors or ultracapacitors. [181, 182] In an electrochemical capacitor system, an electrolyte solution is confined between two electrodes like a battery, but instead of using a highly redox-active electrode coupled with corresponding electrolyte that can store energy over a long period of time, an electrochemical capacitor involves either very fast-

acting surface reactions (inducing “pseudo-capacitive charge storage”) or non-redox double-layer formation. This design results in an energy storage device that allows faster charge/discharge rates than a battery but still stores more energy than a conventional capacitor. It thus bridges the gap between two devices for applications such as electric car accelerators and short-term backup power. Not surprisingly, the requirements for electrolytes in this system are similar to those of batteries. Because phosphazene electrolytes have been shown to be electrochemically stable ionic conductors, their application in the supercapacitor field is a logical future development.

Another of the promising future directions for phosphazene electrolytes is in solar cell development. Although most conventional solar cells are based on solid inorganic materials (mainly semiconductors such as silicon), recent advances in the field have yielded designs in which hybrid materials and electrolytes can play an important role. For example, the dye-sensitized solar cell system [183, 184] utilizes redox-active electrolytes as an essential part of their photoelectron generation design. In addition to the usual requirements of an electrolyte system, a solar cell component material also needs good photochemical stability and, in some cases, optical transparency. Phosphazenes have been used in optical materials in the past [185, 186], and these materials are promising candidates for solar cell applications. Our preliminary studies in this direction are discussed in Chapter 4.

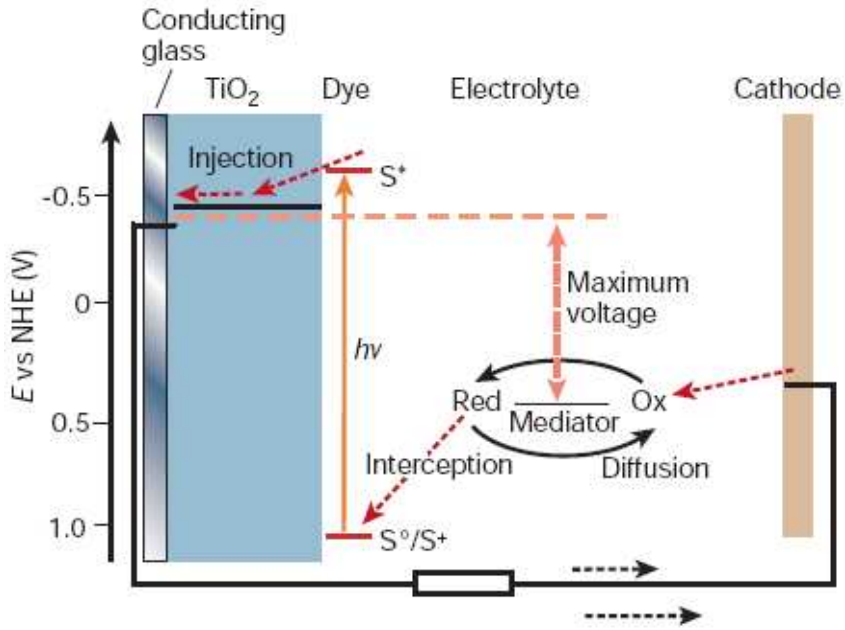

Figure **1-9**: Schematic operation diagram of dye-sensitized solar cells [184].

Lastly, the effective transformation of one energy type to another has always been a popular topic in phosphazene studies. This includes sub-topics such as electro-luminance and electro-actuators [187, 188]. Although this direction covers a wide array of topics, research that involved direct eletro-response of electrolyte materials are much less common. Most of the previous studies involved responsive electrolytes that convert other energy types, such as thermal energy, into kinetic energy. For example, the lower critical solution temperature (LCST) effect is a kind of behavior certain hydrogel materials exhibit, which causes the material to shrink below a certain temperature [189, 190]. By ultilizing such effects, thermo-responsive phosphazene electrolytes that expand when heated and contract when cooled have been developed [191 - 194]. Recent progress

in the field however opened up new possibilities for electroactive phosphazene electrolyte systems. One example of such actuator research based on a responsive hydrogel is described in Chapter 6.

1.6. Summary

Phosphazene electrolytes are interesting and useful materials for the field of energy research due to the remarkable characteristics of the basic chemical structure as well as the availability of various synthetic pathways that allows design versatility. Although most of the applications have been focused on batteries and fuel cells, there are a number of other directions that can be potentially promising for future research.

The rest of this thesis is devoted to various aspects of recent developments in this field: Chapter 2 and 3 contain a discussion of the conductivity and fire safety of ethyleneoxy phosphazene gel electrolytes, respectively. Chapter 4 expands the topic of ethyleneoxy phosphazene to dye sensitized solar cell systems, and uses this material as a model for the study of electrode-electrolyte interfaces. In Chapter 5 the effect of pendant polymer structuring on methanol fuel cell membrane performance is described. Finally, Chapter 6 focuses on the electroactivity of a mixed-substituent phosphazene electrolytes and their viability as electrochemical actuator materials.

1.7. References

[1] Aono, H.; Imanaka, N; Adachi, G.Y. *Acc. Chem. Res.* **1994,** *27,* 265

[2] Reuter, B.; Hardel, K. *Naturwissenshaften* **1961,** *48*, 161

[3] Owens, B. B.; Argue, A.G. *Science* **1967,** *157,* 308

[4] Takahashi, T.; Ikeda, S.; Yamamoto, O. *J. Electrochem. Soc.* **1972,** *119,* 477

[5] Tatsumisago, M.; Shinkuma, Y.; Minami, T. *Nature* **1991,** *354*, 217

[6] Mark, J.E.; Allcock, H.R.; West, R. *Inorganic polymers;* Prentice Hall; Englewood Cliffs, New Jersey, 1992.

[7] Carraher, C.E.; Sheats, J.E.; Pittman, C.U. Eds. *Organometallic polymers;* Academic; New York, 1978

[8] Ciardelli, F.; Tsuchida, E.; Wohrle, D. *Macromolecule-metal complexes;* Springer; New York, 1996

[9] Archer, R.D. *Inorganic and organometallic polymers;* Wiley-VCH; New York, 2001

[10] Stark, F.O.; Falender, J.R.; Wrigth, A.P. In *Comprehensive organometallic chemistry. The synthesis, reactions and structures of organometallic compounds, UK edn.;* Wilkinson, G; Stone, F.G.A.; Abel, E.W. eds. Pergamon; Oxford, 1982, vol 2, pp 305

[11] Ziegler, J.M.; Fearon, F.W.G. *Silicon-based polymer science;* American Chemical Society; Washington, D.C., 1990

[12] Jones, R.G.; *Silicon-containing polymers;* The Royal Chemical Society; Cambridge, 1995

[13] Brook, M. A. *Silicon in organic, organometallic and polymer chemistry;* Wiley Interscience; New York, 2000

[14] Manners, I. *Macromol. Symp.* **2003,** *196,* 57

[15] Allcock, H. R. *Polym. Prepr.* **2000,** *41,* 553

[16] Allcock, H. R. *Heteroatom ring systems and polymers;* Academic; New York, 1967

[17] Allcock, H. R. *Chemistry and applications of polyphosphazenes;* Wiley Interscience; Hoboken, New Jersey, 2002

[18] Allcock, H. R. *Phosphorus-nitrogen compounds. Cyclic, linear, and high polymeric systems;* Academic Press; New York, 1972

[19] Manners, I. *Angew. Chem. Int. Ed. Engl.* **1996,** *35,* 1602

[20] Allcock, H. R. *Current Opinion in Solid State & Materials Science* **2007**, *10,* 231-240

[21] Honarkar, H.; Rahimi, A. *Monatshefte fur Chemie* **2007,** *138,* 923–933

[22] Gleria, M.; De Jaeger, R. *Top. Curr. Chem.* **2005,** *250,* 165–251

[23] Chandrasekhar, V.; Thomas, K. R. J. *Struct. Bond.* **1993,** *81,* 41

[24] Allcock, H. R. *Chem. Eng. News* **1985,** *63,* 22

[25] Allcock, H. R.; Kugel, R. L. *J. Am. Chem. Soc.* **1965,** *87,* 4216

[26] Allcock, H. R.; Kugel, R. L. *Inorg. Chem.* **1966,** *5,* 1716

[27] Liebig, J.; Wohler, J. *Justus. Liebig. Ann. Chem.* **1834,** *11,* 139

[28] Allcock, H. R. *Chemical Revlews*, **1972,** *72(4),* 315-355

[29] Allcock, H. R.; Kugel, R. L.; Valan, K. J. *Inorg. Chem.* **1966,** *5,* 1709

[30] Gleria, M.; De Jaeger, R. Eds. *Phosphazenes. A worldwide insight;* Nova; Hauppauge, 2004

[31] Allcock, H. R.; Austin, P. E.; Neenan, T. X.; Sisko, J. T.; Blonsky, P. M.; Shriver, D. F. *Macromolecules* **1986,** *19,* 1508

[32] Allen, C. W.; Hneihen, A. S. *Phosphorus Sulfur Silicon* **1999,** *146,* 213

[33] Carriedo, G. A.; Garcia-Alonso, F. J.; Gomez-Elipe, P.; Fidalgo, J. I.; Garcia-Alvarez, J. L,; Presa-Soto, A. *Chem. Eur. J.* **2003,** *9,* 3833

[34] De Jaeger, R.; Gleria, M. *Prog. Polym. Sci.* **1998,** *23,* 179

[35] Konecny, J. O.; Douglas, C. M.; Gray, M. Y. *J. Polym. Sci.* **1960,** *42,* 383

[36] Kajiwara, M.; Shiomoto, K. *Polym. Commun.* **1984,** *25,* 93

[37] Scopelianos, A. G.; Allcock, H. R. *Macromolecules* **1987,** *20,* 432

[38] Sennett, M. S.; Hagnauer, G.L.; Singler, R. E. *Polym. Mater. Sci. Eng.* **1983,** *49,* 297

[39] Sennett, M. S.; Hagnauer, G. L.; Singler, R. E.; Davies, G. *Macromolecules* **1986,** *19,* 959

[40] Potts, K. M.; Hagnauer, G. L.; Sennett, M. S.; Davies, G. *Macromolecules* **1989,** *22,* 4235

[41] Mujumdar, A. N.; Young, S. G.; Merker, R. L.; Magill, J. H. *Makromol. Chem.* **1989,** *190,* 2293

[42] Mujumdar, A. N.; Young, S. G.; Merker, R. L.; Magill, J. H. *Macromolecules* **1990,** *23,* 14

[43] Mujumdar, A. N.; Young, S. G.; Merker, R. L.; Magill, J. H. *Polym. Sci.* **1991,** *1,* 70

[44] Honeyman, C. H.; Manners, I.; Morrissey, C. T.; Allcock, H. R. *J. Am. Chem. Soc.* **1995,** *117,* 7035

[45] Allcock, H. R.; Crane, C. A.; Morrissey, C. T.; Nelson, J. M.; Reeves, S. D.; Honeyman, C. H.; Manners, I. *Macromolecules* **1996,** *29,* 7740

[46] Allcock, H. R.; Reeves, S. D.; de Denus, C. R,; Crane, C. K. *Macromolecules* **2001,** *34,* 748

[47] Allcock, H. R.; Reeves, S. D.; Nelson, J. M.; Crane, C. A. *Macromolecules* **1997,** *30,* 2213

[48] Nelson, J. N.; Primrose, A. P.; Hartle, T. J.; Allcock, H. R. *Macromolecules* **1998,** *31,* 947

[49] Nelson, J. M.; Allcock, H. R. *ACS Polym. Prep.* **1998,** *39,* 631

[50] Allcock, H. R.; Reeves, S. D.; Nelson, J. M. Manners, I. *Macromolecules* **2000,** *33,* 3999

[51] Allcock, H. R.; Prange, R. *Macromolecules* **2001,** *34,* 6858

[52] Nelson, J. M.; Allcock, H. R. *Macromolecules* **1997,** *30,* 1854

[53] Singler, R. E.; Schneider, N. S.; Hagnauer, G. L. *Polym. Eng. Sci.* **1975,** *15,* 321

[54] Allen, G.; Lewis, C. J.; Todd, S. M. *Polymer* **1970,** *11,* 31

[55] Allcock, H. R.; Connolly, M. S.; John, T. S.; Al-Shali, S. *Macromolecules* **1987,** *21,* 323

[56] Stewart, F. F.; Harrup, M. K.; Luther, T. A.; Orme, C. J.; Lash, R. P. *J. Appl. Polym. Sci.* **2001,** *80,* 422

[57] Allcock, H. R.; Kugel, R. L. *J. Am. Chem. Soc.* **1965,** *87,* 4216

[58] Allcock, H. R.; Kugel, R. L.; Valan, K. *J. Inorg. Chem.* **1966,** *5,* 1709

[59] Goldschmidt, F.; Dishon, B. *J. Polym. Sci.* **1948,** *3,* 481

[60] Rose, S. H. *J. Polym. Sci. B* **1968,** *6,* 837

[61] Mochel, V. D.; Cheng, T. C. *Macromolecules* **1978,** *11,* 176

[62] Cheng, T. C.; Mochel, V. D.; Adams, H. E.; Longo, T. F. *Macromolecules* **1980,** *13,* 158

[63] Blonsky, P. M.; Shriver, D. F.; Austin, P. E.; Allcock, H. R. *J. Am. Chem. Soc.* **1984,** *106,* 6854

[64] Allcock, H. R.; Austin, P. E.; Neenan, T. X.; Sisko, J. T.; Blonsky, P. M.; Shriver, D. F. *Macromolecules* **1986,** *19,* 1508

[65] Allen, G.; Lewis, C. J.; Todd, S. M. *Polymer* **1970,** *11,* 31,

[66] Allcock, H. R.; Kim, Y. B. *Macromolecules* **1994,** *27,* 3933

[67] Singler, R. E.; Hagnauer, G. L.; Schneider, N. S.; LaLiberte, B. R.; Sacher, R.E.; Matton, R. W. *J. Polym. Sci. Polym. Chem. Ed.* **1974,** *12,* 433

[68] Thompson, J. E.; Reynard, K. A. *J. Appl. Polym. Sci.* **1977,** *21,* 2575

[69] Dieck, R. L.; Goldfarb, L. *J. Polym. Sci. Polym. Chem. Ed.* **1977,** *15,* 361

[70] Allcock, H. R.; Fuller, T. J.; Evans, T. L. *Macromolecules* **1980,** *13,* 1325

[71] Allcock, H. R.; Austin, P. E. *Macromolecules* **1981,** *14,* 1616

[72] Allcock, H. R.; Austin, P. E.; Rakowsky, T. F. *Macromolecules* **1981,** *14,* 1622

[73] Allcock, H.R.; Neenan, T.X.; Kossa, W.C. *Macromolecules* **1982,** *15*, 693

[74] Neenan TX, Allcock, H.R. *Biomaterials* **1982**,*3*,78

[75] Di Marco PG, Giro, G., Gleria, M, Lora, S. *Thin Solid Films* **1986**, *135*,157

[76] Haddon, R.C., Chichester-Hicks, S.V. *Macromolecules* **1989**, *22*, 1027

[77] Minto, F., Scoponi, M., Gleria, M., Pradella, F., Bortolus, P. *J Inorg Organomet Polym* **1992**, *2*, 405

[78] Gleria, M., Minto, F., Scoponi, M., Pradella, F., Carassiti, V. *Chem Mater* **1992**, *4*, 1027

[79] Medici, A., Fantin, G., Pedrini, P., Gleria, M., Minto, F. *Macromolecules* **1992**, *25*, 2569

[80] Gleria M, Minto F, Flamigni L, Bortolus P *J Inorg Organomet Polym* **1992**, 2, 329

[81] Gleria, M., Minto, F., Fontana, G., Bertani, R., Facchin, G. *Macromolecules* **1995**, 28:4399

[82] Allcock, H.R.,Kugel, R.L. *Inorg Chem* **1966**, 5,1716

[83] Allcock, H.R., Mack, D.P. *J Chem Soc Chem Commun* **1970**, 685

[84] Allcock, H.R., Cook, W.J., Mack, D.P. *Inorg Chem* **1972**, *11*, 2584

[85] Allcock, H.R., Kolich, C.H., Kossa, W.C. *Inorg Chem* **1977**, *16*, 3362

[86] White, J.E., Singler, R.E., Leone, S.A. *J Polym Sci, Polym Chem Ed* **1975**, *13*, 2531

[87] Gleria, M., Minto, F., Lora, S., Bortolus, P., Ballardini, R. *Macromolecules* **1981**, *14*, 687

[88] Welker, M.F., Allcock, H.R., Grune, G.L., Chern, R.T., Stannett, V.T. *Polym Mater Sci Eng* **1992**, *66*, 259

[89] Haddon, R.C., Chichester-Hicks, S.V. *Macromolecules* **1989**, *22*, 1027,

[90] Carriedo, G.A., Jimenez, J., Gomez-Elipe, P., Alonso, F.J.G. *Macromol Rapid Commun* **2001**, *22*, 444

[91] Carriedo, G.A., Alonso, F.J.G.,Vizcaino, S.L,Valenzuela, C.D.,Yutronic, N. *Phosphorus Sulfur Silicon* **2003**, *178*, 1549

[92] Allcock, H.R., Patterson, D.B., Evans, T.L. *J Am Chem Soc* **1977**, *99*, 6095

[93] Allcock, H.R., Evans, T.L., Patterson, D.B. *Macromolecules* **1980**, 13, 201

[94] Evans, T.L., Allcock, H.R. *J Macromol Sci Chem* **1981**, *A16*, 409

[95] Allcock, H.R. *Polymer* **1980**, *21*, 673

[96] Allcock, H. R. *J. Inorganic and Organometallic Polymers and Materials* **2007**, *17*, 349-360

[97] Nicholson, P.S., Whittingham, M.S., Farrington, G.C., Smeltzer, W. W., Thomas, J. (eds) *Solid State Ionics*-91, **1992**, North-Holland, Amsterdam

[98] Bonino, F., Ottaviani, M., Scrosati, B., Pistoia, G. *J Electrochem Soc* **1988**, *135*, 12

[99] Blonsky, P.M., Shriver, D.F., Austin, P.E., Allcock, H.R. *J Am Chem Soc* **1984**, *106*, 6854

[100] Blonsky, P.M., Shriver, D.F., Austin, P.E., Allcock, H.R. Polym Mater Sci Eng 1985, 53, 118

[101] Allcock, H.R., Napierala, M.E., Cameron, C., O'Connor, SJM *Macromolecules* **1996**, *29*, 1951

[102] Allcock, H.R., O'Connor, SJM., Olmeijer, D.L., Napierala, M.E., Cameron, ChG. *Macromolecules* **1996**, *29*, 7544

[103] Allcock, H.R., Olmeijer, D.L., O'Connor, J.M. *Macromolecules* **1998**, *31*, 753

[104] Cowie, J.M.G. *Makromol Chem Macromol Symp* **1992**, *53*, 43

[105] Andrei, M., Cowie, J.M.G., Prosperi, P. *Electrochim Acta* **1992**, 37, 1545

[106] Allcock, H.R., Napierala, M.E., Cameron, C.G., O'Connors, S.J.M. Macromolecules, **1996**, *29*, 1951

[107] Allcock, H.R., Kellam, E.C. *Solid State Ionics*, **2003**,*156*,401

[108] Allcock, H.R., Olmeijer, D.L. *Macromolecules* **1998**, *31*, 8036

[109] Allcock, H.R., Napierala, M.E., Olmeijer, D.L., Best, S.A., Merz, K.M. *Macromolecules* **1999**, *32*, 732

[110] Luther, T.A., Stewart, F.F., Budzien, J.L., LaViolette, R.A., Bauer, W.F., Harrup, M.K., Allen, N.S., Elayan, A. *J Phys Chem B* **2003**, *107*, 3168

[111] Gao, L., Macdonald, D. D., *J. Electrochem. Soc.* **1997**, *30*, 3184

[112] Allcock, H. R., Welna, D. T., Stone, D. A. *Macromolecules* **2005**, *38*, 10406

[113] Tonge, K.M., Shriver, D.F. *J Electrochem Soc* **1987**, *134*, 269

[114] Allcock, H.R., Kwon, S., Riding, G.H., Fitzpatrick, R.J., Bennett, J.L. *Biomaterials* **1988**, *9*, 509

[115] Bennett, J.L., Dembek, A.A., Allcock, H.R.,Heyen, B.J., Shriver, D.F. *Chem Mater*, **1989**,*1*, 14

[116] Nazri, G.A., Meibuhr, S.G. *J Electrochem Soc* **1989**, *136*, 2450

[117] Allcock, H.R., Nelson, C.J., Coggio, W.D. *Polym Mater Sci Eng* **1993**, *68*, 76

[118] Kaskhedikar, N., Paulsdorf, J., Burjanadze, M., Karatas, Y., Roling, B.,Wiemhofer, H.D. *Solid State Ionics* **2006**, *177*, 2699

[119] Brusatin, G., Guglielmi, M., De Jaeger, R., Facchin, G., Gleria, M., Musiani, M. *J Mater Sci* **1997**, 32, 4415

[120] Adamic, K.J., Greenbaum, S.G., Abraham, K.M., Alamgir, M., Wintergill, M.G., Fontanella, J.J. *Chem Mater* **1991**, *3*, 534

[121] Kaskhedikar, N., Paulsdorf, J., Burjanadze, M., Karatas, Y., Wilmer, D., Roling, B., Wiemhofer, H.D. *Solid State Ionics* **2006**, *177*, 703

[122] Kim, C., Kim, J.S., Lee, M.H. *Synthetic Metals* **1998**, *98*, 153

[123] Allcock, H.R., Chang, Y., Welna, D.T. *Solid State Ionics*, **2006**, *177*, 569

[124] Allcock, H.R., Kellam, E.C., Morford, R.V. *Solid State Ionics* **2001**, *143*, 297

[125] Morford, R.V., Kellam, E.C., Hofmann,M.A., Baldwin, R., Allcock,H.R. *Solid State Ionics* **2000**, *133*, 171

[126] Inoue, K., Nishikawa, Y., Tanigaki, T. *J Am Chem Soc* **1991**, *113*, 7609,

[127] Inoue, K., Nishikawa, Y., Tanigaki, T. *Macromolecules* **1991**, *24*, 3464

[128] Inoue, K., Nishikawa, Y., Tanigaki, T. Solid State Ionics **1992**, *58*, 217

[129] Inoue, K., Tanigaki, T., Yuan, Z. *Polym Adv Technol* **1993**, *4*, 74

[130] Allcock, H.R., Laredo, W.R., Kellam, E.C., Morford, R.V. *Macromolecules* **2001**, *34*, 787

[131] Allcock, H.R., Laredo, W.R., Morford, R.V. *Solid State Ionics* **2001**, 139, 27

[132] Inoue, K., Miyamoto, H., Itaya, T. *J Polym Sci Part A: Polym Chem* **1997**, *35*, 1839

[133] Allcock, H.R., Sunderland, N.J., Ravikiran, R., Nelson, J.M. *Macromolecules* **1998**, *31*, 8026

[134] Allcock, H. R.; Welna, D. T.; Stone, D. A. *Macromolecules* **2005**, *38*, 10406

[135] Stone, D. A., Allcock, H. R. *Macromolecules* **2006**, *39*, 4935

[136] Welna, D. T.; Stone, D. A.; Allcock, H. R. *Chemistry of Materials* **2006**, *18*, 4486

[137] Welna, D. T.; Stone, D. A.; Allcock, H. R. *Chemistry of Materials* **2007**, *19*, 2473

[138] Ganapathiappan, S., Chen, K., Shriver, D.F. *Macromolecules* **1988**, *21*, 2299

[139] Chen, K., Shriver, D.F. *Chem Mater*, **1991**, *3*, 771

[140] Ganapathiappan, S., Chen, K., Shriver, D.F. *J Am Chem Soc*, **1989**, *111*, 4091

[141] Allcock, H.R.; Welna, D.T.; Maher, A.E. *Solid State Ionics* **2006**, *177*, 741

[142] Chen, D., Cui, Y., Wang, X., Tang, X. *J Appl Polym Sci*, **2002**, *86*, 709

[143] Kiyohisa, T., Yuhko, T., Yasuhiro, H., Takeshi, Y., *J Soc Mater Sci*, **1988**, *37*, 1397

[144] Allcock, H.R., Austin, P.E., Neenan, T.X., Sisko, J.T., Blonsky, P.M., Shriver, D.F. *Macromolecules* **1986**, *19,* 1508

[145] Reed, C.S., Taylor, J.P., Guigley, K.S., Coleman, M.M., Allcock, H.R. *Polym Eng Sci* **2000**, *40*, 465

[146] Allcock, H.R., Taylor, J.P. () *Polym Eng Sci* **2000**, *40*, 1177

[147] Quinn, E.J., Dieck, R.L. *J Fire Flammability* **1976**, *7*, 5

[148] Nazri, G.A., MacArthur, D.M., O'Gara, J.F. *Polym Prepr*, **1989**, *30,* 430

[149] Morford, R. V.; Welna, D. T.; Kellam, C. E.; Hofmann, M. A.; Allcock, H. R. *Solid State Ionics*, **2006**, *177*, 721

[150] Fei, S. and Allcock, H.R. *J. Power Sources* **2010**, *195*, 2082

[151] Carrette, L., Friedrich, K.A., Stimming, U. *Fuel Cells* **2001**, *1*, 1

[152] Nature **2006**, *441*, 1046-1047

[153] Deluca, N. W.; Elabd, Y. A. *Polymer Electrolyte Membranes for the Direct Methanol Fuel Cell: A Review Journal of Polymer Science: Part B: Polymer Physics*, **2006**, *44*, 2201

[154] Viral Mehta and Joyce Smith Cooper *Review and analysis of PEM fuel cell design and manufacturing Journal of Power Sources* **2003**, *114*, 32-53

[155] Savadogo, O. *J. New Mater. Electrochem. Syst.* **1998.** 1:47–66

[156] Jones DJ, Rozi`ere J. 2001. *J. Membr. Sci.* 185:41–58

[157] Kreuer, K.D., J. *Membr. Sci.*, **2001**, *185*, 29

[158] Kreuer, K.D.. In *Handbook of Fuel Cell Technology*, ed. W Vielstich, A Lamm, H Gasteiger, **2003**, *420*. London: Wiley & Sons

[159] Rikukawa, M., Sanui, K. *Prog. Polym. Sci.* **2000**, *25*, 1463

[160] Graves, R., Pintauro, P.N. *J Appl Polym Sci* **1998**, 68, 827

[161] Guo, Q., Pintauro, P.N. *J. Membr. Sci.* **1999**, 154, 175

[162] Carter, R., Evilia, R.F., Pintauro, P. *J. Phys. Chem.* **2001**, 105, 2351

[163] Fedkin, M.V.; Zhou, X.Y.; Hofmann, M.A.; Chalkova,E.; Weston, J.A; Allcock, H.R., *Mater Lett* **2002**, *52*, 192

[164] Tang, H., Pintauro, P.N., Guo, Q., O'Connor, S. *J Appl Polym Sci* **1999**, *71*, 387

[165] Carter, R.; Wycisk, R.; Yoo, H.; Pintauro, P. *Electrochem. Solid-State Lett.* **2002**, 5, 195

[166] Allcock, H.R., Fitzpatrick, R.J. *Chem. Mater.* **1991**, *3*, 1120

[167] Allcock, H. R.; Fitzpatrick, R. J.; Salvati, L. *Chem. Mater.* **1991**, *3*, 1120

[168] a) Allcock, H. R. *Acc. Chem. Res.* **1979**, *12*, 351; b) Allcock, H. R.; Klingenberg, E. H.; Welker, M. F. *Macromolecules* **1993**, *26*, 5512

[169] Wycisk, R., Pintauro, P.N. *J. Membr. Sci.* **1996**, *119*, 155

[170] Montoneri, E., Gleria, M., Ricca, G., Pappalardo, G.C. *Makromol. Chem.* **1989**, *1989*, 191

[171] Tang, H., Pintauro, P.N. *J. Appl. Polym. Sci.* **2001**, *79*, 49

[172] Wycisk, R., Pintauro, P., Wang, W., O'Connor, S. *J. Appl. Polym. Sci.* **1996**, *59*, 1607–17

[173] Graves, R., Pintauro, P. *J. Appl. Polym. Sci.* **1998**, 68, 827

[174] Guo, Q., Pintauro, P.N. *J. Membr. Sci.* **1999**, *154*, 175

[175] Allcock, H.R., Hoffmann, M.A., Ambler, C.A., Morford, R.V. *Macromolecules* **2002**, *35*, 3484

[176] Allcock, H.R., Hoffmann, M.A., Ambler, C.A., Lvov, S.N., Zhou, X.Y. *J. Membr. Sci.* **2002**, 201, 47

[177] Hoffmann, M.A., Ambler, C.A., Maher, A.E., Chalkova, E., Zhou, X.Y., *Macromolecules* **2002**, *35*, 6490

[178] Chalkova, E., Zhou, X.Y., Ambler, C.A., Hoffmann, M.A., Weston, J.A., *Electrochem. Solid-State Lett.* **2002**, *5*, 221

[179] Fei, S.-T.; Wood, R. M.; Lee, D. K.; Stone, D. A.; Chang, H.-L.; Allcock, H. R. *J. Membrane Science* **2008**, *320*, 206

[180] Allcock, H. R.; Wood, R. M. *J. Polm. Sci. Part B, Polymer Physics*, **2006**, *44*, 2358

[181] Simon, P.; Gogotsi, Y. *Nature Materials* **2008**, *7*, 845

[182] Burke, A. *Electrochimica Acta* **2007**, 53, 1083

[183] Gratzel, M. *Journal of Photochemistry and Photobiology C: Photochemistry Reviews* **2003**, *4*, 145

[184] Gratzel, M., *Nature* **2001**, *414*, 338

[185] Allcock, H. R.; Bender, J. D.; Chang, Y.; McKenzie, M.; Fone, M. M. *Chemistry of Materials* **2003**, *15*, 473

[186] Olshavsky, M.; Allcock, H. R. *Macromolecules* **1997**, *30*, 4179

[187] Fei, S.-T.; Phelps, M. V. B.; Wang, Y.; Barrett, E.; Gandhi, F.; Allcock, H. R. *Soft Matter* **2006**, *2*, 397

[188] Allcock, H. R.; Chang, Y.; Stone, D. A. *J. Polymer Science* **2006**, *44*, 69

[189] Taylor, L.D.; Cerankowski, L.D. *J. Polym. Sci.* **1975**, *13*, 2551

[190] Yoshida, M.; Asano, M.; Safranj, S.; Omichi, H.; Spohr, R.; Vetter, J.; Katakai, R. *Macromolecules* **1996**, *29*, 8987

[191] Allcock, H. R.; Austin, P. E.; Neenan, T. X.; Sisco, J. T.; Blonsky, P. M.; Shriver, D. F. *Macromolecules* **1986**, *19*, 1508

[192] Michels, B.; Waton, G.; Zana, R. *Langmuir* **1997**, *13*, 3111

[193] Heskins, M.; Guillet, J.E. *J. Macromol. Sci., Part A2* **1968**, 1441

[194] Chang, Y.; Powell, E.S.; Allcock, H.R.; Park, S.M.; Kim, C. *Macromolecules*, **2003**, *36*, 2568

Chapter 2

Recent Progress with Ethyleneoxy Phosphazenes as Lithium Battery Electrolytes

2.1. INTRODUCTION

Among the various possible applications for phosphazenes described in the last chapter, one of the most interesting is in lithium battery electrolytes **[1]**. Lithium batteries are among the most widely used primary and secondary modern energy storage devices. As noted in the introduction, lithium metal and lithium ion batteries are electrochemical devices that generate electricity from lithium sources based on either metallic lithium electrodes or intercalation compounds such as lithium–cobalt/lithium– magnesium complexes. The numerous advantages of lithium batteries allow them to be used in a wide variety of energy storage applications, especially where reliable, repeatable charge-discharge characteristics are needed **[2].**

As with many other energy storage devices that rely on similar electrochemical principles, the performance of electrolyte components relates directly to the performance of the assembled battery. **[2 - 4]** The first and formost consideration of a battery electrolyte is that whether it has a high ionic conductivity. For the electrochemical reaction to produce electron flow, the lithium ions must be able to transverse from one electrode to another, and the output of electrons relate with the movement of ions on a charge-by-charge basis following electroneutrality principles. As such, the conductivity

of the ions in the electrolyte directly translates to the internal resistance of the battery, and thus affects the power output of a cell following the basic V=IR equation. This is especially impartant in the case of polymeric electrolytes, as the existence of larger molecular weight species generally restricts the mobility of ions.

A number of phosphazene – based lithium battery electrolytes have been reported in the past, mainly focused on solid polymer electrolyte systems. **[5-7]** These types of materials have shown good performance in assembled-cell conditions and are known to be compatible with other battery components such as carbon and metal oxide electrodes [**1,8**] while maintaining better performance compared to many of the existing solid electrolytes. On the other hand, the potential of phosphazene compounds as *gel* electrolyte components has not been as thoroughly explored. **[9, 10]** Similarly, liquid electrolyte systems are part of another field where phosphazene research is lacking. Since phosphazenes have high thermal stability, low volatility, and exhibit fire retardant behavior, it is possible to develop component materials that are resistant to leaks, pressure buildup and fire – which are the most common problems encountered for battery systems. **[2,11]**

Among the possible polyphosphazene molecular designs, species with ethyleneoxy side groups deserve special attention, as this family of materials is known to maintain a liquid state as oligomers. They also have higher conductivities compared to similarly structured poly (ethylene oxide) (PEO) alternatives, mostly due to their low crystallinity and main chain flexibility. The materials are also known to have good

compatibility with traditional electrolyte materials such as propylene carbonate, which leads to a wide range of possibilities for gel electrolyte compositions. **[1]**

For example, linear polyphosphazenes with oligo-ethyleneoxy side groups have ionic conductivities above 10^{-5} Scm^{-1} when used as gum (solvent free) electrolytes **[5,6]**. Moreover, small molecule cyclic phosphazenes with the same ethyleneoxy side groups have been used either as stand-alone electrolytes or as plasticizers for gel electrolytes, and they are known to function well as solvents and as additives that increase the ionic conductivity of the base macromolecular electrolyte **[7,9].** Related studies showed that, when used as a plasticizer for poly(ethylene oxide) electrolytes, the conductivity of the resulting gel electrolyte increased from ~10^{-5} to ~10^{-3} Scm^{-1} at 50 ◦C **[12]**.

We discuss here the conductivity of ethyleneoxyphosphazene-based electrolytes with and without the addition of propylene carbonate, as well as comparing the performance of gel electrolytes based on other polymeric compounds. The phosphazene materials used in this study are summarized in **Figure 2-1**. For the electrochemical evaluations, we prepared lithium salt electrolytes of each material and carried out alternating current impedance ionic conductivity experiments for different salt concentrations. The lithium triflate–propylene carbonate system was selected as the model base electrolyte for better comparison with earlier phosphazene studies.

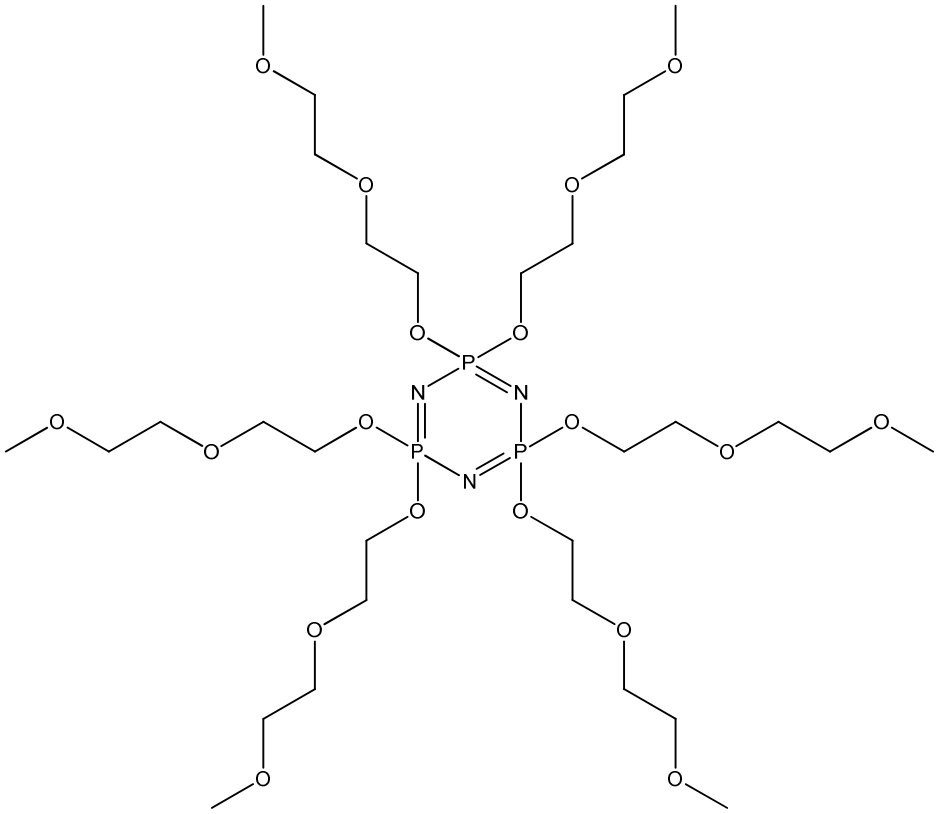

1

MEE Trimer

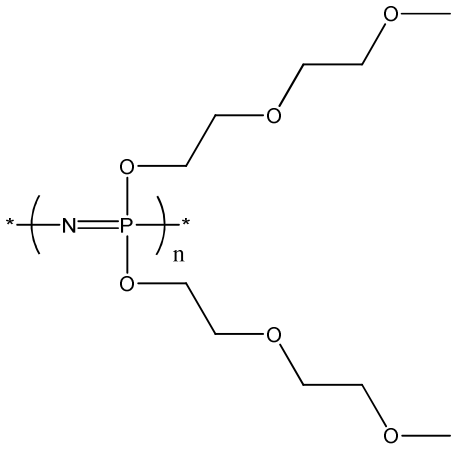

2

MEEP

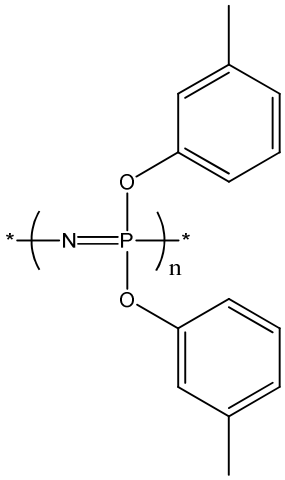

3

MCPHOS

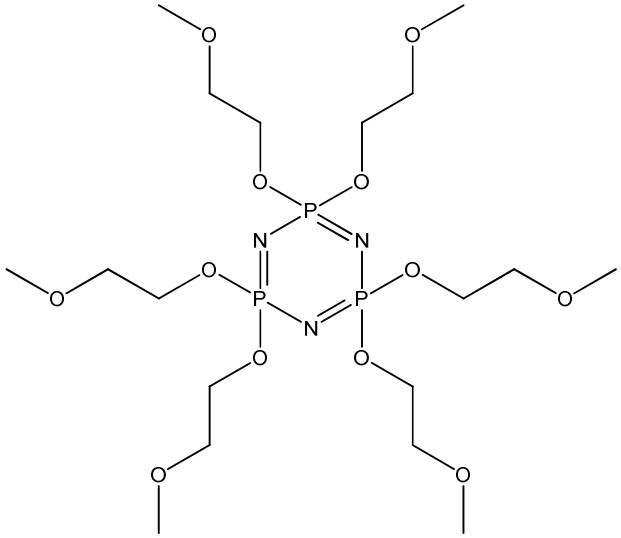

4

ME Trimer

Figure **2-1**: Types of phosphazene compounds used in this study. The following acronyms are used throughout this chapter and are explained as follows: MEE trimer: hexa (methoxyethoxyethoxy) cyclotriphosphazene (compound 1). MEEP: poly (bis-methoxyethoxyethoxy) phosphazene (compound 2). MCPHOS: poly (bis-m-cresol)

phosphazene (compound 3). ME trimer: hexa (methoxyethoxy) cyclotriphosphazene (compound 4).

2.2. EXPERIMENTAL

2.2.1. Materials

Hexachlorocyclotriphosphazene, $(NPCl_2)_3$, was obtained from Fushimi Chemical and Pharmaceutical Co. Ltd., Japan. The compound was purified by recrystallization from heptane, and sublimation at 40 ◦C and 0.05mmHg vacuum. Celite, sodium metal, lithium trifluoromethylsulfonate ($LiCF_3SO_3$), di(ethylene glycol)methyl ether, and propylene carbonate were obtained from Aldrich. Diethyl ether, hexanes, tetrahydrofuran (THF), and methylene chloride (CH_2Cl_2) were purchased from VWR. Di(ethylene glycol) methyl ether and propylene carbonate were purified by vacuum distillation. The diethyl ether, hexanes, THF, and CH_2Cl_2 were purified through copper/ silica catalytic drying columns. All other chemicals were used as received.

2.2.2. Characterization

Molecular and materials characterization was carried out by ^{1}H and ^{31}P NMR spectroscopy with the use of a Bruker AMX-360 instrument. Conductivity measurements were made using a HP-4192A impedance analyzer and a two-point solid or liquid

conductivity cell. The cell constant was calibrated with a set amount of standard sodium chloride electrolytes of various concentrations. In the case of anhydrous samples, the cell was dried under reduced pressure for 24 h and was refilled with dry nitrogen before measurements.

2.2.3. Syntheses

All synthesis reactions are based on literature procedures **[5, 6, 9, 13, 14, 15]** with modifications as described below.

2.2.3.1. Hexa(methoxyethoxyethoxy)cyclotriphosphazene (MEE trimer) (1)

Di(ethylene glycol) methyl ether (68 ml, 0.57 mol) was added to a suspension of sodium metal (6.55 g, 0.28 mol) in THF (400 ml), and the mixture was stirred and heated gently until all the solid sodium had been consumed. The fully reacted mixture was then added to a solution of hexachlorocyclotriphosphazene (15 g, 0.043 mol) in THF (100 ml). The reaction mixture was stirred and heated gently for 16 h, then cooled to room temperature. The THF was removed under reduced pressure, and the remaining mixture was re-dissolved in CH_2Cl_2 and purified via a water extraction. The solvent was then removed, the product was re-dissolved in an ether–hexane mixture at the maximum possible concentration, and the solution was stored at low temperature (−65 ◦C) until a clear phase-separation was obtained. The lower portion was separated and dried, redissolved in CH_2Cl_2, mixed with activated carbon to remove colored impurities, and

filtered with a short Celite column, followed by a final removal of CH_2Cl_2 under reduced pressure. The product was a clear, slightly yellow oil. Yield: 77.9%. ^{31}P NMR: 17.7311ppm (s, 3P, NPN). ^{1}H NMR: 3.282ppm (s, 3H, OCH_3); 3.449ppm (t, 2H, $MeOCH_2$); 3.553ppm (m, 4H CH_2OCH_2); 4.006ppm (t, 2H, $POCH_2$).

2.2.3.2. Hexa (methoxyethoxy) cyclotriphosphazene (ME trimer) (4)

For this synthesis the reaction was carried out as described above for hexa(methoxyethoxyethoxy)cyclotriphosphazene, except ethylene glycol methyl ether was used in place of di(ethylene glycol) methyl ether and the time for both steps under mild heating was extended to 32 hours. Yield: 67.2%. ^{31}P NMR: 17.7298ppm (s, 3P, NPN). ^{1}H NMR: 3.282ppm (s, 3H, OCH_3); 3.449ppm (t, 2H, $MeOCH_2$); 4.006ppm (t, 2H, $POCH_2$).

2.2.3.3. Poly[bis(methoxyethoxyethoxy)phosphazene] (MEEP) (2) and poly (bis-m-cresol) phosphazene (MCPHOS) (3)

Both syntheses were carried out by following previously published procedures **[6, 9, 13, 14]**.

2.2.4. Electrolyte solution preparation

Two alternative methods were employed for electrolyte preparation. Unless otherwise noted in the description, liquid samples were always formulated to maintain

1M lithium ion concentration, while the salt-electrolyte weight ratios for gel electrolytes were set to be the same as 1M $LiCF_3SO_3$ in propylene carbonate. Propylene carbonate (PC) containing mixtures were generally formulated to achieve a 75:25 solid- or phosphazene- to propylene carbonate weight ratio unless otherwise noted.

2.2.4.1. Solvent-free electrolytes

The electrolyte formulation procedures based on "neat" phosphazene compounds without the addition of propylene carbonate are described below, with liquid and non-liquid final materials following separate procedures.

2.2.4.1.1. Liquid electrolytes

Formulation of liquid electrolytes was achieved by dissolving $LiCF_3SO_3$ salt directly in the electrolyte mixture under nitrogen. As a typical example, the conductivity measurements for the electrolyte solutions of MEE trimer/$LiCF_3SO_3$ salt were carried out for samples of various concentrations by adding $LiCF_3SO_3$ to a 2:1 THF:MEE trimer mixture and removal of the THF later in vacuum. Liquid MEE trimer (3.5771 g, 3ml), pre-dissolved in THF (5 ml), was mixed with $LiCF_3SO_3$ in 1.3, 2.6, 3.7, 6, 9.3, 11.3, 28.7, 37.7, and 44.7 wt% ratios **[5, 7, 13, 15]**. Stirring was applied to ensure proper mixing. The solvent was then removed from the resulting mixture at reduced pressure.

2.2.4.1.2. Solid and gel electrolytes

For solid, gum and gel samples where solid polymeric components were involved, the electrolyte materials were pre-dissolved in the minimum amount of THF (5 ml) before addition of the lithium salt and mixing. After the salts were fully dissolved the organic solvent was removed slowly under reduced pressure to form a homogenous membrane. The electrolyte samples were otherwise prepared using the same procedure and weight ratios as described for liquid electroytes

2.2.4.2. Electrolytes containing propylene carbonate

Propylene carbonate-based samples were prepared using the same total sample weight as the corresponding no-carbonate samples in each case: a base of propylene carbonate–phosphazene or propylene carbonate - polymer blend was mixed with $LiCF_3SO_3$ in appropriate ratios. For concentration – related experiments, the mixture was again formulated for a final ratio of 1.3, 2.6, 3.7, 6, 9.3, 11.3, 28.7, 37.7, or 44.7 wt% $LiCF_3SO_3$ in base blend. For propylene carbonate–liquid trimer mixtures and 75:25 weight ratio propylene carbonate–phosphazene polymer mixtures, $LiCF_3SO_3$ was first blended with propylene carbonate in predetermined amounts to maintain the final concentrations as described above. MEE trimer or MEEP polymer were then added to the solution until the components formed a homogeneous solution. For propylene carbonate–MEEP mixtures of 25:75 and 50:50 weight ratios, the polymer was first dissolved with the lithium salt in THF to form a homogeneous solution. The solvent was then removed under reduced pressure. The resultant solid electrolyte was then allowed to absorb

propylene carbonate at ratios described above for 2 weeks under an inert atmosphere until a uniform gel electrolyte was formed.

2.3. DISCUSSION

2.3.1. Phosphazene synthesis

Poly (bis-methoxyethoxyethoxy) phosphazene (MEEP), hexa (methoxyethoxyethoxy) cyclotriphosphazene (MEE trimer), and poly (bis-m-cresol) phosphazene (MCPHOS) (Figure 2-1, compound 1-3) were synthesized based on previously reported procedures. **[6,9,13]** For the hexa (methoxyethoxy) cyclotriphosphazene (ME trimer) (Figure 2-1, compound 4) the reaction conditions were adjusted from the hexa (methoxyethoxyethoxy) cyclotriphosphazene synthesis by longer heating times: The reactivity of the methoxyethoxy sodium salt with the trimer was found to be lower than that of MEE sodium salt, and large excess of side group alkoxide or heating was required to drive the reaction to completion. The reactivity of the alcohol to sodium metal was also low, and additional mild heating was also applied in this step. Although rearrangement of POR bonds to NOR units was a possible competing process, no evidence of such reactions was found.

2.3.2. Single-solvent electrolyte conductivity

The conductivity measurements for electrolyte solutions of MEE trimer / $LiCF_3SO_3$ salt were completed for samples of various concentrations. It is interesting to note that while the MEE trimer is a liquid, the observed viscosity increased notably with increased salt concentration in our samples, especially at higher salt concentrations where the conductivity starts to drop. We have observed similar behavior with MEEP, and suspect that ionic crosslinking occurs in the system. The same reasoning can also be applied here. The conductivity of the methoxyethoxy (ME) trimer – Li salt solutions were found to be lower than those of their MEE trimer counterparts, which is expected due to lower oxygen content and shorter side chains that have lower degrees of freedom. The conductivity values of ME trimer MEE trimer samples are compared in **Figure 2-2.**

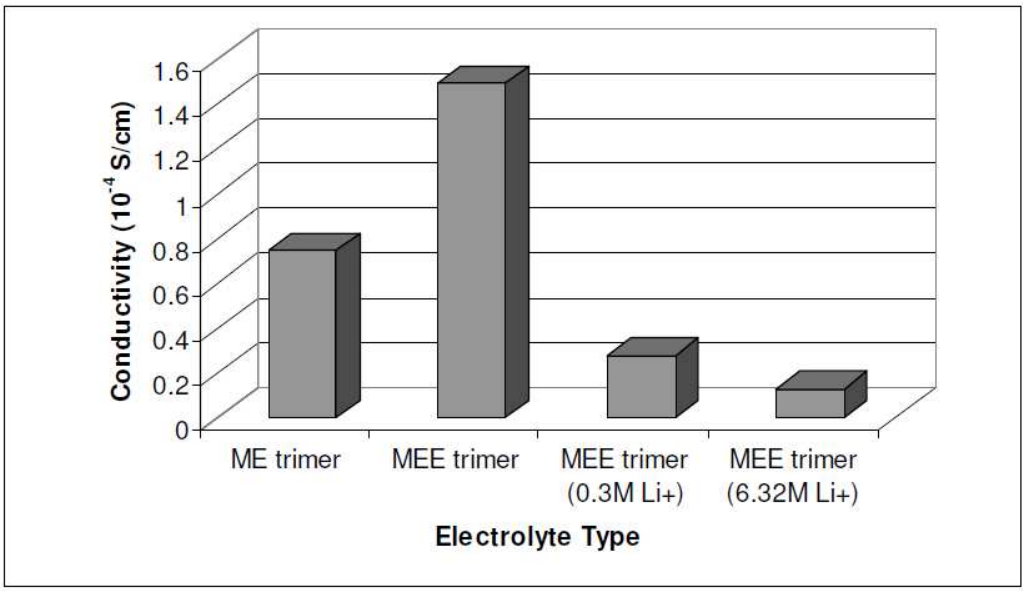

Figure **2-2**: Comparison of ionic conductivities for liquid ME trimer and MEE trimer electrolytes. All numbers reported here are averages of at least 6 samples. Note error bars in this case are too small to show in figure (1%).

2.3.3. Mixed-solvent electrolyte conductivity

The conductivity results for mixed-component electrolytes formed by the addition of 25wt% propylene carbonate to phosphazenes are shown in **Figure 2-3.** Because propylene carbonate is a good solvent for the lithium ion system, the mixed electrolytes have a better performance than the neat (solvent free) phosphazene electrolytes. This holds true even for liquid oligomeric phosphazenes. The effects are especially significant for polymeric phosphazene materials, as the added propylene carbonate also acts as a plasticizer and enhances the ion mobility within the polymer framework. This result

correlates well with previous literature **[9]**. Other polymer-propylene carbonate mixtures were also tested for ion conductivity but, with the exception of poly(ethylene oxide) (PEO) – based samples, the values were generally low compared to the MEEP sample. The difference was especially interesting in the case where non-conductive components such as isotatic polypropylene (iPP) and poly (bis-m-cresol) phosphazene (MCPHOS) were compared with ethyleneoxy phosphazenes, despite the electrolyte fabrication from the two non-conducting compounds resulted in a paste-like mixture and gel-like samples, respectively**.** It is reasoned that, because the use of nonconducting polymeric fillers gives a much lower conductivities than using ion-conducting polymeric species such as MEEP, the conductive nature of the polymer matrix contributes greatly to the overall ion mobility.

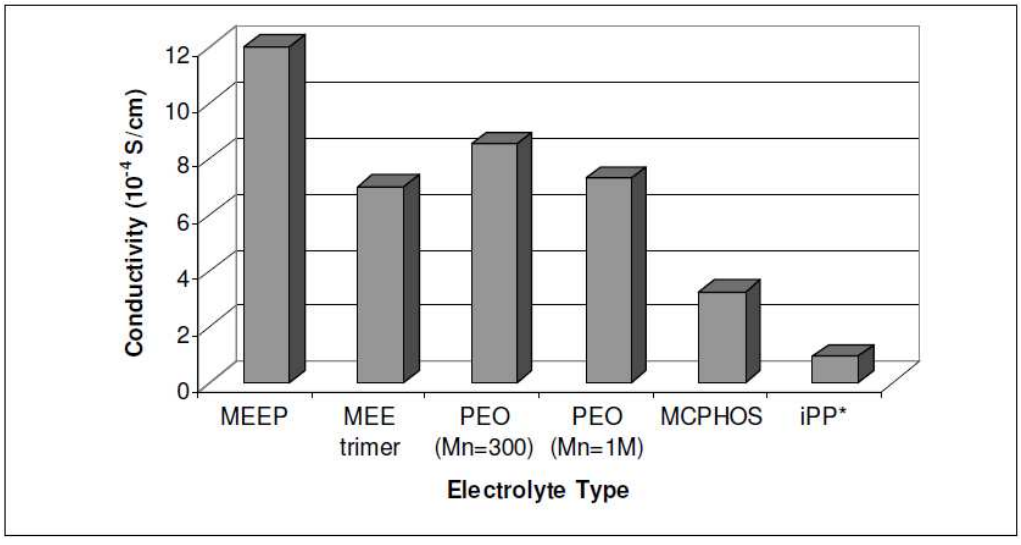

Figure **2-3**: Comparison of mixed electrolyte conductivity. All numbers reported here are averages of at least 6 samples. Note error bars in this case are too small to show

in figure (1%). With the exception of isotactic polypropylene (iPP) electrolytes which are 75:25 wt ratio paste of solid beads and propylene carbonate, all samples were homogenous gels or liquid mixtures.

2.3.4. Component ratio effects on ionic conductivity

The third part of this project was focused on comparative conductivity studies of electrolytes that contain methoxyethoxyethoxy polymeric- or small molecule cyclic phosphazenes with different concentrations of propylene carbonate and lithium salt additives. The conductivity results are shown in **Figures 2-4 and 2-5.** The salt concentrations were chosen to approximate to 0.1–1M values in the liquid electrolyte at lower ranges, while the Li:O atomic ratios were targeted to 1:4–1:8 at the higher ranges in accordance with previous solid electrolyte experiments **[5,7,13,15]**. The 1.5×10^{-4} Scm^{-1} maximum conductivity of the MEE trimer electrolyte was in agreement with other liquid phosphazene electrolytes reported previously.

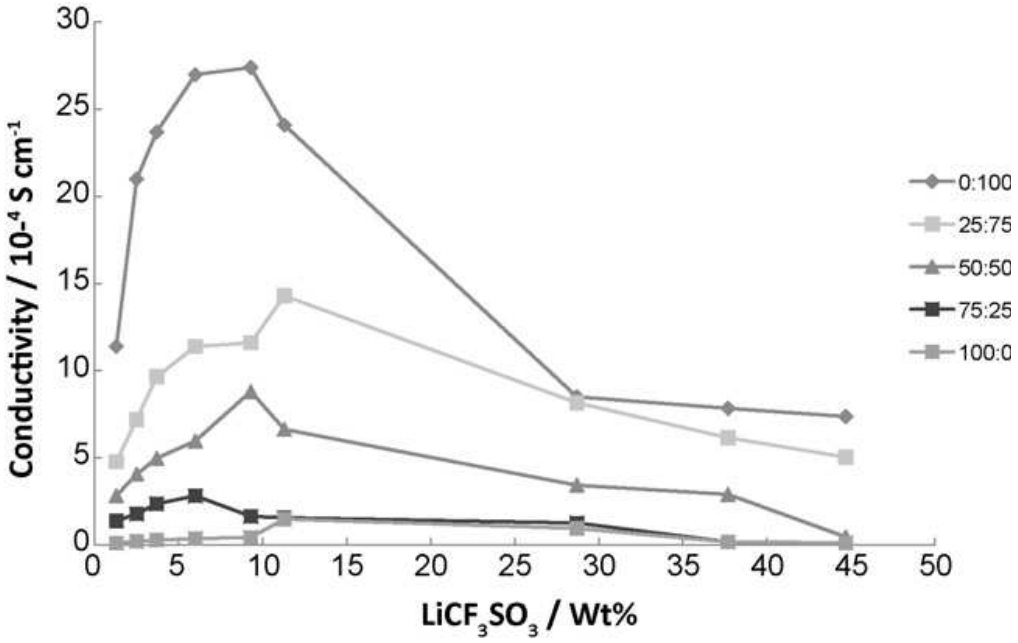

Figure **2-4**: Conductivity data for MEE trimer–propylene carbonate mixtures for different phosphazene : propylene carbonate weight ratios. All numbers reported here are averages of at least 6 samples. Note error bars in this case are too small to show in figure (1%).

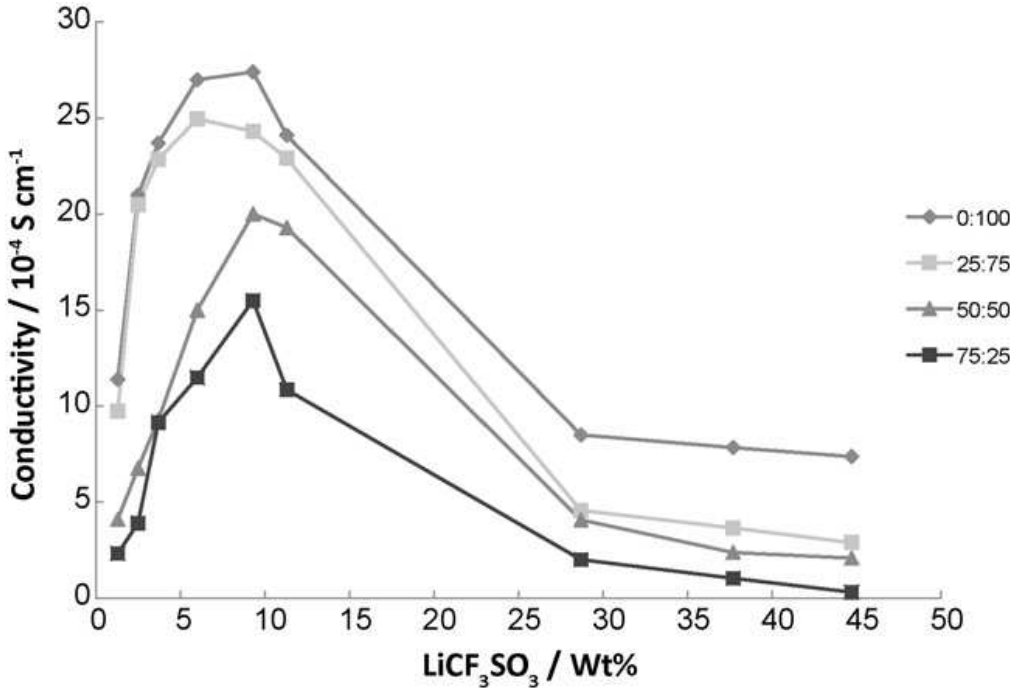

Figure **2-5**: Conductivity data of MEEP – propylene carbonate mixtures for different phosphazene : propylene carbonate weight ratios. All numbers reported here are averages of at least 6 samples. Note error bars in this case are too small to show in figure (1%).

Mixtures of methoxyethoxyethoxyphosphazenes with propylene carbonate generally had higher ionic conductivities than the pure phosphazene compounds, as shown in **Figures 2-4** and **2-5**. This is not unexpected, because the addition of a highly

ion-conductive, low viscosity liquid plasticizer should increase the ion mobility. Thus, both polymeric and cyclic trimeric methoxyethoxyethoxyphosphazenes are acceptable additives to propylene carbonate, since their existence does not significantly compromise the conductivity of the organic carbonate-based electrolyte system even at relatively high weight ratios. However, an unexpected result is that *the polymeric MEEP – propylene carbonate mixtures had higher ionic conductivities than comparable MEE trimer – propylene carbonate mixtures.*

The observation points to that the addition of propylene carbonate to MEEP has a significant effect on the conductivity, while, for MEE trimer, the increase was not obvious until the amount of propylene carbonate was raised to approximately 50 wt% **(Figure 2-6**). Because similar numbers have been reported in the past for MEEP – propylene carbonate mixtures **[12]**, the possibility of conductive contamination can probably be ruled out. However, considering that pure MEEP has a lower ionic conductivity and higher viscosity than MEE trimer, this result still requires investigation and explanation, especially for the samples with low propylene carbonate content where the viscosities of the MEEP – propylene carbonate mixtures are higher than those of MEE trimer – propylene carbonate mixtures.

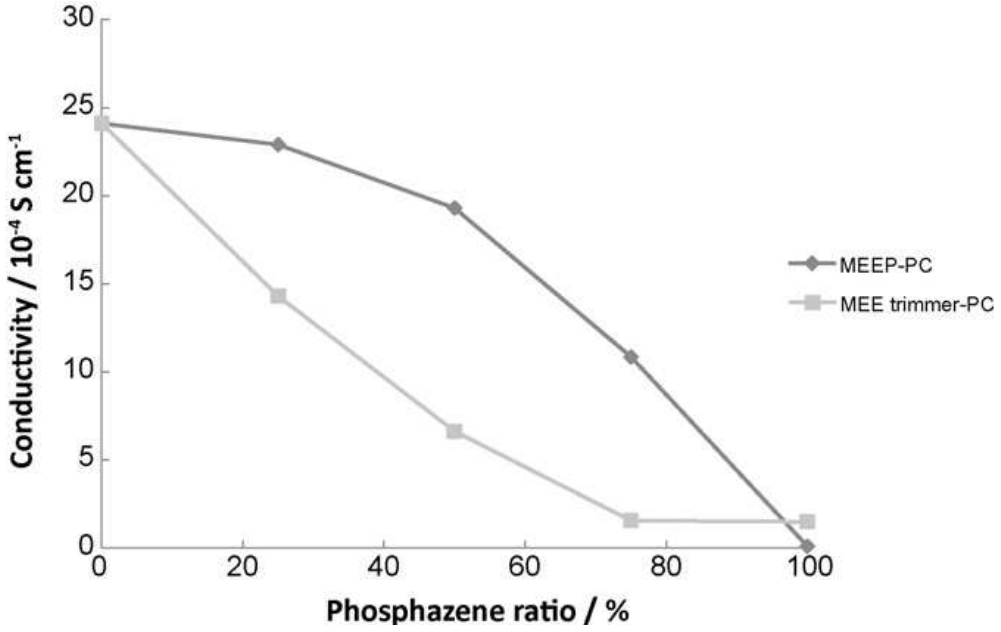

Figure **2-6**: Comparison of ionic conductivity around the optimal Li^+ concentration. All numbers reported here are averages of at least 6 samples. Note error bars in this case are too small to show in figure (1%).

A possible explanation for the behavior of the high polymer is that the "swinging-arm" ion transport mechanism often invoked for branched polymer electrolytes is applicable to this system. This mechanism supposes that ions can be transported between side chains through their random thermal movements, and that this process is actually assisted by the existence of a continuous, flexible polymer backbone if the matrix is swollen by a compatible ion-conducting liquid medium. A possible additional effect is the preservation of the ion transport properties of propylene carbonate within a larger

molecular framework of MEEP polymer. Instead of a homogeneous mixture of solvent molecules that encase the ions, as in the case of propylene carbonate alone or of MEE trimer–propylene carbonate systems, the MEEP chains may form large coils or a supporting matrix when suspended in etheric solvents. Such a system can be viewed as composed of islands or webs of MEEP floating in a sea of propylene carbonate, essentially providing ion conductive channels through a solution that is composed mainly of propylene carbonate.

On the other hand, polymers that have a lower compatibility with propylene carbonate may still form an *entangled matrix* that is swollen by propylene carbonate, and the ionic conductivity would be hindered by the solid matrix. However, both of these assumptions require additional proof by comparing our results to liquid solvent compatible gel systems that are known to have low ionic conductivities.

2.4. CONCLUSIONS

We have demonstrated the viability of liquid and gel lithium battery electrolytes based on ethyleneoxy phosphazenes. The conductivity of liquid oligomeric phosphazene electrolytes is acceptable for some energy storage applications, while the addition of propylene carbonate greatly enhances the performance of the resultant gel electrolytes. Further developments will depend on investigation of other component requirements, such as the fire retardant properties that are described in the next chapter.

2.5. REFERENCES

[1] Mark, J.E., Allcock, H.R., West, R., *Inorganic Polymers,* Prentice Hall, New Jersey, **1992**

[2] Tarascon, J.-M.; Armand, M. *Nature,* **2001**, *414***,** 359

[3] Striebel, K.A.; Zaghib, K.; Guyomard, D. Electrochemical Society, Meeting Staff *Lithium and Lithium-Ion Batteries: Proceedings of the International Symposium*, Electrochemical Society, Incorporated Electrochemical Society Proceedings **2004**, *2003-28*, 394

[4] Masataka, W.; Osamu, Y. *Lithium ion batteries: Fundamentals and performance* Wiley-VCH, **2008**

[5] Nazri, G. *Chemistry of Materials,* **1989**, *1***,** 370

[6] Allcock, H. R.; Sunderland, N. J.; Ravikiran, R.; Nelson, J. M. *Macromolecules*, **1998**, *31*, 8026

[7] Kaskhedikar, N.; Burjanadze, M.; Karatas, Y.; Wiemhöfer, H. D. *Solid State Ionics,* **2006**, *177***,** 3129

[8] Ahn, S.; Kim, H.-S.; Yang, S.; Do, J. Y.; Kim, B. H.; Kim, K. *Journal of Electroceramics,* **2008,** *23,* 289-294

[9] Allcock, H. R.; Ravikiran, R.; O'Connor, S. J. M. *Macromolecules,* **1997**, *30,* 3184

[10] Morford, R. V.; Kellam III, E. C.; Hofmann, M. A.; Baldwin, R. Allcock, H. R. *Solid State Ionics,* **2000,** *133***,** 171

[11] Zhang, S. S. *Journal of Power Sources* **2006,** *162*, 1379

[12] Morford, R.M.; Welna, D.T.; Kellam III,C.E.; Hofmann, M.A.; Allcock, H.R. *Solid State Ionics* **2006**, *177*, 721

[13] Lyon, R.E.; Speitel, L.; Walters, R.N.; Crowley, S. *Fire Mater*. **2003**, *27*, 195

[14] Carriedo, A. A.; Fernndez-Catuxo, L.; Alonso, F. J. G.; Elipe, P. G.; Gonzlez, P. A.; Snchez, G. *Journal of Applied Polymer Science,* **1996**, *99*, 1879-1885

[15] Xu, K.; Ding, M.S.; Zhang, S.; Allen, J.L.; Jow, T.R. *J. Electrochem. Soc.* **2002**, 149, A622

Chapter 3

Methoxyethoxyethoxyphosphazenes as ionic conductive fire retardant additives for lithium battery systems

3.1. Introduction

As discussed in the previous chapters, the main advantage of lithium batteries is their high energy density, which makes them smaller and lighter than other batteries such as nickel–cadmium devices. This makes lithium batteries especially suitable for applications where lightweight or compact power sources are required, such as portable electronic devices and electric vehicles.

On the other hand, one of the biggest drawbacks of rechargeable lithium batteries is their flammability. The high energy density of lithium batteries is accompanied by the high reactivity of their metallic or composite lithium components and by the flammability of their small-molecule, organic solvent-based electrolytes. This makes them susceptible to combustion or even explosions under certain conditions such as over-charging or short circuits caused by defects or physical damage. Numerous lithium-battery related fires have been reported in recent years, leading to recalls and restrictions [1].

Although various protective devices have been designed to reduce the incidence of battery-induced accidents, problems persist. This is an especially important problem for energy storage in electrical automobiles due to the large batteries that are required.

The avoidance of secondary damage after accidents or short circuits is especially important for such an application [2]. A number of strategies have been implemented to improve the fire safety of secondary lithium batteries [3,4]. In addition to methods such as reducing the amount of flammable components in the battery, a major challenge is the development of fire retardant additives. Fire retardant materials include those that are truly nonflammable and which can physically contain a fire, and those that inhibit exothermic reactions via chemical reactions to prevent a fire [5,6].

Many fire retardant species contain phosphorus compounds [7–11] because organophosphorus molecules are efficient radical scavengers and flame quenching materials. Combustion processes are essentially exothermic free-radical reactions, and the existence of radical capture species impedes combustion by quenching the mechanism. Other types of fire retardants include nitrogen-containing compounds that release inert gaseous by-products to form a highly porous char that provides thermal insulation and prevents the combustion from spreading [12,13]. Most fire retardant additives for lithium batteries are integrated into either the electrode or the electrolyte. However, because such additives cannot contribute to the electrochemical reaction, they usually have a negative effect on the battery efficiency. Other important concerns for practical additive materials include electrochemical stability under actual operational conditions, as well as a straightforward synthesis procedure suitable for scale-up.

In addition to their versatility in reaction chemistry and overall stability in electrochemical environments [14,15], one of the most important advantages of many phosphazene compounds is their flame resistance or fire retardance properties [16]. This

makes phosphazenes particularly good candidates for fire retardant materials in batteries. In other applications, studies have shown that phosphazene crosslinkers in polyurethanes cause the originally highly flammable material becomes self-extinguishing [17]. Other phosphazenes are effective as fire retardants for wood-based materials, where the weight loss during burning was cut in half by the application of a cyclic triphosphazene coating [18]. The currently available phosphazene fire retardant additives are principally amino- or oxy- derivatives of methyl or phenyl substituted cyclic trimers. These compounds are relative easy to synthesize and have been reported to have useful fire retardant properties [19,20]. This is particularly evident for amino derivatives. However, when used in batteries these molecules lower the electrochemical efficiency of the cell. For aminophosphazene compounds there is also the problem of spontaneous degradation under typical electrochemical working conditions. Thus, the need exists for new fire retardant additives that will maintain or enhance the ionic conductivity of the cell, retain a high energy density, and increase the safety of lithium batteries.

An attractive solution is the incorporation of ionically conductive fire retardant additives into the organic electrolyte. As noted in earlier chapters, previous studies have shown that certain phosphazene compounds are themselves suitable as electrolytes for lithium batteries due to their acceptable ionic conductivities [21-25]. It was also reported that these polymers have a high onset temperature of thermal degradation (~235 ◦C) together with a modest heat release capacity [23]. There are also studies where, when phosphazenes were used as plasticizers for other solid electrolyte systems, the flammability of the electrolyte was lowered below the combustion standard while still

maintaining good electrochemical performance [26]. By using these species as pure electrolytes or additives to organic solvent electrolytes, it should be possible to construct a fire-resistant lithium battery with a high energy density [27]. Moreover, small-molecule liquid cyclic phosphazenes that bear oligo-ethyleneoxy side groups should be useful as electrolyte additives or as stand-alone liquid electrolytes without decreasing the overall efficiency of the battery, as suggested in the last chapter. High molecular weight, long-chain species can be used as the basis of gel electrolytes or as semi-solid spacer matrix materials.

In this work, we have performed in-depth studies of the safety performance of various phosphazene compounds as liquid electrolyte additives, gel electrolyte additives, and stand-alone electrolyte components. As in the previous chapter, the materials focused on here includes the polymeric methoxyethoxyethoxypolyphosphazene (MEEP), the small-molecule methoxyethoxyethoxy cyclotriphosphazene (MEE trimer), and the methoxyethoxyethoxy cyclotriphosphazene (ME trimer) (Figure 3-1). The main focus of this study is on the fire retardant properties and electrochemical performance of both the pure compounds and their mixtures with classical organic solvent-based electrolytes. For fire retardant properties, we analyzed the combustion properties of the electrolytes through direct burning tests modified from ASTM standard procedures. The lithium triflate ($LiCF_3SO_3$)–propylene carbonate (PC) system was selected as the model base electrolyte for better comparison with earlier phosphazene studies. The phosphazene systems should have a comparable performance to commercial electrolytes while providing better fire safety.

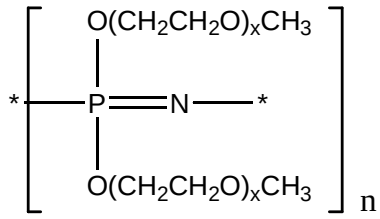

Figure **3-1**: Structure of a polyphosphazene with oligoethyleneoxy side chains.

In this particular study we focused on the methoxyethoxyethoxy polyphosphazene high polymer (MEEP), which has an x value of 2 andan n value up to 15000; the methoxyethoxyethoxy cyclotriphosphazene (MEE trimer), which has an x value of 2 and an n value of 3; and methoxyethoxy cyclotriphosphazene (ME trimer), which has an x value of 1 and an n value of 3. Mixed electrolytes are referred to in the chapter based on their abbreviations: For example, a 75:25 mixture of methoxyethoxyethoxy cyclotriphosphazene and propylene carbonate (PC) is abbreviated as a 75:25 MEE trimer – PC sample.

3.2. Experimental

3.2.1. Materials, synthesis, formulation and characterization

The materials and procedures for electrolyte fabrication and characterization were described in Chapter 2. Grade 691 glass microfiber filter paper was purchased from VWR.

Nextel 312 aluminum–silicone–boron oxide fiber was obtained from 3M. Both substrates were used as received.

3.2.2. Flammability test procedures

3.2.2.1. Wick test

Liquid flammability tests were carried out by the addition of a 2 g electrolyte sample contained in a small (5mm deep) glass cup. A 1cm×1 cm glass fiber paper (VWR Grade 691 glass microfiber filter paper) was soaked in the electrolyte for 1min. The paper was then supported vertically by the side of the cup as a wick, and was ignited by a butane flame held in contact with the edge of the paper. Two separate experiments with different conditions were carried out for each material. In the first experiment the lighter flame was removed when a free-standing flame was observed, and in the second test the flame remained at the wick for 10 seconds before it was removed. Unless otherwise noted, the experimental results reported were based on whichever method resulted in the shortest contact of the butane flame with the filter paper. Once the ignition source was removed, the flame was timed until it self-extinguished and was recorded in each case.

3.2.2.2. Fiber test

This test was a modified procedure based on ASTM D-5306. A 12-cm length of 3M Nextel 312 aluminum–silicon–boron oxide fiber (900 Denier Ply-twisted 2.7 twist

per inch 3/4 yarn, 390 yrds lb^{-1}) was weighed and soaked in the electrolyte solution for 1min. The yarn was then tensioned via weights at both ends and pretreated by a standard method, weighed to calculate the average amount of electrolyte absorbed per unit length, then suspended horizontally and ignited from one end. The flame was allowed to burn over 1 cm before the timing was started, and the timing ended either when the flame self-extinguished or when the flame had traveled 5 cm, whichever came first. The flame propagation was calculated by dividing the actual distance the flame traveled by the time taken for the flame to travel. The average fuel consumption rate was calculated by multiplying the electrolyte weight per length by the flame propagation rate.

3.3. Results and discussion

3.3.1. General aspects for fire retardant properties

The fire retardant behavior of these compounds is of major interest. Although no commonly accepted tests are available for the flammability of electrolytes, a number of methods are possible based on previous studies [10–12,15,19,28]. However, our attempts to test various phosphazene systems showed that many of the methods employed in other programs caused samples to self-extinguish too quickly to allow the detection of differences between various compositions. Thus, we have modified existing methods to artificially sustain a flame by introducing a larger surface area, so that the variations between different samples can be examined thoroughly. In addition, we believe that both

the self-extinguish time and the flame propagation behavior are important indicators of fire retardant behavior, although the latter is rarely reported. Similarly, the consumption rate of the electrolytes may also give some insight into the nature of the actual combustion process. As such, we have chosen methods which used non-flammable matrices that absorb the electrolyte samples in order to provide stable platforms for all three measurements. This provides a close mimic of the behavior of an electrolyte in a working battery.

3.3.2. Self-extinguishing rate

The self-extinguishing time measurements using a glass fiber wick method were performed with a container of electrolyte ignited from a piece of glass fiber supported by the side of the glass cup container, and the extinguish time of the resulting flame was timed (Figure 3-2).

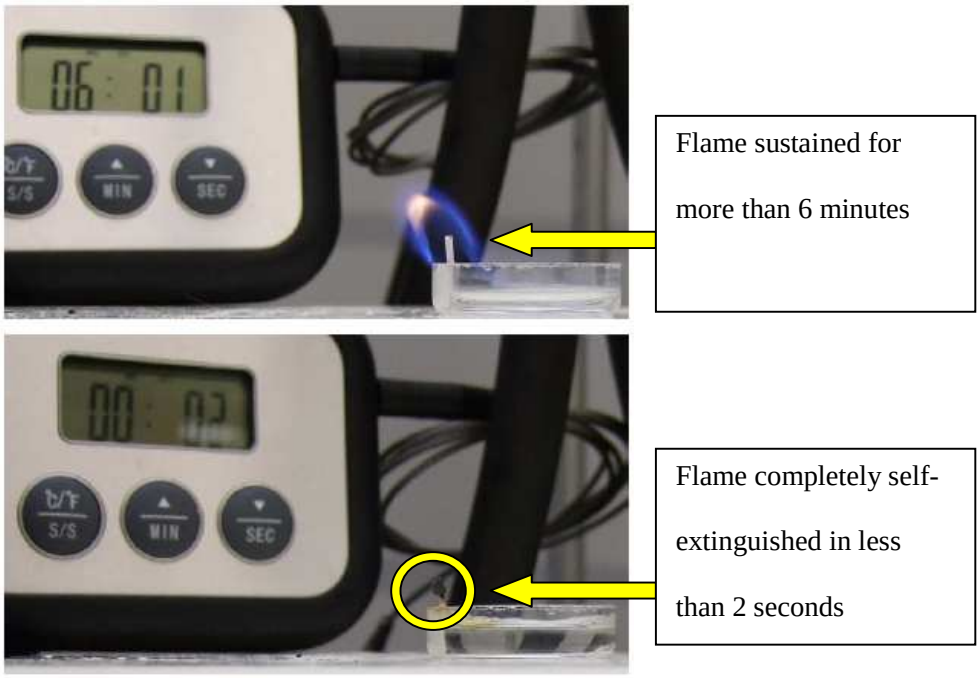

Figure **3-2**: Self-extinguish time experiment setup. Above: sustaining flame of pure propylene carbonate. Below: rapidly self-extinguished flame of MEE trimer.

To eliminate any non-reproducible error from ignition flames and observational error, as well as to mimic the difference between flash ignitions versus constant heat source ignitions, we compared the results of removing the ignition source after observation of a sustaining flame versus removal after a set period of time. The results showed that the difference is relatively minor for the samples we are investigating: in terms of the relative performance of the samples there is no significant difference. While it is not possible to compare MEEP flammability directly with other materials, because MEEP is a gum rather than a liquid, and it cannot be readily absorbed into the wick

during combustion, it is still possible to estimate comparisions through the performance of phosphazene–propylene carbonate mixtures. The flammability of samples with a higher phosphazene content was lower in all the electrolyte types we have investigated. For the undiluted liquid electrolyte materials, MEE trimer is less flammable than propylene carbonate, and ME trimer shows an even lower flammability **(Figure 3-3)**. This is related to the ratio of phosphorus to carbon and oxygen, because organic C, H, and O species should be more combustable, and a higher ratio of these elements should lead to higher flammability.

On the other hand, for mixed phosphazene-propylene carbonate electrolytes, the mixtures with the polymeric components are interestingly less flammable than those composed of only liquid components (i.e. small molecule solutes). For example, the experimental results with MEEP – propylene carbonate show a lower flammability than for MEE trimer – propylene carbonate, with a significantly shorter self-extinguish time (Figure 3-4). This is probably due to the lower volatility of MEEP, which decreases the overall vapor pressure of the flammable species, and effectively reduces the flammable fuel supply with a higher energy barrier. This could also be due to the fact that the lower volatility and better thermal stability of the polymer causes it to form a solid protective layer, while the liquid components evaporate. It was also observed that samples with a high content of phosphazene materials tend to produce large amounts of char after combustion.This is consistent with the radical stabilization effect of organic phosphorus fragments, which are expected to hinder exothermic chain reactions and lower the temperature of the flame, thus promoting char formation. This may be one of the reasons

for the difference in self-extinguishing behavior between different samples. MEE trimer – propylene carbonate mixtures had lower viscosities and thus had less efficient coating capacities than the MEEP – propylene carbonate mixtures. On the other hand, the charring effect of the phosphazenes still caused the samples to self-extinguish after a short period of time compared with clean-burning pure propylene carbonate (Figure 3-2 and 3-4).

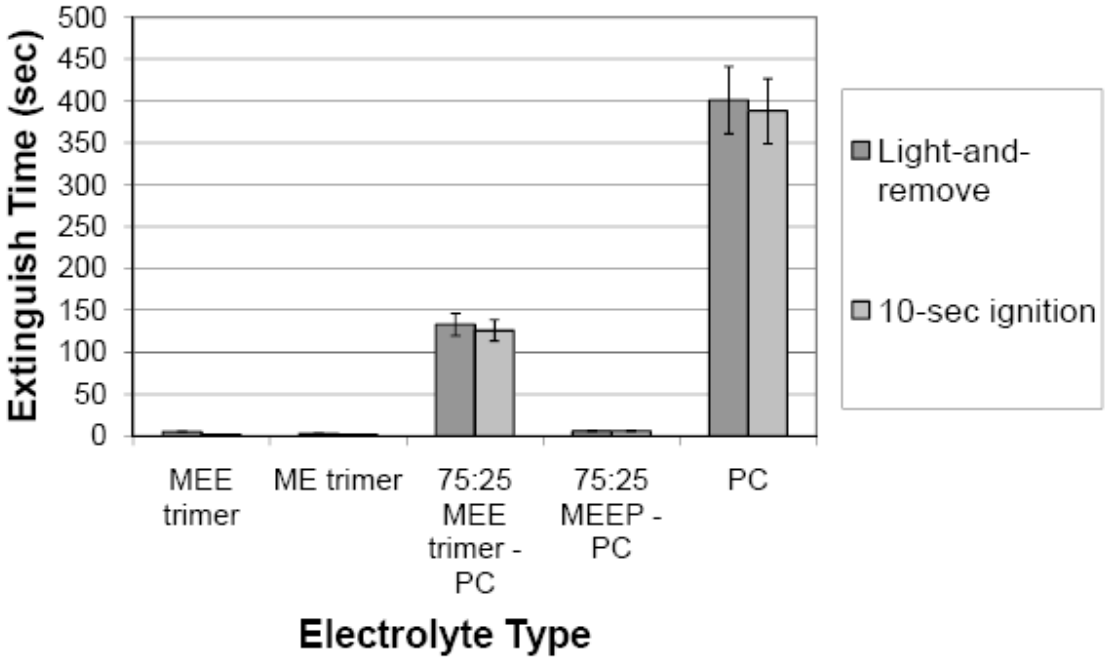

Figure **3-3**: Comparison of self-extinguish behavior between single-solvent and mixed-solvent electrolytes of different composition. All numbers reported here are averages of at least 6 samples. See caption of Figure 3-1 for sample definitions.

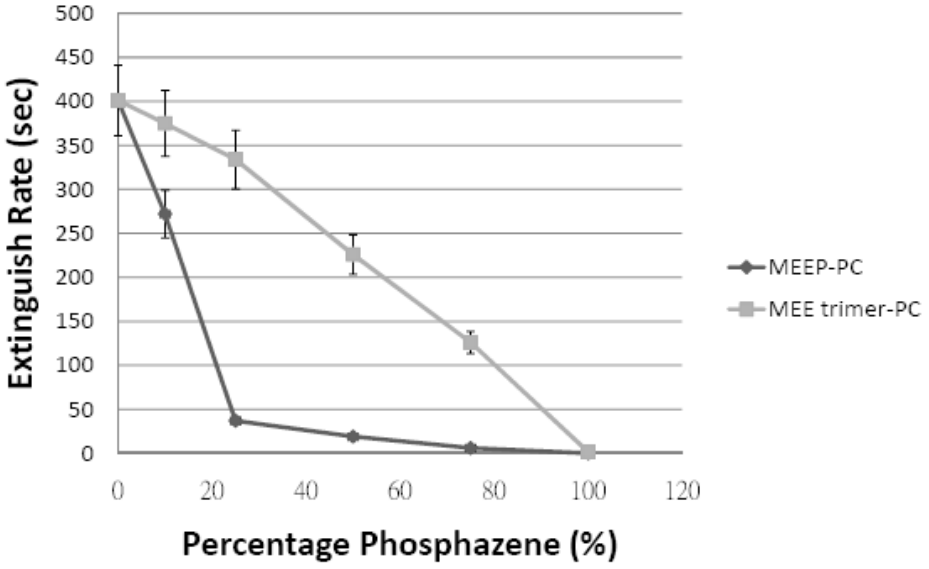

Figure **3-4**: Results of self-extinguishing test based on different phosphazene – propylene carbonate ratios. All numbers reported here are averages of at least 6 samples.

3.3.3. Linear flame propagation

Flame propagation tests using ceramic fibers were adapted from hydraulic fluid characterization methods (ASTM D-5306), where the speed of an ignited flame traveling from one end of the fiber to another is used to compare flammability (Figure 3-5). Our results show that the addition of phosphazene components indeed reduces the average flame propagation rate in a propylene carbonate electrolyte. Increases in the amount of propylene carbonate in the mixture increases the flammability as expected. Higher

concentrations of the non-flammable $LiCF_3SO_3$ component also decreased flame propagation, although it shows a much reduced effect after a certain point (Figures 3-6 and 3-7) This “level-off” effect is likely due to both the carbons and oxygens in the composition maintaining a minimal flammability despite the amount of non-flammable inorganic components, as well as the limit of our ability to characterize the low-flammability self extinguishing samples. The results are promising since the phosphazene additives not only lower the flammability significantly, but the optimal concentration range of $LiCF_3SO_3$ (where the fire retardant effect levels off) for all samples overlap with the optimal range for conductivity. On the other hand, the results show no significant difference between the MEE trimer and MEEP in terms of their impact on linear flame progression.

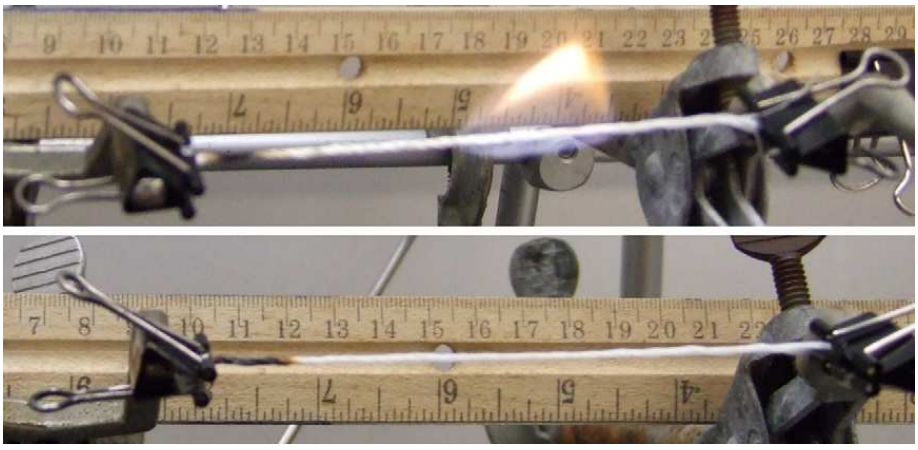

Figure **3-5**: Experimental setup for linear flame propagation test. Above: rapid progressing flame of propylene carbonate sample. Below: self-extinguished MEE trimer sample.

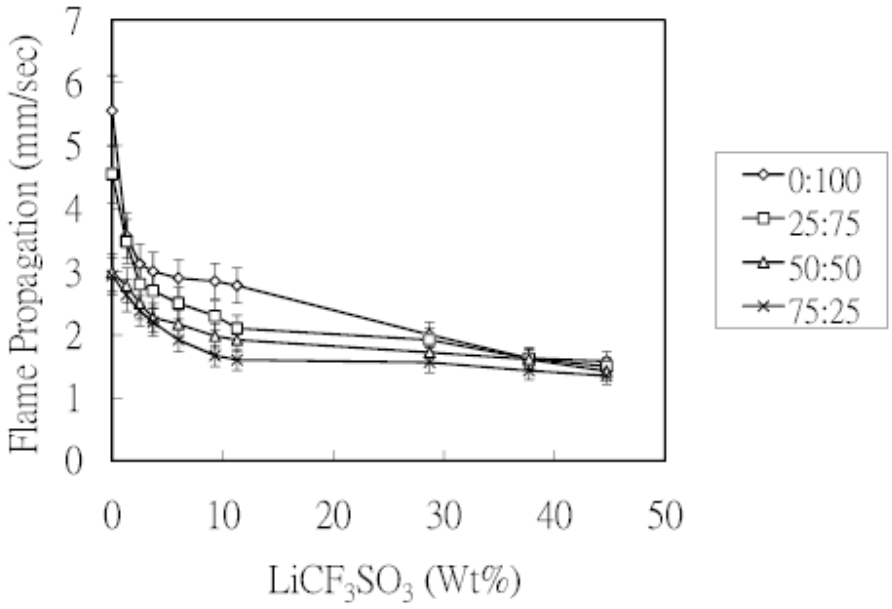

Figure **3-6**: Linear flame propagation of MEEP – propylene carbonate mixtures. All numbers reported here are averages of at least 6 samples. Note the diminishing effect of increase in lithium salt concentration.

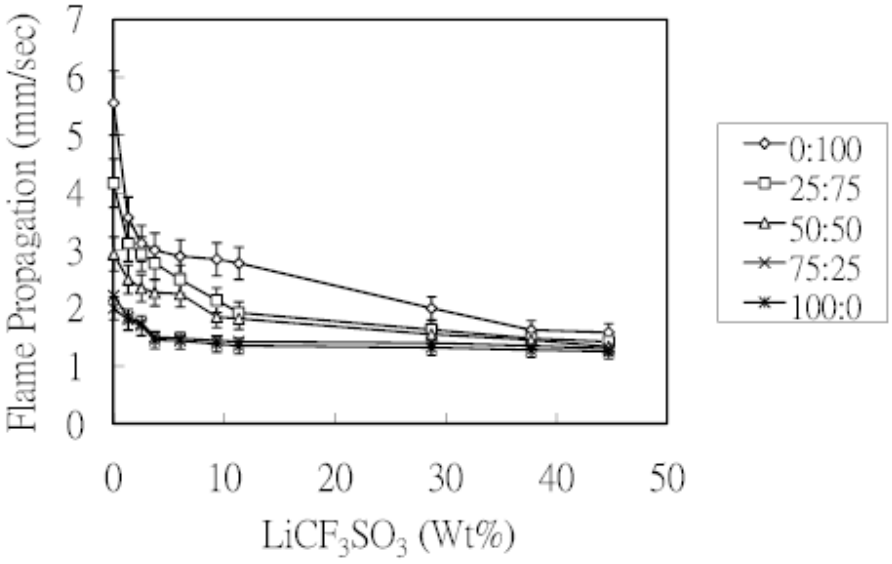

Figure **3-7**: Linear flame propagation of MEE trimer – propylene carbonate mixtures. All numbers reported here are averages of at least 6 samples. The "level off" point comes earlier than the polymeric MEEP additive.

3.3.4. Fuel consumption rate

Conversion of flame progression data to fuel consumption was accomplished by dividing the weight of absorbed electrolyte by the flame propagation speed, and the results show some interesting differences between the two data sets despite use of the same method. At lower lithium salt concentrations, the addition of MEEP seemed to induce a similar fuel consumption rate as in the linear flame propagation tests, but at very high salt concentrations the electrolyte appeared to be consumed faster, causing a reversed trend (**Figures 3-8 and 3-9**). Although the difference is relatively minor, such a

result suggest that the variation at the high $LiCF_3SO_3$ salt concentrations compared to wick tests could be related to the viscosity of the electrolyte solution, because higher viscosities would lead to a thicker coating of the electrolyte on the ceramic fiber, and the difference in the amount of absorbed electrolyte per unit length would impact the effective surface area and thus the fuel consumption rate. In fact, with higher viscosity samples it was sometimes observed that parts of the electrolyte were melted and dripped from the fiber rather than being consumed by the flame, which could also contribute to the difference. Similarly, the trend of flammability at higher concentrations reverses slightly for MEE trimer versus MEEP when a high percentage of MEEP is present in the mixture, again closely tied to the apparent viscosity. The viscosity effect is also believed to be the reason for the “bumps” in trend for samples between 5~10% salt concentration, as the extra electrolyte uptake linked to the appearent viscosity increase matches these trends as being nonlinear. The balance of surface tension, gravity and “wiper” material interactions is also believed to play an important role here. As such, more investigation will be required to find a more appropriate test to compare with the results of existing methods for a clear picture.

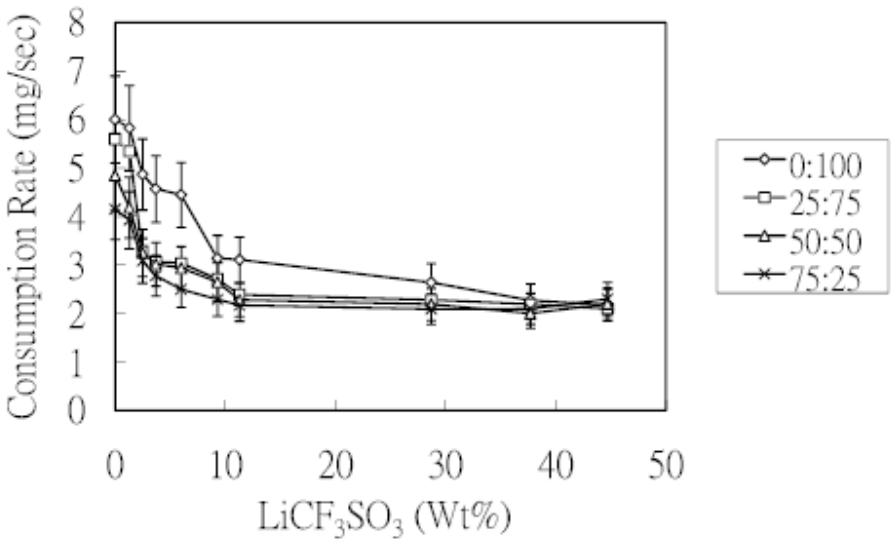

Figure **3-8**: Fuel consumption rates of MEEP – propylene carbonate mixtures. All numbers reported here are averages of at least 6 samples. Note the reversal trends at certain concentrations due to increase in viscosity and thus more fuel per length.

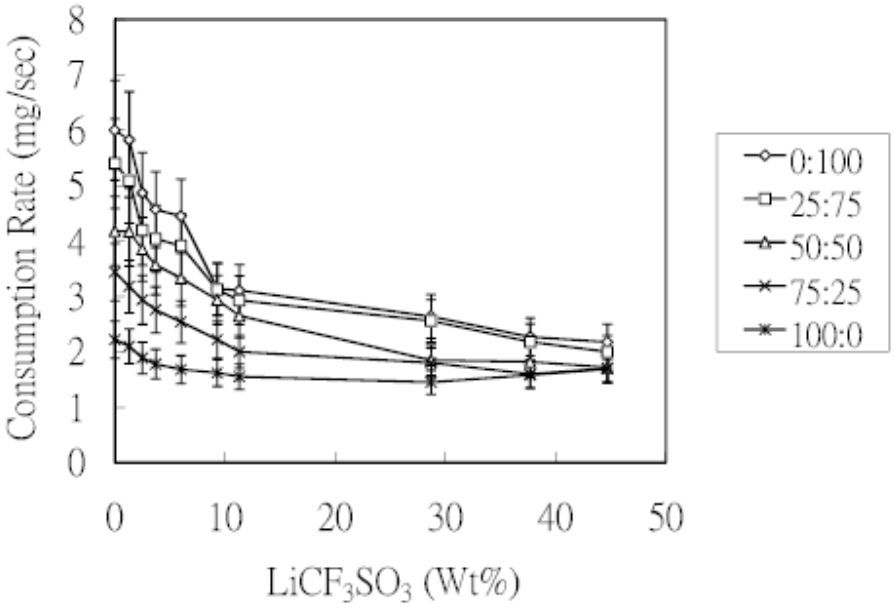

Figure **3-9**: Fuel consumption rates of MEE trimer – propylene carbonate mixtures. All numbers reported here are averages of at least 6 samples. Reversal trend showed up at concentrations similar to polymeric MEEP samples.

3.4. Conclusions

We have developed fire-retardant electrolyte systems based on the methoxyethoxyethoxy-substituted phosphazene high polymer and low molecular weight oligomer systems and have developed testing methods to estimate their flame retardant ability. These can be compared with their electrochemical performance as described in Chapter 2. As a stand-alone electrolyte the methoxyethoxyethoxyphosphazene cyclic trimer has shown very good self-extinguishing behavior with acceptable conductivity.

When mixed with propylene carbonate solvent, both the cyclic oligomer and MEEP polymer showed good compatibility with the organic medium and a significant reduction of flammability while retaining good ionic conductivity. Additional tailoring of the side groups attached to the phosphazene skeleton should further improve the fire safety of lithium battery electrolyte systems. Future research will be focused on an in-depth electrochemical study geared toward assembled commercial batteries, including cyclic voltammetry studies of component stabilities as well as the effect of different salt types.

3.5. Acknowledgements

We thank Dr. Daniel Welna, David Lee, and Dr. Toshiki Fushimi for helpful discussions and suggestions.

3.6. References

[1] Jacoby, M. *C&EN* **2007,** *85,* 26–28.

[2] Terada, N.; Yanagi, T.; Arai, S.; Yoshikawa, M.; Ohta, K.; Nakajima, M.; Yanai, A.; Arai, N. *J. Power Sources* **2001,** *100,* 80–92.

[3] Aurbach, D.; Talyosef, Y.; Markovsky, B.; Markevich, E.; Zinigrad, E.; Asraf, L.; Gnanaraj, J. S.; Kim, H. J. *Electrochim. Acta* **2004,** *50,* 247–254.

[4] Balakrishnan, P. G.; Ramesh, R.; Kumar, T. P.; *J. Power Sources* **2006,** *155,* 401–414.

[5] Nelson, G. L. in: Nelson, G. L. Eds., *Fire and Polymers II: Materials and Tests for Hazard Prevention,* American Chemical Society, Washington, DC, 1995, pp. 1–26.

[6] Zhang, S. S. *J. Power Sources* **2006,** *162,* 1379–1394.

[7] Green, J. in: Wilkie C. A. Eds., *Fire Retardancy of Polymeric Materials,* Marcel Dekker Inc., New York, 2000, p. 147.

[8] Wang, Q.; Sun, J.; Yao, X.; Chen, C. *Electrochem. Solid-State Lett.* **2005,** *8,* A467–A470.

[9] Zhang, S. S.; Xu, K.; Jow, T. R. *J. Power Sources* **2003,** *113,* 166–172.

[10] Li, W.; Campion, C.; Lucht, B. L.; Ravdel, B.; DiCarlo, J.; Abaraham, K. M. *J. Electrochem. Soc.* **2005,** *152,* A1361–A1365.

[11] Dixon, B. G.; Morris, R. S.; Dallek, S. *J. Power Sources* **2004,** *138,* 274–276.

[12] Inoue, K.; Nakamura, H.; Ariyoshi, S.; Takagi, M.; Tanigaki, T. *Macromolecules* **1989,** *22,* 4466–4469.

[13] Izquierdo-Gonzales, S.; Li, W.; Lucht, B. L. *J. Power Sources* **2004,** *135,* 291–296.

[14] Nazri, G.; McArthur, D. M.; Ogara, J. F. *Chem. Mater.* **1989,** *1,* 370–374.

[15] Fei, S. T.; Phelps, M. V. B.; Wang, Y.; Barrett, E.; Gandhi, F.; Allcock, H. R. *Soft Matter* **2006,** *2,* 397–401.

[16] Mark, J. E.; Allcock, H. R.; West, R. *Inorganic Polymers,* Prentice Hall, New Jersey, 1992.

[17] Reed, C. S.; Taylor, J. P.; Guyglei, K. S.; Coleman, M. M.; Allcock, H. R. *Polym. Eng. Sci.* **2000,** *40,* 465–472.

[18] Chen-Yang, Y. W.; Chuang, J. R.; Yang, Y. C.; Li, C. Y.; Chiu, Y. S. *J. Appl. Polym. Sci*. **1998,** *69*, 115–122.

[19] Bridgestone News Release 2002/11/20 (Japan), http://www.bridgestone.co.jp/english/news/021120.html.

[20] Xu, K.; Ding, M. S.; Zhang, S.; Allen, J. L.; Jow, T. R. *J. Electrochem. Soc.* **2002,** *149*, A622–A626.

[21] Nazri, G. *Chemistry of Materials*, **1989,** *1*, 370-374

[22] Allcock, H. R.; Sunderland, N. J.; Ravikiran, R.; Nelson, J. M. *Macromolecules* **1998,** *31*, 8026–8035.

[23] Lyon, R.E.; Speitel, L.; Walters, R. N.; Crowley, S. *Fire Mater*. **2003,** *27*, 195–208.

[24] Allcock, H. R.; Ravikiran, R.; O'Connor, S. J. M. *Macromolecules* **1997,** *30*, 3184–3190.

[25] Kaskhedikar, N.; Burjanadze, M.; Karatas, Y.; Wiemhofer, H.D. *Solid State Ionics* **2006,** *177*, 3129–3134.

[26] Morford, R. M.; Welna, D. T.; Kellam III, C. E.; Hofmann, M.A.; Allcock, H.R. *Solid State Ionics* **2006,** *177*, 721–726.

[27] Fei, S.; Allcock, H. R. *Mater. Res. Soc. Symp. Proc.* **2009,** 1127-T01-05.

[28] Akashi, H.; Sekai, K.; Tanaka, K. *Electrochim. Acta* **1998,** *43*, 1193–1197.

Chapter 4

Electrolyte infiltration in polymer-based dye-sensitized solar cells

4.1. INTRODUCTION

This chapter summarizes a study of polymer-based dye-sensitized solar cell regarding improved electrolyte infiltration into nanoporous electrodes. Solar cells, or photovoltaic cells, are devices capable of generating electricity directly when exposed to sunlight [**1.2]**. This technology has attracted considerable attention because it is viewed as one of the ultimate "green energy" options [**3 – 8]**. However, a few technical problems remain to be solved before the technology can be more widespread, a major one being that the cost of solar electricity is currently about 5-20 times that of conventional power. [**4, 6, 7, 8]** To overcome these restrictions, a number of alternative solar cell designs have been introduced [**9-15**] As mentioned in Chapter 1, among them one of the most promising recent developments is the "Dye Sensitized Solar Cell" (DSSC) [**12]**, This type of solar cell uses a layer of nano-scale semiconductor particles (usually titanium oxide), fused into a mesoporous film and stained with light absorbing dyes, which eject electrons into the transparent electrode (usually titanium oxide) when the dye is excited by light. A

layer of a redox active species (commonly an I^-/I_3^- mixture suspended in a liquid electrolyte) is present to provide an electron-replenishing medium. [**11-13]**

As mentioned in Chapter 2, one of the most important factors in limiting the performance of an electrochemical device based on mobile ions is the conductance of the electrolyte, and this also holds true in the case of dye solar cells **[11-13]**. In general, the liquid electrolytes currently used are based on organic solvents such as acetonitrile in order to maximize this conductivity. The serious drawback of liquid electrolytes is their vulnerability to long term environmental damages: The volatility and the possibility of leakage during extended operation, especially at elevated temperatures, leads to the necessary complexity of sealing the unit. Thus, these devices are frequently unreliable under severe thermal and oxidative conditions, and this seriously limits the manufacturing options and lowers the lifetime of the cell.

Use of a solid polymer electrolyte is a logical solution to this problem. [**16]** Solid polymer electrolyte systems have a number of advantages compared to liquid electrolytes, including high dimensional stability and ease of processing. However, the main drawback of solid (i.e. unplasticized) polymer electrolytes is the low ionic conductivity brought about by limited ion mobility in the solid matrix of even the most flexible polymers. Also, the TiO_2 layers used by most dye solar cells are made by the stacking of nanocrystals. This results in a porous anode with random channels a few nanometers wide (5~15nm pore size). Ideally, the electrolyte should be in contact with the entire dye-functionalized TiO_2 surface. However, this is difficult for polymer electrolyte systems, because twisted

narrow channels require the polymeric molecules to uncoil before they can enter the pores. This entropically-unfavorable process prevents full contact of the electrolyte with the TiO_2 surface, and is often seen as a major reason for the low efficiency of solid polymeric DSSCs compared to gel or liquid electrolyte systems [**17-20]**.

The ideal polymer electrolyte for nanopore infiltration should be fully amorphous and flexible enough at the molecular level to allow dissolved ions to hop from one polymer molecule to another, facilitated by the thermally induced movements of the flexible chains. The previous chapters have shown that polymer electrolytes with high ionic conducting properties, such as those with oligoethylene oxide side chains **(Figure 4-1) [21, 22, 23]**, can be synthesized by linking ion conductive side chains to a flexible polyphosphazene backbone. This approach provides access to amorphous polymers with good thermal- and photo-stability.[**21]** Another important point among their main advantages over other polymers is the low glass transition temperature and absence of crystallinity – that is, they remain highly flexible even at low temperatures due to the unusual mobility of the P-N backbone. This leads to completely amorphous materials that , in addition to faster ion transport compared to polymers with crystalline domains such as poly(ethylene oxide), are also good thermoplastic compounds that are suitable for melt-processing. This is one potential solution to the pore-infiltration dilemma described above. They are also highly adhesive, and promote a more stable interface between electrodes and the electrolyte layer. We expect this group of solid electrolytes to perform well in solar cells based on their good record in lithium battery systems.

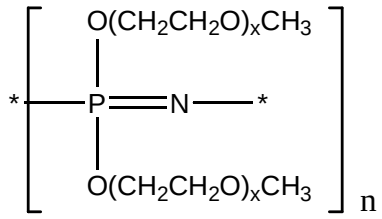

Figure **4-1**: Structure of a polyphosphazene with oligoethyleneoxy side chains. [**21**] In this particular study we focus on the methoxyethoxyethoxy polyphosphazene (MEEP), which has an x value of 2 and an n value up to 15000, and methoxyethoxyethoxy triphosphazene (MEE trimer), which has an x value of 2 and an n value of 3.

Also, semiconductor nanorod "bed of nails" arrays have been suggested as the optimal arrangement for minimization of excitation and charge carrier diffusion lengths.[**24]** By organizing nanorods to produce wide, straight channels, it should be possible to increase the infusion of oligomers and polymers into the array and thus generate a high area of surface contact. Thus, through nanoengineering of the TiO_2, we can compare the effect of different nanorod arrays with varied channel sizes, rod shape, array alignment, or surface morphology. [**25]**

We report here the results of combining the thermoplastic phosphazene electrolyte system with various cell assembly methods as well as nanostructured electrodes on electrolyte infiltration and performance in a dye solar cell. The viability of phosphazenes as a basis for polymer electrolyte components in dye solar cells has been tested. The conductivity of the electrolytes and the corresponding cell efficiency under various assembly conditions has been investigated through EIS and photocurrent analysis. The

pore-filling properties of the polymer electrolyte have also been explored through cross-section SEM studies and have been compared with the electrochemical data.

4.2. EXPERIMENTAL

4.2.1. Materials

Hexachlorocyclotriphosphazene, $(NPCl_2)_3$, was obtained from Fushimi Chemical and Pharmaceutical Co. Ltd., Japan and Nippon Fine Chemicals. The compound was purified by recrystallization from heptane, and sublimation at 40 ◦C and 0.05mmHg vacuum. Celite, sodium metal, anhydrous lithium iodide, propyl-methyl-imidazolium iodide (PMII), iodine, di(ethylene glycol)methyl ether, anhydrous acetonitrile, ethanol, and *tert*-butanol were obtained from Aldrich. Diethyl ether, hexanes, tetrahydrofuran (THF), and methylene chloride (CH_2Cl_2) were purchased from VWR. N-719 dye, FTO – glass, and titanium dioxide nanoparticles (nc-$TiO_{2)}$ were obtained from Solaronix. Di(ethylene glycol) methyl ether was purified by vacuum distillation. The diethyl ether, hexanes, THF, and CH_2Cl_2 were purified through copper/ silica catalytic drying columns. All other chemicals were used as received.

4.2.2 Characterization

All characterization of the chemicals was achieved by ^{1}H and ^{31}P NMR spectroscopy with use of a Bruker AMX-360 instrument. Conductivity measurements were made using a HP-4192A impedance analyzer and a two-point liquid or solid conductivity cell. Photocurrent and photovoltage measurements were obtained from test cells using Keithley 7002 - HD source meter and Oriel 77250 150 W Xe Lamp fitted with AM1.5 filter. All electrochemical experiments are repeated to aquire at least 6 data points before reporting average numbers unless otherwise noted. SEM was done with an FEI Philips XL-20 model instrument supplied by MCL. EDS and BSE scans were done using an FEI Quanta 200 environmental SEM fitted with Oxford Inca 200 EDS supplied by MCL.

4.2.3. Synthesis of methoxyethoxyethoxy polyphosphazene (MEEP) and hexamethoxyethoxyethoxy cyclotriphosphazene (MEE trimer)

These syntheses were carried out according to previous literature with no modification [**26,27]**.

4.2.4. Synthesis of short chain poly[bis(methoxyethoxyethoxy polyphosphazene)] (MEEP)

This synthesis of a short chain chlorophosphazene was carried out according to previous literature with no modification [**28]**. Replacement of chlorine atoms by the MEEP-type side groups was carried out in the same way as for MEEP high polymer. [**29]**

4.2.5. Electrolyte solution mixture preparation

In a typical experiment, MEEP polymer (0.1g) was dissolved in 5ml of acetonitrile with an appropriate ratio of LiI and I_2. The solution was stirred overnight to ensure even mixing, and was used directly in the cell assembly for efficiency tests. For ionic conductivity experiments, the same sample solution was freed from solvents either under atmospheric conditions for 60hr, under vacuum conditions for either 1hr or 16hr, or 60^{o}C for either 1hr or 16hr.

4.2.6. Electrode fabrication

Nanoparticle- based nanoporous titanium oxide electrodes were fabricated based on modified published procedures [**11, 30]**: transparent fluorine-doped tin oxide (FTO) - glass substrates (1 in. × 1 in.) were pre-treated by immersing in isopropanol and sonication for 20 min, followed by 20 min sonication in ethanol. The substrate was then rinsed with deionized water and air-dried. A few drops of nc-TiO_2 paste formulated based on previously reported procedures **[30]** were spread onto the conductive side of the FTO/glass using a razor blade. Cellophane tape spacers were applied to opposite edges of the electrode to control the thickness of the doctor-bladed nc-TiO_2 films. The samples were then sintered at 475 ˚C for 30 min and cooled to 180 ˚C, followed by immersion in a 0.3 mM solution of N-719 dye in a mixture (50:50) of acetonitrile and *tert*-butanol for 48 hr. Nanocolumn-based titanium oxide substrates and platinum nanoparticle electrodes were fabricated based on published procedures **[11, 25, 30, 31].** Comparison samples of

identical TiO_2 structures fabricated on silicon wafers were also prepared for SEM studies in order to eliminate possible complication caused by stress or strain during cross-section fracture.

4.2.7. Test solar cell assembly

To each TiO_2 electrode the electrolyte was applied via solution casting: A spacer made from stretched Parafilm was applied around the perimeter of the TiO_2. Four drops of the acetonitrile-MEEP solution was then applied to the 5mm x 5mm electrode surface and allowed to dry in air for 30 minutes, and the process was repeated until the thickness of the polymer film matched that of the spacer. The assembly was then allowed to dry further under appropriate conditions as described for each of the experiments below, and the platinum counter-electrode was assembled on top of the electrolyte layer and clamped in place following a standard photo-conversion efficiency characterization setup with conditions defined in ASTM G-173-03.

4.2.8. SEM scans for cross-section of MEEP-TiO_2 infusions

MEEP polymer was solution-cast (0.15g dissolved in 5ml of acetone) on a nanoporous TiO_2 on Si wafer by the procedure described above. The resulting sample is dried overnight either under atmospheric or vacuum conditions, at room temperature or 60^oC. The sample was then crosslinked with 20Mrad gamma radiation by explosure to a ^{60}Co source at the Pennsylvania State University Breazeale Nuclear Reactor facility, and

then frozen in liquid nitrogen before being fractured on the edge with a glass-cutter. The cross section was gold-spluttered for 30sec before SEM analysis to ensure high quality imaging except for EDS and BSE runs that operated under low-vacuum settings.

4.3. RESULTS AND DISCUSSION

4.3.1. Viability of MEEP phosphazene as a solar cell electrolyte component

The focus of this research is to understand the effect of electrolyte infiltration on the dye solar cell system. As mentioned in the introduction, the basic design of a dye solar cell and experimental experience implies that a high molecular weight polymer electrolyte should have poor infiltration into the nanoporous electrode. This led to a poor electrode - electrolyte interface due to a reduced surface area with which the electrolyte is in contact with the electrode, and only a fraction of the photoelectron-generating dyes could be recharged by the electrolyte once they eject the photo-excited electrons. This leads to either the rapid back-electron transfer from the TiO_2 to the dye that dissipates

absorbed photo energy into unusable heat, or it causes redox degradation of the dye – both of which lower the effectiveness of the solar cell.

By the use of a low-Tg polymer as the basis of a polymer electrolyte, it was expected that the degree of electrolyte infiltration can be controlled by changes in the cell fabrication conditions. For example, the application of heat during the process should lower the viscosity of the electrolyte and lead to better infiltration. The effectiveness of each assembled cell can be compared through analytical methods. Then the trend can be cross-checked by ion conductivity measurements of the electrolytes after different processing conditions, as well as by cross-section SEM of polymer - electrolyte assemblies. In this way it is possible to differentiate between changes in cell performance due to change in electrolyte infiltration from the cell performance changes due to changes in the performance of electrolyte itself.

For the purpose of measuring the effectiveness of the new solar cells constructed in this project, the single cell energy conversion efficiency (η, percentage of light energy converted into electrical energy), as defined in **equation 4-1**, was used:

$$\eta = \frac{P_m}{E \times A_c} \quad \text{(Equation 4-1)}$$

where Pm is the maximum power output of the cell in W, E is the input light irradiance in W/m^2, and Ac is the effective surface area of our cell in m^2.

The tests were carried out under standard conditions of 25 °C, 1000 W/m^2 irradiance and AM1.5 filters. The benchmark cells to which the new cell designs

were compared were conventional acetonitrile electrolyte and nano-TiO2 electrode systems sensitized by the N719 dye, which obtained 7-8% efficiency reproducibly under AM1.5 irradiation. By contrast, most polymer electrolyte dye cells reported have around 1% efficiency under the same conditions [16].

A variety of MEEP-based solar cell electrolytes have been formulated by dissolving the polymer with an iodide salt and iodine in either acetone or acetonitrile, then evaporating the solvent until a dry, even film was formed on the electrode surface of the test cell. The efficiencies for nanosphere-type dye cell assemblies as well as the ionic conductivities of these electrolytes have been tested, and the results are listed in **Figure 4-2**. The results show that the polymeric MEEP system performs better when the concentration of iodine and iodide are both high, which is different from the conventional liquid electrolyte system based on acetonitrile. It is possible to form homogeneous electrolyte systems with very large amounts of LiI / I_2, as demonstrated by sample 2 where the 1:1:1 LiI : I_2 : MEEP mixture is macroscopically homogeneous. At the same time, the composition of this mixture depends on whether the polymer can be considered a solvent in such cases, and the conduction mechanism may be different compared to other polymer electrolyte systems. Also, the resulting clay-like material was more difficult to fabricate into coherent films.

At the same time, application of heat during the solvent removal process instead raises the efficiency of sample **1** (see **Figure 4-2**) from 0.187% to 0.257%, which suggests that there may still be some degree of infiltration effects. The efficiency of our

MEEP-based dye solar cells are roughly similar to many other solid electrolyte systems [**16]**, which is expected since the solid electrolyte system has a uniformly lower ionic conductivity compared to liquid systems.

One interesting result is that the highest single-sample efficiency to date is 2.97% for a MEEP electrolyte drip-cast using acetonitrile as solvent, with a number of other samples also showing efficiencies above 2%. However, the results obtained in these cases were not reproducible and were thus not taken into account when calculating the average efficiency results. This is suspected to be a solvent retention effect – i.e. the "dried" polymer electrolyte in this case is behaving more like a gel electrolyte. Analysis of electrolyte sample composition by NMR supported this possibility by showing that up to 8% of solvent (molar concentration relative to one repeating unit of polymer) remained after 120 hours of room temperature drying atmospheric conditions.

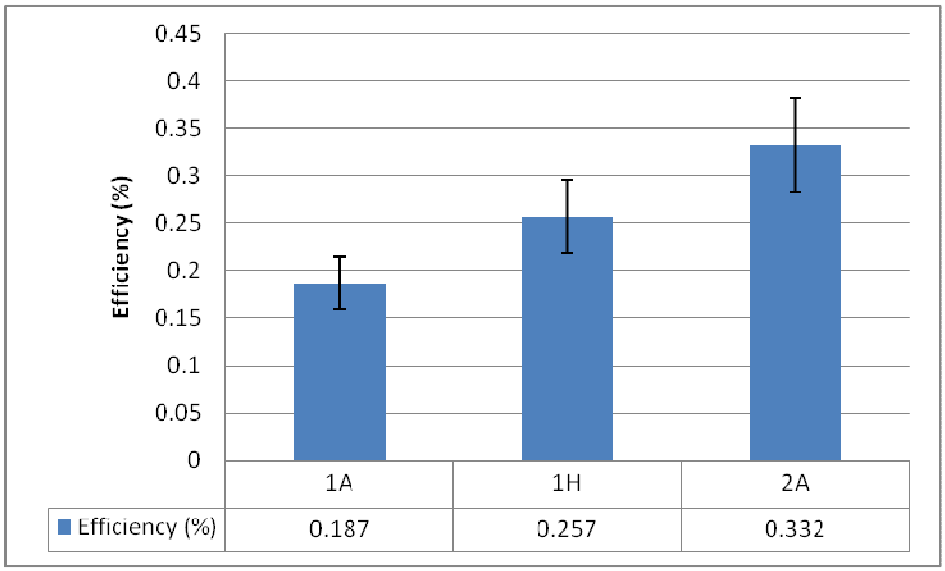

Figure **4-2**: Cell efficiency results for different electrolyte formulations and solvent removal methods. Sample 1: 1:1:10 (wt ratio) LiI:I_2:MEEP. Sample 2: 1:1:1 LiI:I_2:MEEP. Samples labeled as "A" solvents were removed under atmospheric conditions, while those labled as "H" were heated for 1hr at 60^{o}C. All numbers reported here are averages of at least 6 samples.

Solvent-removal using different conditions was also monitored through ionic conductivity measurements, and the results are shown in **Figure 4-3**. As shown here, most of the various solvent-removal conditions led to similar decreases in conductivity, which matched the NMR observation that 4~5% of the solvent still remained. Only when both heat and reduced pressure were applied for extended periods of time (which resulted in a significant decrease in the conductivity), did the NMR fail to detect any signs of residual solvent. While this showed the effect of solvent within the solid electrolyte as a plasticizer as well as a mobile ion shuttle, it did not account for the possible loss of iodine in the solvent removal process. This was suspected based on observations during combined treatment by heat and reduced pressure.

To eliminate such bias, reference samples were made in which a solution of MEEP and iodide salt dissolved in an organic solvent was first prepared. A film of electrolyte was then deposited on test cell electrodes as with previous samples, followed by treatment with heat and reduced pressure to remove all traces of solvent as confirmed by NMR. The sample was then exposed to a fixed amount of iodine vapor within a sealed container until a homogeneous mixture had been formed and no residual iodine unabsorbed by the electrolyte was detected. The result is also shown in **Figure 4-3** (sample 1N). This iodine-vapor infused sample showed better ionic conductivity

compared to samples prepared by direct dissolution – film casting of iodine-containing electrolyte treated through the same solvent removal procedure. Both of the conductivity numbers are lower than those of solvent-containing samples. This further indicated that at least some loss of ionic conductivity, and in turn cell efficiency, was probably due to iodine loss during the solvent removal procedures. Another important finding is that, other than the change caused by the loss of solvents, the NMR analysis showed no detectable change before and after the solvent removal, which eliminated the possibility of chemical reactions of the MEEP polymer during solvent removal procedures.

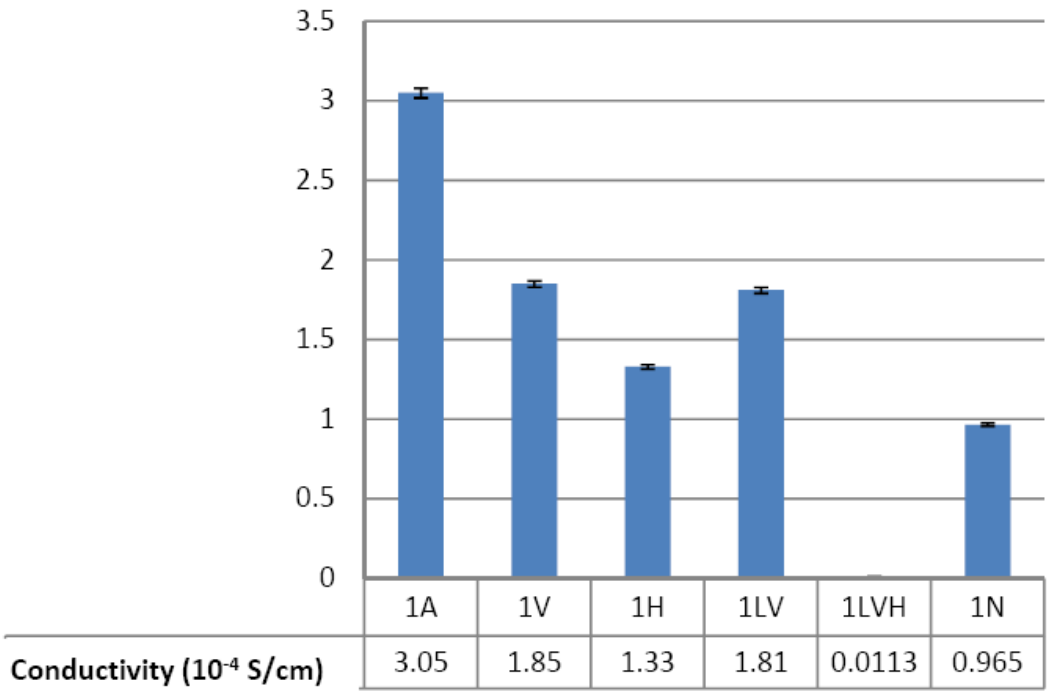

Figure **4-3**: Ionic conductivity results for sample 1 under different solvent removal conditions. Sample 1V: solvent removed under reduced pressure for 1 hour. Sample 1LV: solvent removed under reduced pressure for 16 hours. Sample 1LVH: solvent removed under reduced pressure and heating for 16 hours. Sample 1N: solvent removed under reduced pressure and heating before application of I_2. All data points are the average of at least 6 runs with standard deviation around 1%. Error bar for sample 1LVH is too small

to show on graph.

4.3.2. Electrolyte infiltration and post-assembly heat treatment of cells

Because MEEP is a low T_g thermoplastic polymer, the electrolyte infiltration into the nanoporous electrode would be expected to increase with temperature. In the above example, this effect is not conclusive due to the more overwhelming effect of composition change. If our assumption is correct that: 1) the large molecular size of polymeric electrolytes leads to low pore infiltration and thus poor dye-electrolyte interface, and 2) for a thermoplastic polymer, an increase in temperature leads to better pore filling, then the efficiency of a polymer electrolyte cell should increase with thermal treatment if no other variables come into play.

The experimental investigation of this prospect was based on the electrochemical behavior of electrodes in two separate sets of experiments. The first set, focused on the limited infiltration ability of the polymer components. It involves TiO_2 nanosphere electrodes of different thickness assembled with the same polymer electrolyte using the same procedure. The results are shown in **Figure 4-4.** It can be seen in this case that there was no significant difference or trend among the samples, which supports the assumption that a poor electrolyte – dye interface is most likely the cause of reduced cell efficiency: As other conditions were held constant, the similar efficiencies points to similar effective

areas of photocurrent generation on the TiO_2 surface where the electrolytes are in contact with the dye to provide electrons.

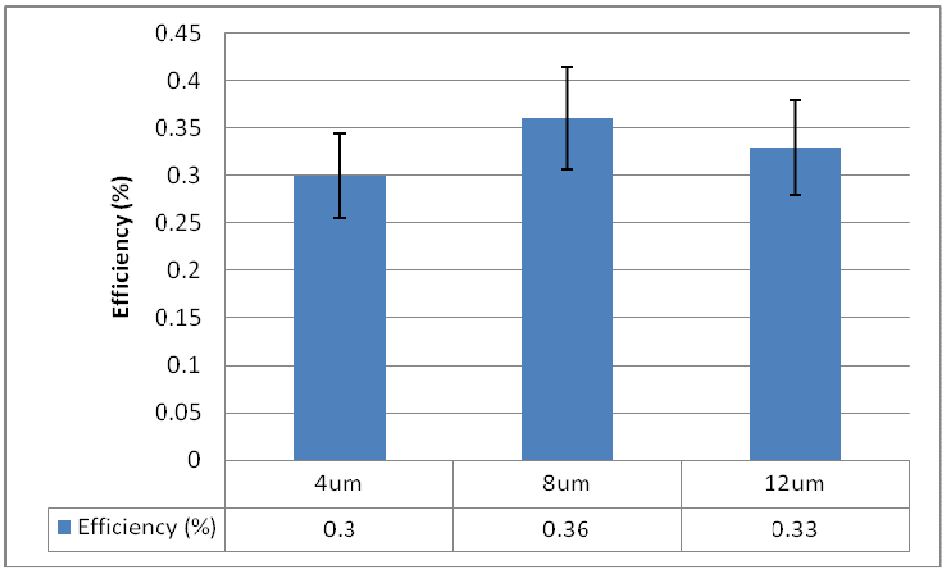

Figure **4-4**: Efficiency results using nanosphere TiO_2 electrodes of different thickness. All data reported here are averages of 6 experiments or more.

The second set of experiments involved the post-assembly heating of the cell, where the cell was assembled and tested for efficiency under normal conditions consistent with the samples mentioned above. The assembled cells were then heated for one hour, allowed to return to room temperature, and tested for photocurrent generation efficiency again. This experimental design was intended to eliminate heat-induced changes in electrolyte composition as well as to observe the thermal stability of the

overall cell assembly. The preliminary efficiency results for various samples are shown in **Figure 4-5**. The baseline sample we used in this case is the linear polymeric MEEP sample **3** (see **figure 4-5** caption for details) where the PMII ionic liquid was used as the iodide source to increase ionic mobility and induce solvent-less mixing. This is compared with an electrolyte sample composed of low molecular weight (5 repeating units) linear MEEP oligomer which is a fluid under room temperature. The small-molecule high-viscosity liquid analog, MEE trimer, was also used as a comparison, the ionic conductivity of which was experimentally determined to be 9.53×10^{-5} S/cm. As shown in this experiment, the efficiency of all the cells tested showed a visible increase after one hour of heat treatment, which supports the assumption of heat-induced increase in electrolyte infiltration. This result is particularly interesting for the MEE trimer system, as the liquid small molecule was anticipated to show better pore infiltration compared to large polymers. In addition, the liquid MEE trimer was able to dissolve iodide salts as well as solid iodine without the assistance of solvents, which eliminated the interference of organic solvents in both ion mobility and electrolyte infiltration. The cells also showed no visible failure after heat treatment, which implies that any volatile components remaining in the cell assembly did not generate sufficient vapor pressure to cause physical damage or leaks in the cell.

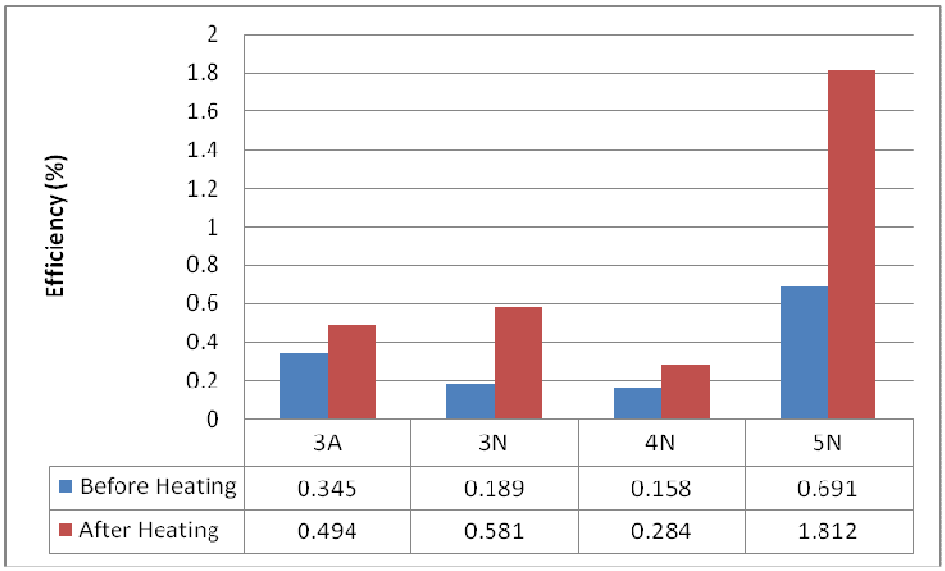

Figure **4-5**: Preliminary cell efficiency results for electrolytes before and after post-assembly heating. The composition of sample 3 is 30:3:100:10 PMII:I_2:MEEP:tBuPy. Samples 4 and 5 are low molecular weight linear MEEP and MEE trimer, respectively, with the ratio of other components the same as sample 1. Sample labeled as "A" solvents were removed under atmospheric conditions before assembly, while samples labeled as "N" did not use any solvents during formulation and were instead force-mixed through mechanical stirring. All data points shown here are averages for 2 experiments and thus the error bars are not included.

4.3.3. Cross-section SEM of electrode – electrolyte assemblies

Another way to investigate the infiltration of polymeric species is through microscopic images of the electrode cross-section after assembly with the electrolyte component. This method has been used in the past to detect the infiltration capacities of solid small molecule hole-conducting species in dye solar cells. The results showed that such methods are effective for visualizing the partial pore-filling effects [**32]**. In our case modification of the method was necessary due to specific challenges for our system: For

liquid systems the cross section method was obviously inappropriate because of their fluid nature, but even for elastic solid polymers the act of cross-section fracture inevitably leads to elongation of the polymer layer and the formation of “overhangs” that interfere with observation. As such, the MEEP samples in this experiment after introduction to the electrode surface were first strengthened through radiation crosslinking, and then cross-sections were obtained using freeze-fracture at liquid nitrogen temperatures.

The results are shown in **Figure 4-6.** By comparing the images, it is apparent that the no-solvent attachment of MEEP as well as solvent-assisted assembly of MEEP at room temperature led to cross sections with a large fraction of open pores, which exemplifies poor electrolyte infiltration. As heat treatment was carried out, areas were observed where the polymeric species infiltrated the nanoporous electrodes and resulted in composite-like filled structures, starting from the direction of polymer application. An increase in the time of heat treatment gradually increased the pore filling percentage, until it reached 100% at 16 hours. This demonstrated the effect of both heat- and solvent-assisted electrolyte infiltration. It also agreed with the cell efficiency study results where an increase in efficiency by post-assembly heating is suspected to be related to improved pore filling of the electrolyte species.

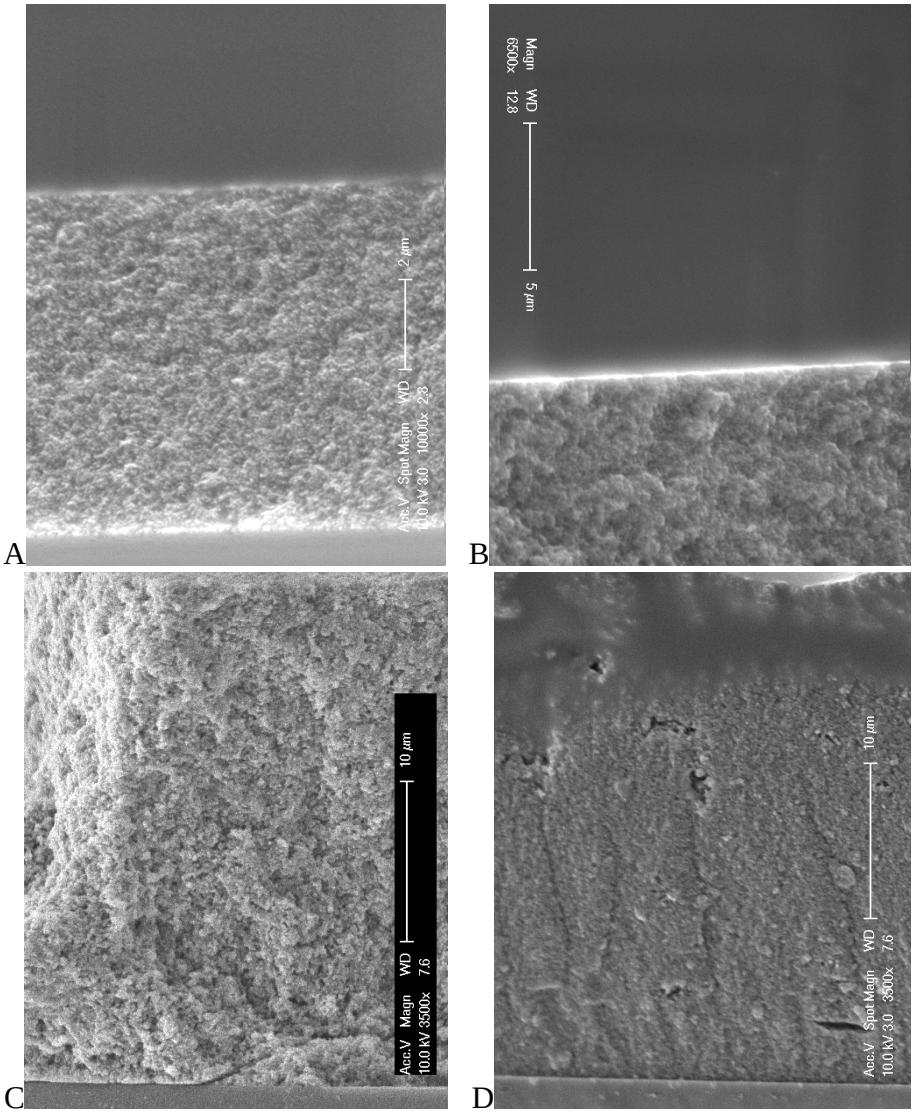
A
Acc.V Spot Magn WD
10.0 kV 3.0 10000x 2.8
2 µm
B
Magn WD
6500x 12.8
5 µm
C
Acc.V Magn WD
10.0 kV 3500x 7.6
10 µm
D
Acc.V Spot Magn WD
10.0 kV 3.0 3500x 7.6
10 µm

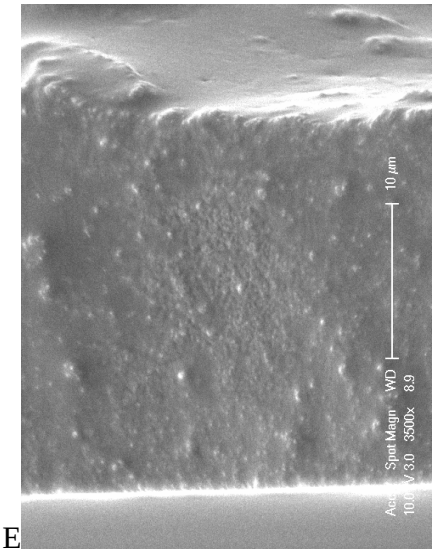

E

Figure **4-6**: Cross-section SEM images of polymer-infiltrated nanoparticle TiO_2 structures. A: Solid polymer applied directly onto the TiO_2 layer. B: Solid polymer melt-cast onto the TiO_2 surface. C: Solution-cast polymer using acetone. D: Combination of solution casting and 1 hour heating. E: Combination of solution casting and 16hr heating.

4.3.4. Effect of column-type electrodes

SEM studies of the type described above have also been applied to the various column-type structures fabricated by oblique angle deposition and thermochemical growth [25,31]. This variation of the e-beam and chemical deposition technique allowed the fabrication of a wide variety of structures ranging from wide stubs to narrow nanowires. Some examples of electrode structures fabricated through this method are shown in **Figure 4-7** a~d. The sets of columns were designed to vary in diameter as well as spacing to confirm their effect on electrolyte infiltration. The cross section SEM after infiltration is shown in **Figure 4-7** e~h. It can be seen from these illustrations that the degree of pore

filling is higher for the columnar structures than for traditional nanoparticle assemblies, even for room temperature assemblies. There is no discernable difference between samples with different column-to-column distances, which may simply be due to the restrictions of current column heights, which is 2um for narrow samples and 5um for wide ones. As the column fabrication procedures improve, we expect to see more pronounced differences in the future.

a 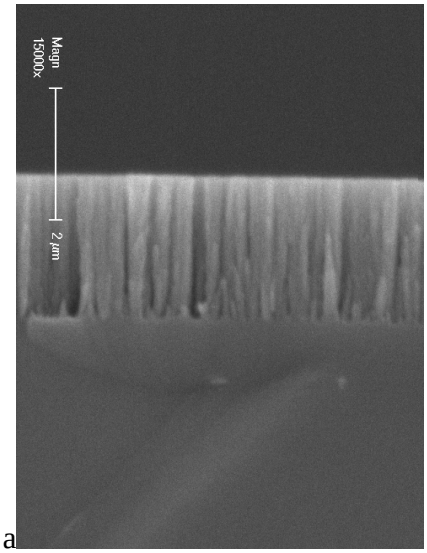

e 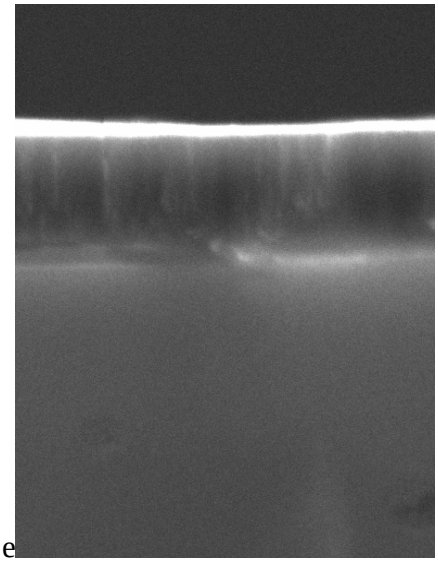

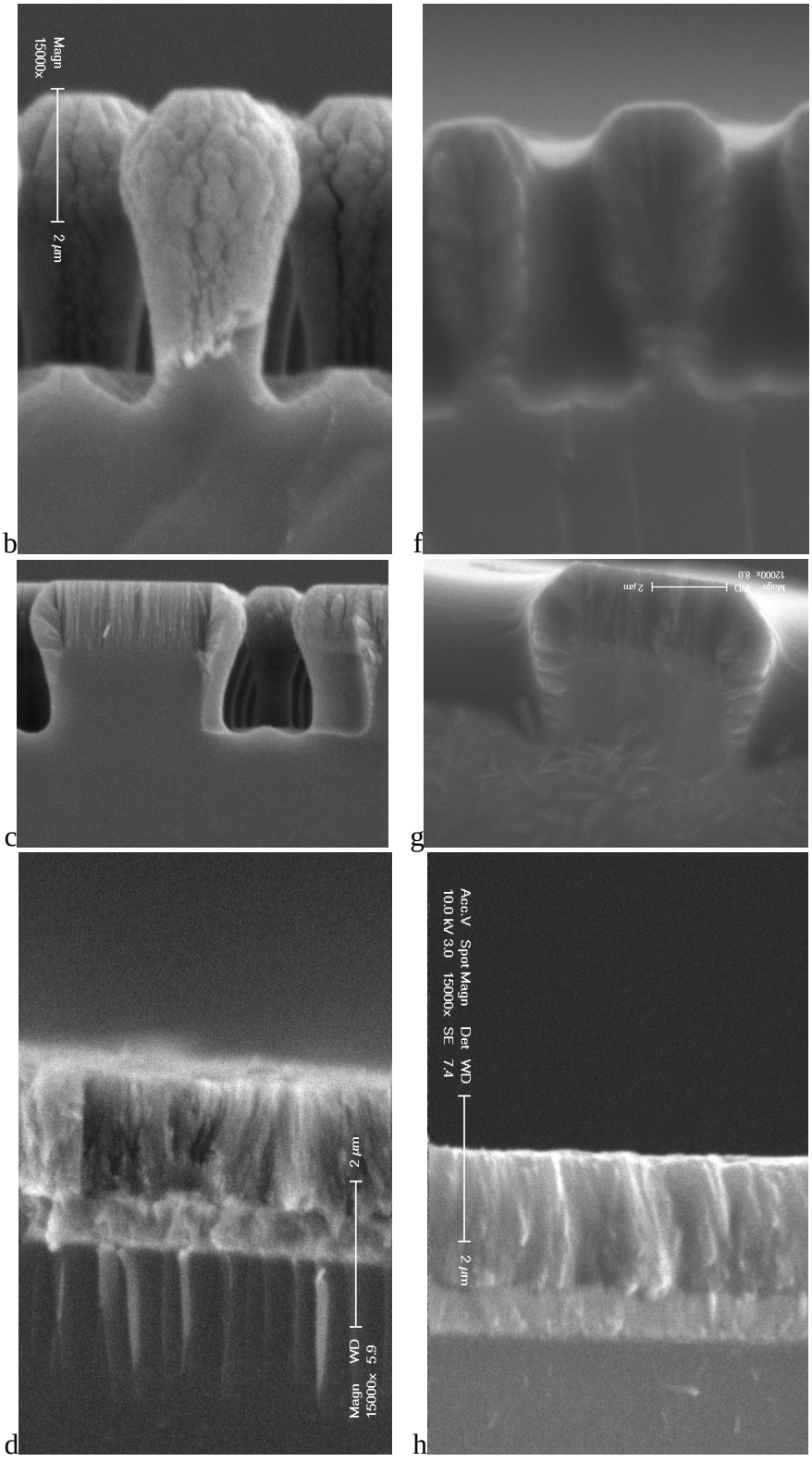
b
Magn
15000x
2 µm
f
c
g
d
Magn WD
15000x 5.9
2 µm
h
Acc.V Spot Magn Det WD
10.0 kV 3.0 15000x SE 7.4
2 µm

Figure **4-7**: Cross section images of various column electrodes before (a~d) and after (e~h) polymer infiltration. Samples are fabricated by Mark W. Horn Group at the Department of Engineering Science and Mechanics using oblique angle deposition **[25]** and Craig Grimes Group at the Department of Electrical Engineering using chemical growth methods **[31]**.

4.3.5. Energy dispersive and back-scattering SEM confirmation of polymer infiltration

While the grayscale pictures using cross-section SEM is a convenient way to estimate the filling percentage of electrolytes in nanoporous substrates, the method may sometimes cause confusion when topographic variations and edge charging interact with electron density of different materials to form complex patterns on the SEM images, as in the case of Figure 4-8 A. As such, a more qualitative analysis method is required to further support our observation for degrees of polymer infiltration.

One useful piece of data is the Energy Dispersive Spectroscopy (EDS), which can function as an elemental analysis method and provide information on the composition of infiltrated species. The result for a typical EDS point-measurement experiment is shown in Figure 4-8 A~C. In this particular case of a polymer-infiltrated column electrode, while the SEM image shows that ther are materials filled between the columns, the grayscale gradient in the image makes it hard to tell if there is indeed full infiltration. By taking EDS measurements at the “top” and “bottom” of the assembly, the analysis showed that the phosphrous signal characteristic of the phosphazene polymer electrolyte was present for both measurements, which indicated full electrolyte infiltration dispite the

visual difference in SEM images in two types of “filling”. EDS methods generally have lower resolution than SEM imaging, but with a line-scan experiment it was still possible to tell the difference between a nanoporous structure fully infiltrated by polymer (Figure 4-9 A) and a structure that shows a more porous, partially infiltrated SEM picture (Figure 4-9 B). The fully infiltrated electrode showed a slow, smooth decline of phosphous signal when the electron beam moved from the polymer-only layer directly above the electrode to the polymer-TiO2 mixture within the electrode and maintained relatively constant throughout the whole electrode. By contrast, in the phosphous signal in a partially infiltrated sample declines rapidly to background noise levels when the electron beam reaches the area shown as being more porous in the SEM images. This shows us the visible pore-filling percentage observed in cross-section images is indeed a good indication of the actual degree of polymer infiltration.

Yet another method of confirming polymer infiltration is the Back-Scatter Electron (BSE) detection SEM, which is more sensitive to differences in the atomic numbers for each element and can thus show more component information. A typical result is shown in Figure 4-8 D, where the polymer composed of lighter atoms are shown in a darker shade to be evenly distributed between the columns, which backscatters more due to the heavier composition atoms. The infiltrated areas in back-scattering results are generally less visible in print due to the weak signal from the polymers, but again they agree with normal SEM images in that it shows evidence of polymer-infiltrated areas at the same spots but with less interference by geometry.

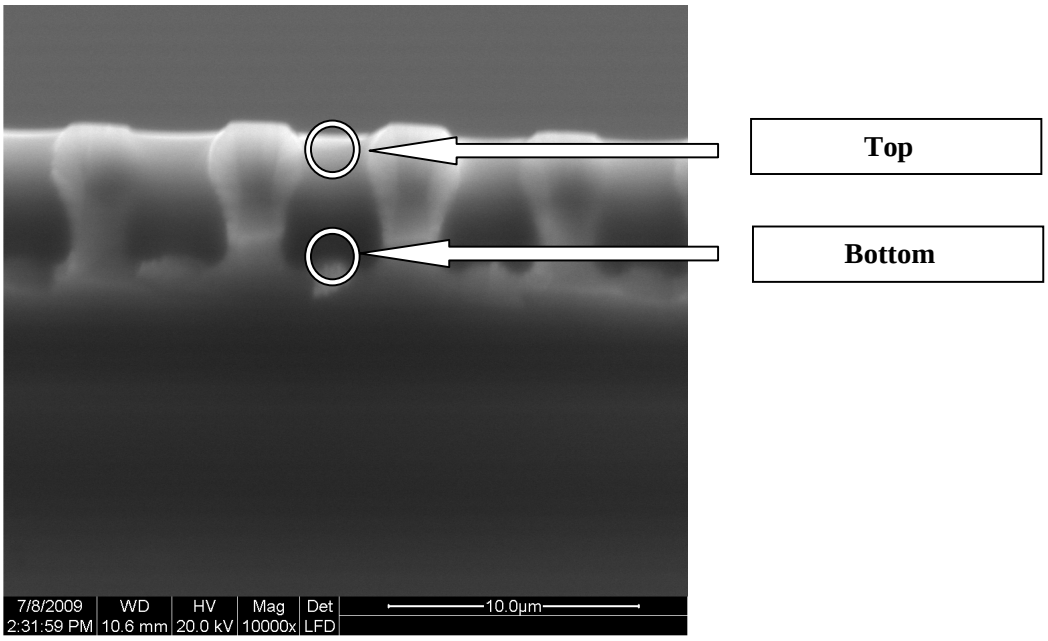

A (Original SEM)

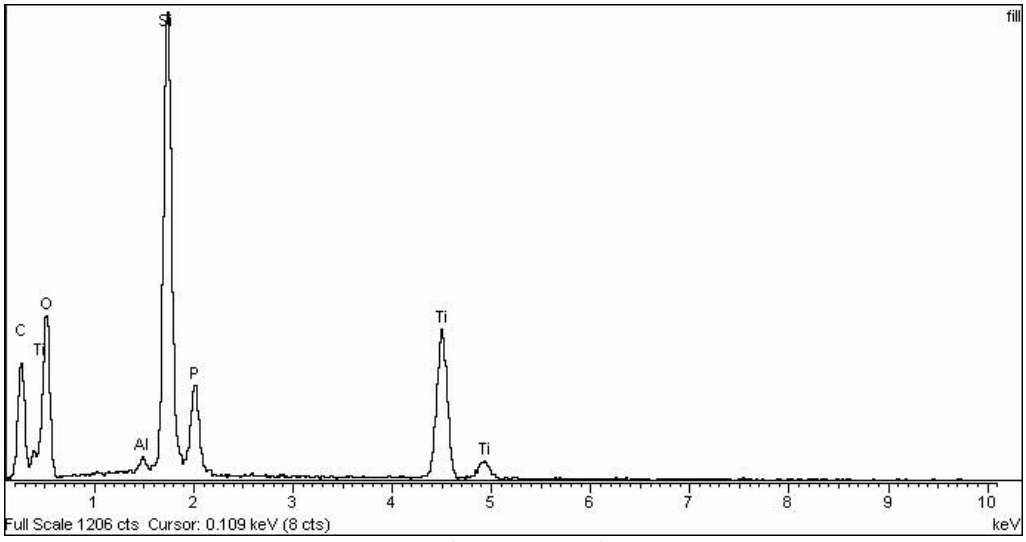

B ("Top" EDS)

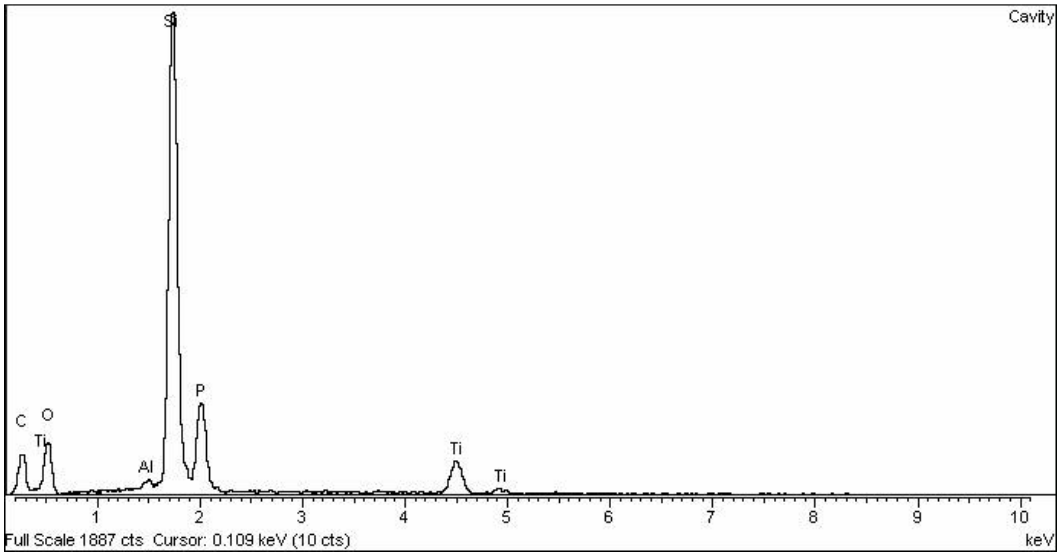

C ("Bottom" EDS)

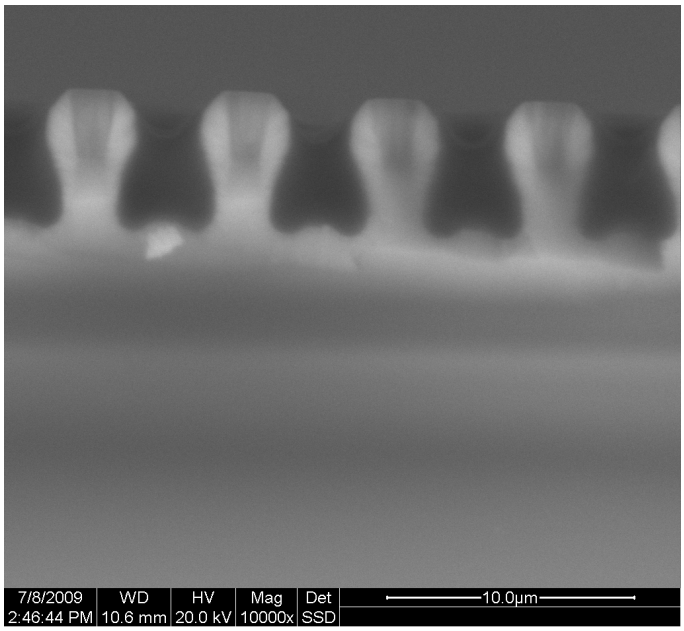

D (BSE image)

Figure **4-8**: EDS and BSE SEM analysis of cross-section column electrode –polymer electrolyte assembly. A: Basic cross-section SEM image of assembly. B: EDS result from top of assembly. C: EDS result from bottom of assembly. D: BSE image of assembly. Note the constant phosphrous signal in both EDS compared to a change in Ti signal due to the change in column width at different points, as well as the "evenly filled" picture in the BSE image as opposed to the color gradient likely caused by charging in the original image A.

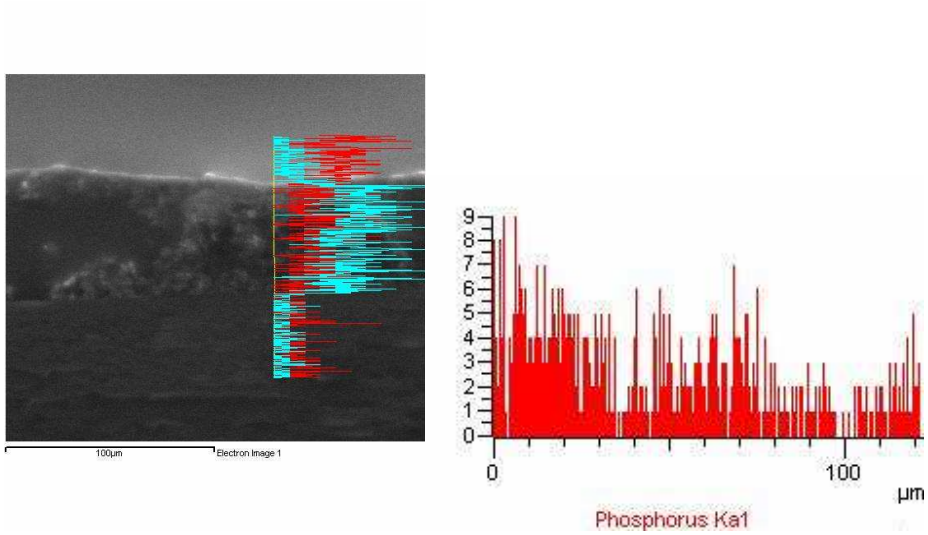

A ("Fully infiltrated" structure)

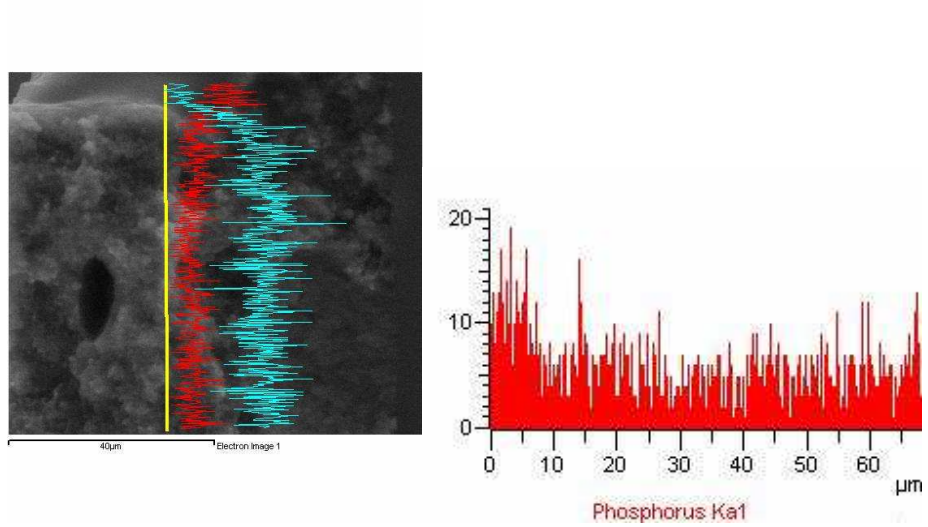

B ("Partially infiltrated" structure)

Figure **4-9**: EDS line scans of polymer-TiO_2 assembly that showed homogeneous "fully infiltrated" SEM image (A) and one that showed porous "partial infiltration" image (B). The red lines in the SEM image as well as in the graphs on the right show the phosporous signal strength which corresponds to the polymer, while the blue lines in the SEM showed Ti signals originated from TiO_2. Note the sharper decline of phosphorous signal in B as opposed to A when the scan crosses from the polymer-only section into the polymer-TiO_2 mixture.

4.3.6. Discussion

The low-Tg thermoplastic polymer electrolyte MEEP holds promise as a candidate for dye solar cell electrolytes. At room temperature, the electrolyte shows a performance similar to those of other polymeric systems, but the performance increases with an increase of I^- and I_2 concentrations to a much larger degree than for liquid electrolyte systems. It can be argued that, with the restricted mass transport within a solid electrolyte system, the increase in the number of charge carriers can compensate for the loss in ionic mobility by direct transfer of electrons between neighboring I^- / I_3^- pairs. Of course, as in traditional polymer electrolyte systems, the increase in ionic nature of the mixture eventually induces sufficient ionic crosslinking in the system to the point where the low ion mobility again becomes the dominating factor.

The strong solvent retention characteristic of the polymer electrolyte system explains our preliminary observation of “deep wetting”: A rough qualitative observation can be made by visually inspecting the conductive glass side of the TiO_2 electrode, as the “bottom” of the TiO_2 assembly that is hardest for the electrolyte to infiltrate. It is also closest to the transparent substrate on which it is fabricated, and is thus visible through the glass. In cells using liquid electrolytes, this visible “bottom” had very different visual characteristics before and after full infiltration of the electrolyte, partially due to the difference of refractive index between air and electrolyte, and partially due to the color of

the electrolyte. When polymer electrolytes were used in this study this change could still be observed, which seemed to contradict the SEM pictures. In cross section microscopy the results clearly showed that under such conditions the polymer could not have achieved full infiltration. The observed “deep wetting” results can be explained by the residual solvent in the assembled cell: In such a polymeric film system, the drying at the air-solution interface can form a protective layer that hinders the evaporation of solvents beneath. In the case of microporous electrodes, the polymer layer can further function as a “cap” on top of the nano-sized channels, through which the liquid components cannot readily evaporate until the structures have been broken open for the cross-section analysis and the liquid part exposed. This essentially led to the existence of a bilayer system in which the electrons pass from a solid electrolyte into a liquid electrolyte before reaching the dye. The advantage of this structure would be that it essentially has the bulk mechanical stability of a solid-state system while retaining an average mass transfer rate similar to that of gel-type systems. Also, the thermal stability of such systems is still acceptable as shown by the post-assembly heating experiments, as the amount of volatile components is relatively small. The disadvantage of this however is that the precise quantity of the liquid solvent remaining may be hard to control, as shown in our experiment results.

4.4. CONCLUSION

The actual filling of nanoporous structures by polymer molecules gave the best results when a combination of solvent assistance and heat-melt processing were applied, as shown by both the cross-sectional imaging as well as the post-assembly heat treatment experiments. Although simple heating is insufficient to promote full infiltration, it did seem to play a major role. As with most melt-processing experiments, longer heating times led to higher degrees of infiltration, even though most of the solvents were known to have been removed in the first hour. The characteristics of our high molecular weight thermoplastic polymer are particularly apparent when compared to small-molecule based studies [**32]**. In the case of our polymer electrolytes, the gradual improvement of pore filling develops in a top-down fashion, with the side exposed to the electrolyte solution showing high polymer content, and with the degree of infiltration decreasing deeper into the surface structure. In contrast, a small-molecule study by Gratzel **[32]** showed relatively even, if incomplete, infiltration of the material within the nanoporous structure. This is also believed to be associated with the application of melt-processing, as void spaces and incomplete infiltration are reasonable outcomes for film casting based on solution evaporation.

The disadvantage of the thermal processing is the probability of changes in electrolyte composition, as we have demonstrated through the solvent removal studies. The open-air heat treatment during solvent removal compared to the sealed environment of post-assembly treatment suggests that component loss occurs rather than thermal -

chemical side reactions. This is supported by the fact that no differences in NMR spectra have been detected for pre- and post- heat treatment samples other than the loss of solvent. In addition, the loss of solvents may not be the only factor. Specifically, the volatility of iodine is a concern, the impact of which we demonstrated through comparing the application of iodine before and after solvent removal. Interestingly, in a closed system such as an assembled cell the volatile iodine did not result in vapor pressure buildup sufficient to cause damage to the cell or otherwise result in unwanted side reactions as many were concerned for these systems.

Titanium dioxide column structures showed promise for allowing improved polymer infiltration into the electrodes, even under room temperature conditions. Although the 2*u*m-limit for our current fabrication methods does not allow for a full comparison with the thickness of nanosphere structures that are generally above 10 microns high, it does give a qualitative view of its effect on infiltration. From the present results, it can be seen that, even when the spacing between columns is similar to the pore size in nanoparticle structures, an improvement in performance was still detected. As we have proposed, one of the main reasons could be that the straight-line opening provided by the void between columns can provide a shorter pathway for the polymer to penetrate deep into the electrode. It also possibly contributes to the improvement because the columns generate open channels as opposed to restricted pores with limited openings. This eliminates the possibility that infiltration is hindered by trapped solvent and vapor in dead-end nanopores, while allowing multiple directions for the polymer flow. With taller

columns it may be possible to achieve larger differences between solvent removal methods and structure variations.

4.5. FINAL COMMENTS

We have described here a study of polymer electrolyte infiltration into electrode surfaces in dye solar cell systems. The feasibility of MEEP phosphazene polymer as a solar cell component has been proved, with efficiency numbers similar to those of other polymer electrolytes and with similar mass transport abilities. The infiltration and thus the dye-electrolyte interface of the thermoplastic polymer system in nanoporous structures showed an improvement by application of thermal-melt procedure through SEM and cell efficiency studies. Possible thermal instability issues have also been considered, with evidence pointing toward solvent retention and iodine loss in an open system. Preliminary results using columnar electrodes show promise for overcoming the difficulties stated above, although further development of the electrode fabrication methods will be necessary. Further studies regarding electrolyte design and cell assembly procedures are needed, which can potentially lead to practical and robust dye solar cells.

4.6. ACKNOWLEDGMENT

We thank the DOE Golden office for funding support. David Lee and Andrew Hess assisted with helpful discussions.

4.7. REFERENCES

1. Fahrenbruch, A. L.; Bube, R. H. *Fundamentals of solar cells.* Academic Press, New York, NY, **1983,** 576

2. Kazmerski, L. L. *Renewable and Sustainable Energy Reviews* **1997,** *1(1-2),* 71-170

3. Lin, G.H.; Carlson D.E. *International Journal of Hydrogen Energy* **2000,** *25,* 807-811

4. Palz, W.; Zibetta, H. *International Journal of Solar Energy,* **1991,** *10,* 11–216.

5. McConnell, R. D. *Renewable and Sustainable Energy Reviews* **2002,** *6(3),* 271-293

6. Gartner, J. *Wired News,* **2005,** March 28

7. Carlson, D. E.; Wronski, C. R. *Applied Physics Letters* **1976,** *28(11),* 671-673

8. Bergmann, R.B. *Applied physics. A, Materials science & processing* **1999,** *69 (2),* 187

9. Chamberlain, G. A. *Solar Cells,* **1983,** *8,* 47-83.

10. Huynh, W. U.; Dittmer, J. J.; Alivisatos, A. P. *Science* **2002,** *295(5564)* 2425 – 2427

11. Gratzel, M. *Journal of Photochemistry and Photobiology C: Photochemistry Reviews* **2003,** *4*, 145–153.

12. O'Regan, B.; Gratzel, M. *Nature* **1991,** *353*, 737

13. Durrant, J. R.; Haque, S. A. *Nature Materials* **2003,** *2*, 362-363

14. Baumann, A.; Bhargava, Y.; Liu, Z.X.; Nemet, G.; Wilcox, J. *MSE/C226,* **2004,** December 6

15. Smestad, G. *Solar Energy Materials and Solar Cells*, **1994,** *32*, 259-273

16. Nogueira, A. F.; Durrant, J. R.; De Paoli, M. A. *Advanced Materials* **2001,** *13(11),* 826 – 830

17. Wang, P.; Zakeeruddin, S. M.; Moser, J. E.; Nazeeruddin, M. K.; Sekiguchi, T.; Gratzel, M. *Nat. Mater.* **2003,** *2*, 402-498.

18. Kubo, W.; Kambe, S.; Nakade, S.; Kitamura, T.; Hanabusa, K.; Wada, Y.; Yanagida, S. *J. Phys. Chem. B* **2003,** *107*, 4374-4381

19. Kim, J. H.; Kang, M. S.; Kim, Y. J.; Won, J.; Park, N. G.; Kang, Y.S. *Chem. Commun.* **2004,** 1662-1663

20. Yang, H.; Yu, C.; Song, Q.; Xia, Y.; Li, F.; Chen, Z.; Li, X,; Yi, T.; Huang C. *Chem. Mater.* **2006,** *18(22),* 5173 - 5177;

21. Blonsky, P. M.; Shriver, D. F.; Austin, P.; Allcock, H. R. *J. Am. Chem. Soc.*, **1984**, *106*(22), 6854-6855.

22. Allcock, H. R.; Austin, P. E.; Neenan, T. X.; Sisko, J. T.; Blonsky, P. M.; Shriver, D. F. *Macromolecules;* **1986**; *19*(6); 1508-1512.

23. Allcock, H. R.; Pucher, S. R.; Tumer, M. L.; Fitzpatrick, R. J. *Macromolecules* **1992,** *25,* 5513-5521

24. Huynh, W. U.; Dittmer, J. J.; Alivisatos, A.P. *Science*, **2002,** *295*, 2425.

25. Horn, M. W.; Pickett, M. D.; Messier R.; Lakhtakia, A. *J. Vac. Sci. Technol. B,* **2004,** *22 (6),* 3426-3430.

26. Fei, S. T.; Allcock H. R. *J. Power Sources 2010,* **195,** 2082-2088

27. Blonsky, P. M.; Shriver, D. F.; Austin, P. E.; Allcock, H. R. *J. Am. Chem. Soc.* **1984,** *106,* 6854

28. Honeyman, C.H.; Manners, I.; Morrissey, C.T.; Allcock, H.R. *J. Am. Chem. Soc.* **1995,** *117,* 7035

29. Paulsdorf, J.; Burjanadze, M.; Hagelschur, K.; Wiemhofer, H.-D. *Solid State Ionics* **2004,** *169,* 25–33

30. Lee, S.-H. A.; Abrams, N. M.; Hoertz, P. G.; Barber, G. D.; Halaoui, L. I.; Mallouk, T. E. *J. Phys. Chem. B* **2008,** *112,* 14415–14421

31. Feng, X.; Shankar, K.; Varghese, O.K.; Paulose, M.; LaTempa T.J.; Grimes, C.A. *NanoLett.,* **2008** *8 (11),* 3781–3786

32. Snaith, H. J.; Humphry-Baker, R.; Chen, P.; Cesar, I.; Zakeeruddin, S. M.; Gratzel, M. *Nanotechnology* **2008,** *19* 424003 (12pp)

Chapter 5

Fuel cells for portable electronic devices: Inorganic–organic hybrid polymers with pendent sulfonated cyclic phosphazene side groups as potential proton conductive materials for direct methanol fuel cells

5.1. Introduction

An increasing need exists for energy sources to power more durable and more portable electronic devices. Most existing portable energy technology is based on primary or secondary (rechargeable) batteries. Batteries are a convenient technology, but they are limited by the fact that, once all their energy has been consumed, they must be discarded or recharged. An open electrochemical device, such as a fuel cell, is a practical solution to these problems. Unlike batteries, which have only a limited amount of chemical energy stored at any time, a fuel cell can generate electricity for as long as a fuel is supplied to the system. Extra fuel can also be transported to remote areas where electricity is not available for recharging batteries [1]. Research in fuel cell technology is also important because of its potential to provide clean energy. Several types of fuel cell technology are available [1], but the form that is considered to be the most applicable to portable electronic devices is the proton exchange membrane (PEM) fuel cell, which typically operates at a moderate temperature (below 80 ◦C) and still retains a high power density. This potential to operate close to room temperature is important, since it reduces the need for thermal insulation and initial warm-up. Unlike high-power applications such as stationary or automotive power generation, where high temperature is an acceptable

tradeoff for high efficiency, portable devices such as cell phones or laptop computers require a power source that functions at or even below room temperature.

The fuel utilized by a PEM fuel cell is also a critical consideration. A promising type of fuel cell for portable electronic devices is the *direct methanol fuel cell* (DMFC), which utilizes liquid methanol directly to produce electrical power. Compared to other possible fuels such as hydrogen, methanol is safer to store, handle, and transport. The bulk and mass of a methanol powered device would also be less than one that is powered by hydrogen because methanol does not require rigid containment [2].

One of the most crucial elements of a DMFC assembly is the electrolyte membrane layer across which protons are transported. Criteria for a practical PEM are chemical stability, good electrode adhesion properties and high proton conductivity [3]. In the case of a DMFC, low methanol crossover is also a crucial requirement [4], because methanol crossover results in a loss of efficiency if the fuel can be oxidized directly at the cathode without producing electrical power. Hence, there is a need to develop a membrane material that can deliver high proton conductivity combined with low methanol permeability. Because both the proton conduction and methanol permeability are often attributed to membrane microstructures [5,6], one promising approach is to introduce new designs that differ from existing ones at a fundamental molecular chemistry level, thereby changing the microstructure and the way the materials interact with either protons or methanol [7,8]. A number of materials have been developed for this purpose and show some degree of success, such as modified Nafion, polybenzimidazoles, and sulfonated poly(ether ketones) [9–12].On the other hand, most

of these materials are hard to fine-tune chemically for optimal performance, and progress in this field had been restricted for this reason.

As mentioned in the introduction, the polyphosphazenes have received much attention [13–17] in this field due to several unique advantages. These include a high level of functionality per repeating unit, control of chemical properties over a wide range of molecular reactions, and a spectrum of different architectures to allow optimization of physical characteristics. Open chain polyphosphazenes were first investigated as proton conducting membranes in hydrogen fuel cells [17]. However, their possible utility in direct methanol fuel cells became apparent in recent years, even though the resistance to methanol crossover still needs to be improved. Consequently, the focus here is on new polymer electrolyte membranes that can combine the aforementioned advantages of phosphazenes with a higher resistance to methanol permeation and better physical properties than the alternatives. Specifically, methods have been developed for the linkage of pendent cyclic phosphazene side groups to organic polymer backbones [18,19]. One advantage of this design is to combine the chemical reactivity and oxidation/reduction stability of phosphazenes with the physical attributes (flexibility, strength and ease of fabrication) of an organic backbone polymer. This approach can yield a variety of functionalized polymers. An organic polymer system that is described here is based on the polynorbornene skeleton, which is accessible by ring opening metathesis polymerization (ROMP) [19,20]. The organometallic-catalyzed ROMP is a useful synthetic approach in the sense that it gives good control over the molecular weight of the polymer while maintaining a high reaction rate, which leads ultimately to a stable performance of the resulting material and ease of scale-up for industrial

manufacturing. It also allows for a wide range of modifications at the monomer stage, which gives more flexibility in designing the polymer [21,22].

Polynorbornenes with pendent cyclic phosphazene units have already been investigated for use as polymer electrolytes for secondary lithium batteries [23] and lithium sea water batteries [24]. These polymers combine the hydrophobicity of the organic polymer with the chemical tailorability of the phosphazene units. Furthermore, because each repeating unit contains a phosphazene ring with five available bonding sites, higher incorporations of functional groups per repeating unit are possible than with typical linear organic or inorganic macromolecules. Consequently, variants of these polymers should also be viable candidates for PEM applications.

Sulfonation of aryl or aryloxy groups is a common approach in the synthesis of proton conducting materials [25–30] because of the high acidity of the sulfonic acid protons coupled with the low methanol solubility of aryloxy groups. Compared to linear polyphosphazene systems, the highly stable phosphazene ring structure should reduce the possibility of side reactions during sulfonation procedures and should extend the lifetime of the membrane. In addition, the sulfonated functional groups are separated from the polymeric main chain and are clustered on the side extensions, which may lead to different interactions for the purpose of proton and methanol migration. Thus, the combination of the two concepts leads to a polymer with pendent cyclophosphazene units that bear sulfonic acid functional groups and hydrophobic, un-functionalized aryloxy units. This is an appealing possibility for the purpose of making a PEM material with high ionic conductivity and low methanol permeability.

In this study, we first synthesized a norbornene monomer with a pendent cyclic chloro-phosphazene side group **(Figure 5-1)**. The monomer was polymerized using a first generation Grubbs' catalyst, and the chlorine atoms in the pendent cyclic phosphazene units were replaced with *m*-cresoxy groups. The polymer was then treated with SO_3, which preferentially reacts at the aryl rings to form sulfonic acid groups **(Figure 5-2)**. The methyl group on the phenoxy side units was utilized to permit subsequent gamma radiation crosslinking in an attempt to further decrease methanol permeability. The objective was to synthesize a polymer that can preserve a conductive pathway for protons while suppressing excessive methanol crossover at room temperature.

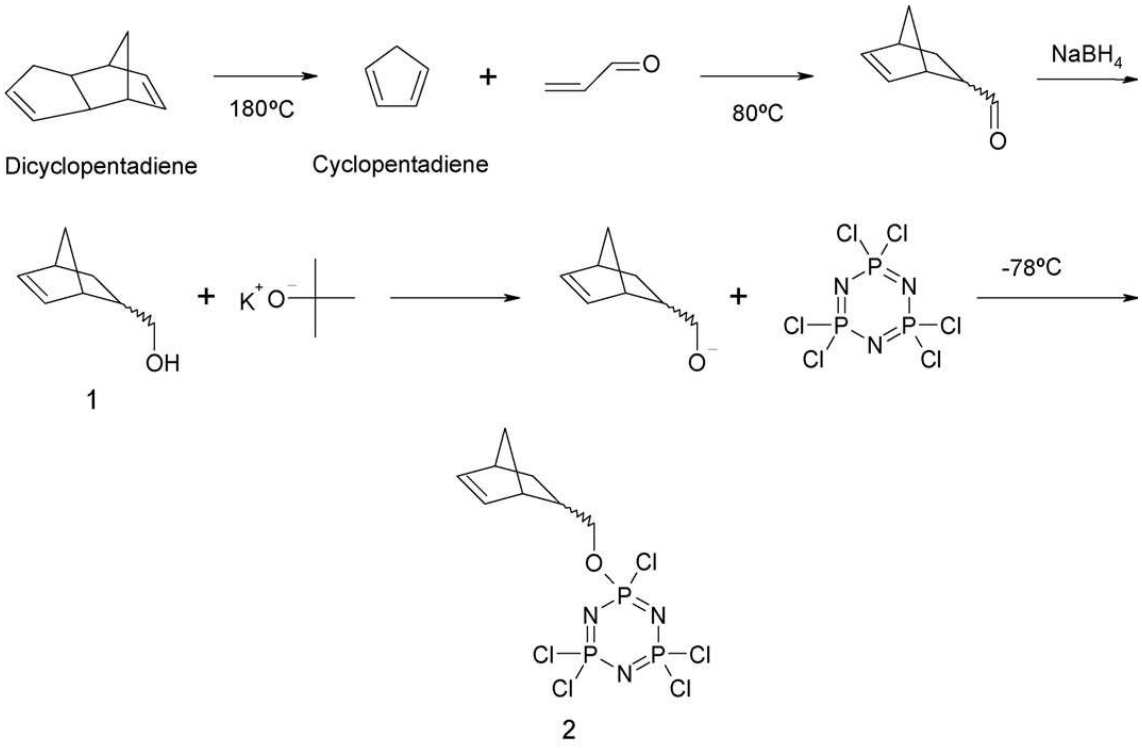

Figure **5-1**: Synthetic scheme for the monomer.

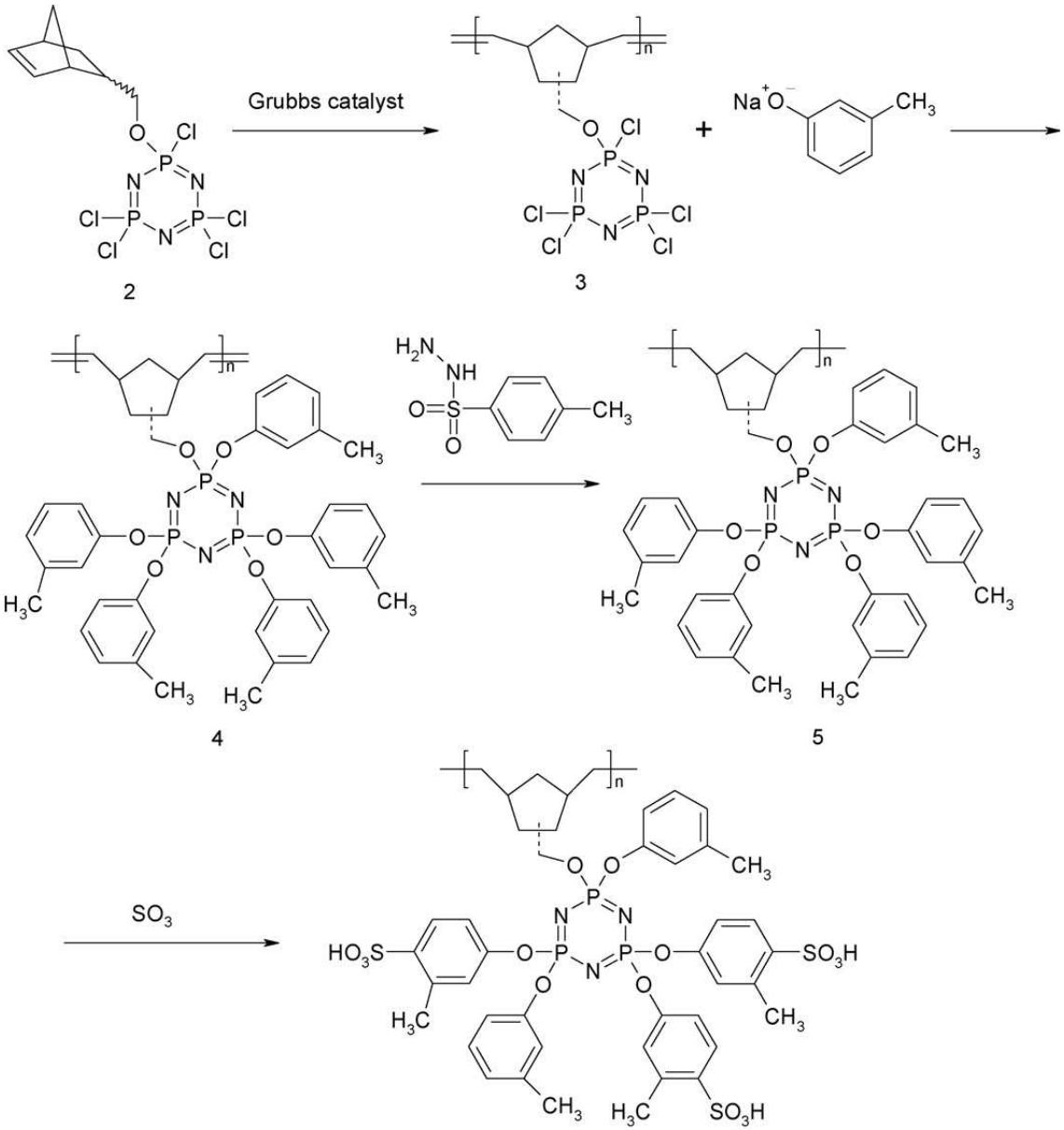

Figure **5-2**: Synthetic scheme for the sulfonated polymer: polymerization, hydrogenation and sulfonation reactions.

5.2. Experimental

5.2.1. Materials

All materials were used as received unless stated otherwise. Sodium (ACS reagent grade), ethyl vinyl ether (99%), bis(tricyclohexylphosphine)benzylidene ruthenium (IV) chloride (97%), *p*-xylene (anhydrous, 99+%), *p*-toluenesulfonhydrazide (97%), 1,2-dichloroethane (99%) and sulfur trioxide (99%) were obtained from Aldrich. Potassium *tert*-butoxide (98%) was obtained from Acros. Hexachlorocyclotriphosphazene was obtained from Fushimi Pharmaceutical Co., Ltd. and was purified by recrystallization twice from heptane followed by sublimation at 30 ◦C at 0.01mmHg. 3-Methylphenol (97%, Aldrich) was distilled over calcium chloride under reduced pressure. Tetrahydrofuran (99.99%, EMD), dichloromethane (99.8%, EMD), and dioxane (99.0%, EMD) were dried by passage through Glass Contour alumina columns before use [31]. Pre-treated Nafion 115 (Dupont) was washed with and soaked in de-ionized water repeatedly for 48 h before being subjected to conductivity, swelling, and methanol crossover tests. De-ionized water with a resistance of 18 Mohms was obtained from a Barnstead Nanopure Diamond water purification system. All synthesis reactions were carried out under an atmosphere of dry nitrogen.

5.2.2. Instrumentation

High field ^{1}H (360 MHz), ^{13}C (90 MHz), and ^{31}P (146MHz) NMR spectra were obtained with a Bruker AMX-360 spectrometer. ^{1}H and ^{13}C NMR peaks were referenced

to external tetramethylsilane. ^{31}P NMR peaks were referenced to external 85% H_3PO_4 with positive shifts recorded downfield from the reference. ^{31}P and ^{13}C spectra were proton decoupled. Molecular weights and polydispersity indices were estimated by use of a Hewlett-Packard 1090 gel permeation chromatograph equipped with Phenomenex Phenolgel 10um linear columns and a HP-1047A refractive index detector. The equipment was calibrated with polystyrene standards. The samples were eluted with 0.1 wt% solution of tetra(*n*-butyl)ammonium nitrate in THF. Glass transition temperatures were obtained with use of a TA Instruments Q10 differential scanning calorimeter (DSC), calibrated with indium, water and cyclohexane standards. Sample dimensions were measured with Mitutoyo Digimatic calipers. Room temperature conductivity was measured using a Hewlett Packard 4192A LF impedance analyzer at a potential of 0.1V and an alternating current frequency range of 5 Hz to 1MHz.

5.2.3. Synthesis of pentachloro-(5-norbornene-2-methoxy)-cyclotriphosphazene (2)

This synthesis and its subsequent polymerization were carried out following a modified published procedure [24]. 5-Norbornene- 2-methanol (**1**) (87.00 g, 0.702 mol) was synthesized according to a previous literature procedure [32], and was dissolved in THF (1.5 L). Potassium *tert*-butoxide (74.62 g, 0.665 mol) was suspended in THF (0.5 L) and was added dropwise to the stirred solution of **1** and allowed to react overnight at room temperature. Hexachlorocyclotriphosphazene (347.00 g, 0.998mol) was dissolved in THF (2 L). Both mixtures were cooled in a dry-ice/acetone bath and the norbornene salt was cannulated into the cyclotriphosphazene solution in a slow, dropwise fashion.

When the addition was complete, the reaction vessel was allowed to warm to room temperature and was stirred overnight. The solution was concentrated by vacuum to yield a brown liquid which was dissolved in diethyl ether and washed with water (3× 700mL). The organic layers were combined, dried over anhydrous $MgSO_4$ and concentrated. The resultant brown oil was placed in a vacuum sublimator. Residual ether was removed in vacuum at room temperature. Excess hexachlorocyclotriphosphazene was removed by sublimation at 40 ◦C at 0.01mmHg for 5 days. Mono-substitution was confirmed by following the process by ^{31}P NMR spectra during and after the reaction. Yield = 259.79 g (68%). ^{31}P NMR ($CDCl_3$) δ (ppm): 22.75 (d, –PCl_2, 2P), 14.90 (t, –PCl(*exo*-ONb), 0.3P), 14.61 (t, –PCl(*endo*-ONb), 0.7P). ^{1}H NMR (CDCl3) δ (ppm): 6.20 (q, 5-H, endo, 0.7H), 6.11 (m, 5-H, exo, 0.3H), 6.11 (m, 6-H, exo, 0.3H), 6.01 (q, 6-H, endo, 0.7H), 4.26 (m, –CH_2O–, exo, 0.3H), 4.08 (dd, –CH_2O–, exo, 0.3H), 3.97 (m, –CH_2O–, endo, 0.7H), 3.77 (dd, –CH_2O–, endo, 0.7H), 2.99 (s, 1-H, endo, 0.7H), 2.86 (s, 4-H, endo, 0.7H), 2.82 (s, 4-H, exo, 0.3H), 2.53 (m, 2-H, endo, 0.7H), 1.89 (m, 3-H, endo, 0.7H), 1.89 (m, 2- H, exo, 0.3H), 1.50 (m, 7-H, endo, 0.3H), 1.40 (m, 1-H, exo, 0.3H), 1.31 (t, 7-H, exo, 0.3H), 1.30 (t, 3-H, exo, 0.3H), 1.20 (m, 3-H, exo, 0.3H), 0.53 (m, 3-H, endo, 0.7H). ^{13}C NMR ($CDCl_3$) δ (ppm): 138.03 (5-C, endo), 137.13 (5-C, exo), 136.00 (6-C, exo), 131.92 (6-C, endo), 73.36 (–CH_2O–, exo), 72.82 (–CH_2O–, endo), 49.32 (7-C, exo + endo), 44.82 (1-C, exo), 43.59 (4-C, endo), 43.26 (4-C, exo), 42.23 (1-C, endo), 41.58 (2-C, exo), 38.76 (2-C, endo), 29.21 (3-C, exo), 28.56 (3-C, endo).

5.2.4. Synthesis of poly[pentachloro-(5-norbornene-2-methoxy)-cyclotriphosphazene] (3)

The monomer to initiator ratio was ~190:1 for all reactions to ensure consistency for each batch. Monomer 2 (21.11 g, 0.0485mol) was degassed under reduced pressure. The monomer was then dissolved in CH_2Cl_2 (200mL). Grubbs' first generation catalyst (0.20 g, 0.243 mmol) was suspended in CH_2Cl_2 (2 mL) and added rapidly to the stirred monomer solution. The polymerization was terminated after 10 s by the addition of 1mL ethyl vinyl ether. The polymer solution was diluted with 500mL THF and was used without further purification.

5.2.5. Synthesis of poly[penta(3-methylphenoxy)-(5-norbornene-2-methoxy)-cyclotriphosphazene] (4)

Sodium metal (5.69 g, 0.247 mol) was suspended in THF (200mL). *m*-Cresol (27.79 g, 0.257mol) was added slowly and was allowed to react overnight. After the reaction was complete, as indicated by the consumption of the sodium metal, the *m*-cresol salt solution was cannulated into the previously prepared polymer **3** solution. The reaction mixture was then refluxed for 5 days.

The resultant solution was concentrated by rotary evaporation and precipitated twice into methanol and twice into hexanes. The product polymer was an adhesive, brown material which was dried in a round bottom flask in preparation for the subsequent reaction. Yield = 31.32 g (81%) from 21.11 g of monomer **2**. 31P NMR ($CDCl_3$) δ ppm: 12.3 (t (endo–exo overlap), $P(OC_6H_4CH_3)(O–CH_2–Nb)$, 1P), 8.8 (d, $P(OC_6H_4CH_3)2$, 2P (86%)), 7.7 (d, $P(OC_6H_4CH_3)2$, 2P (14%)) 1H NMR ($CDCl_3$) δ ppm: 6.8 (m, Ar*H*, 20H),

5.25ppm (s, br, C*H* C*H*, 2H), 3.5 (d, OCH_2, 2H), 2.2 (s, ArCH_3, 15H), 1.65 (m, cyclopentane ring, 7H).

5.2.6. Hydrogenation of the polymer backbone to poly[penta(3-methylphenoxy)-(5-norbornene-2-methoxy)-cyclotriphosphazene] (5)

p-Xylene was added to the round bottom flask containing the purified polymer **4** (31.31 g, 0.0394mol), and stirring was maintained overnight to dissolve the polymer. A large excess of *p*-toluenesulfonhydrazide (73.37 g, 0.394mol) was added to the polymer solution and the solution was refluxed for 3 h. The solution was then concentrated by evaporation and the product was precipitated into methanol. This polymer was redissolved in THF and precipitated into methanol twice. The polymer obtained was dried under vacuum to yield an adhesive off-white material. A molecular weight of 190 kDa and a PDI of 2.6 were estimated for the polymer. The T_g of the polymer was found to be 2 ◦C by DSC. Yield = 21.84 g (69%). 1H NMR ($CDCl_3$) δ ppm: 6.8 (m, Ar*H*, 20H), 3.5 (d, OCH_2, 2H), 2.2 (s, ArCH_3, 15H), 1.65 (m, cyclopentane ring and –CH_2CH_2– overlap, 11H).

5.2.7. Sulfonation procedure (6A–6E)

Polymer **5** (19.81 g, 0.0249 mol) was dissolved in dichloroethane and was cooled in an ice bath. Aliquots of a 1M SO_3 solution in dichloroethane were added to the polymer solution slowly according to the desired degree of sulfonation. The reaction was allowed to proceed for 3 h and was quenched by the addition of 50mL saturated NaOH

solution in 1:1 water and ethanol mixture. At this point, the polymer had precipitated from the solution as a dark brown solid. The solution was evaporated to dryness under reduced pressure and the polymer was soaked for 24 h in successive cycles in de-ionized water, 0.1M aqueous NaOH, de-ionized water, 0.1M aqueous HCl and de-ionized water. Finally, water was removed from the polymer in a vacuum oven at 0.1mmHg and 40 ◦C.

5.2.8. Film casting and radiation crosslinking (7A–7E, 8)

Dried polymer **6** (5.00 g) was dissolved in 100mL of *N*,*N*-dimethylacetamide. Six 10cm×10cm membranes were cast from this solution on polypropylene plates. The membranes were dried under vacuum at 24 ◦C for 48 h and at 80 ◦C for 24 h. The membranes obtained were brown, flexible, and had an average thickness of 210um. The membranes were then crosslinked by exposure to 20MRad (Sample **7A**–**7E**) or 40MRad (Sample **8**) gamma irradiation from a ^{60}Co source at the Pennsylvania State University Breazeale Nuclear Reactor facility.

5.2.9. Determination of IEC values

The neutral condition ionic exchange capacity (IEC) titration experiment was selected as the evaluation method for the equivalent amount of active acid groups introduced [33]. This is based on the fact that the number of protons available for actual ionic exchange is a better indication of the number of free protons that would dissociate and contribute to actual conductivity than the results from other experimental methods

such as NMR. The protons from the acidic group in the polymer were exchanged with Na^+ ions by soaking a 0.10 g sample of the polymer in 50 mL of a 2M NaCl solution for 48 h with occasional shaking. Aliquots of the solution (10 mL) were titrated with 0.01MNaOH to calculate the amount of protons released by the polymer. The IEC value is reported as moles of protons per gram of polymer.

5.2.10. Determination of water and methanol swelling

The polymers were soaked in de-ionized water for 24 h at 24 ◦C, after which time the polymers were removed from water and excess liquid on the surface was removed by gently pressing the polymer between two halves of a filter paper. The degree of swelling is defined as the following **Equation 5-1**:

$$\text{water swelling}\,(\%) = \left[\frac{\omega_{\text{wet}} - \omega_{\text{dry}}}{\omega_{\text{dry}}}\right] \times 100 \qquad \textbf{(Equation 5-1)}$$

ω_{wet} and ω_{dry} are the weights of wet and dry polymer, respectively.

Methanol swelling experiments were carried out in a similar manner, except that either pure methanol or a 10%(v/v) methanol aqueous solution was used instead of water.

5.2.11. Determination of methanol permeability

Methanol permeability was measured through a modified published method [34,35]. The apparatus used is shown in **Figure 5-3**. A film of the polymer was sandwiched between the two halves of the apparatus and was sealed tightly to prevent

leaks. One chamber of the apparatus was filled with a 10% solution of methanol in water; the other with de-ionized water. After 24 h at room temperature, the methanol content of the de-ionized water was evaluated by ^{1}H NMR spectroscopy by comparing the methanol CH_3 peak integration to the OH peak and by calibration via a series of standard solutions. Nafion 115 was used in this experiment as a standard sample, and was evaluated by the same procedures to ensure that the results are comparable.

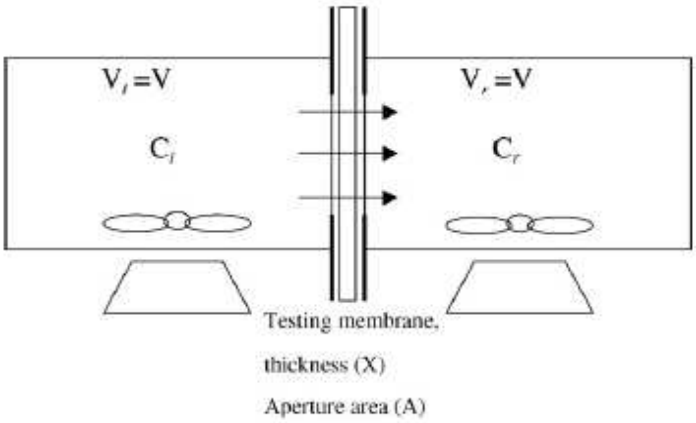

Figure **5-3**: Schematic diagram for methanol permeability measurements.

5.3. Results and discussion

5.3.1. Polymer synthesis

In the synthesis of monomer **2**, a 0.4M excess of hexachlorocyclotriphosphazene and a low reaction temperature were employed to ensure replacement of only one

chlorine atom per hexachlorocyclotriphosphazene ring by the norbornene unit. This was confirmed by ^{31}P NMR spectroscopy. Although the monomer initially had a 0.3:0.7 ratio of exo:endo norbornene, the isomer ratio changed to 0.14:0.86 after polymerization as evidenced by ^{31}P NMR spectra of **4**. It is speculated that one of the isomers is more reactive than the other due to the positioning of the bulky cyclic phosphazene group. Similar observations have been made in the ring opening metathesis polymerizations of other norbornene systems [36,37]. The different reactivity of the isomers can also be used to explain the large polydispersity index in the polymer. The backbone of the polymer was then hydrogenated to suppress crystallinity and to prevent side reactions during the subsequent sulfonation procedure. Hydrogenation was carried out using *p*-toluenesulfonhydrazide following a procedure adapted from Cohen and co-workers [38]. The complete saturation of the backbone was indicated by the disappearance of the alkene peak at 5.25ppm in the 1H NMR spectra from polymer **4** to polymer **5**.

5.3.2. Sulfonation and IEC values

The addition of SO_3 to polymer **5** introduced sulfonic acid groups at the aryl rings. Previous studies have indicated that sulfonation occurs primarily at the *para*-position of the aryl rings [39]. From **Figure 5-4**, it is clear that the IEC values show a linear relationship with the amount of SO_3 added. Hence, this sulfonation procedure allows accurate control of the IEC value. From an extrapolation of the line in **Figure 5-4**, it appears that sulfonation began after 0.383Mequivalents of SO_3 per repeat unit were added. This observation is consistent with the work of Montoneri et al. [40] and Wysick

and Pintauro [41] who explained that SO_3 should coordinate first to the lone pair electrons of the phosphazene nitrogen atoms during sulfonation of aryloxy substituted polyphosphazenes. They reported that sulfonation of the aryl rings did not occur until <50% of the phosphazene nitrogen atoms were complexed with SO_3. Our results deviate from theirs because we estimate that sulfonation of the aryl rings occurs after only 13% of the phosphazene nitrogen atoms have been complexed with SO_3 (3 nitrogen atoms per repeat unit, hence 0.383/3×100 = 13%). Sulfonation of the aryl rings occurred at a lower level of added SO_3, probably because the nitrogen atoms in the rigid cyclic phosphazene trimer ring are less accessible than those in a flexible linear polyphosphazene polymer. A comparison of the materials used during this study is summarized below (**Table 5-1**).

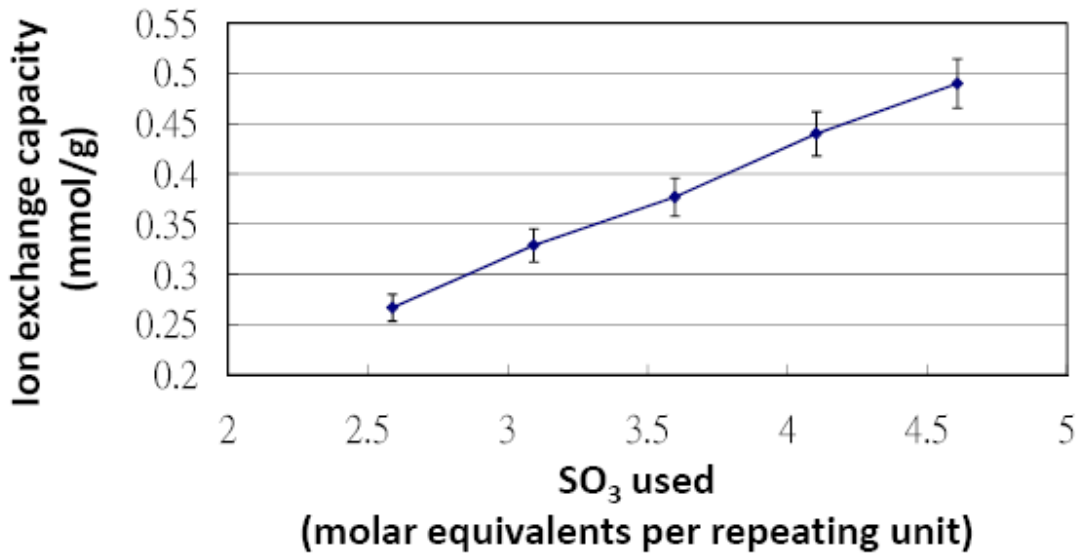

Figure **5-4**: IEC values of the polymer versus the amount of SO_3 used for sulfonation. Data reported are averages of at least 6 samples.

Table **5-1**: Properties of uncrosslinked sulfonated polymers. Samples were made in duplicates of 6 for average results.

Sample	SO_3 used	IEC	Water Swelling
	(mole eq)	(mmol/g)	(%)
6A	2.588	0.27	35.80
6B	3.093	0.33	55.03
6C	3.598	0.38	105.18
6D	4.103	0.44	202.73
6E	4.608	0.49	309.99

5.3.3. Crosslinking and physical property changes

To ensure mechanical stability, restrict water uptake, and lower the methanol crossover of the new membrane materials, ^{60}Co gamma radiation treatment was used in our study to induce free radical crosslinking. The membranes were fabricated according to the above procedures, exposed to radiation, and compared with samples untreated by radiation. The membranes had an average thickness of 170–250um and showed no measurable dimensional change after radiation treatment. The *T*g of the material increased as expected after both the sulfonation and crosslinking treatments. The mechanical strength of the materials improved after crosslinking, especially when in the water-swollen state. Thus, the following studies were conducted on the crosslinked films only. The results of these studies are summarized in **Table 5-2**.

Table **5-2**: Performance data for crosslinked sulfonated polymers. All samples were made in duplicates of 6 for average of results. The methanol crossover results reported here are diffusion coefficient numbers based on static experimental conditions **[35].**

Sample	IEC	Crosslink	Conductivity	Tg
	(mmol/g)	(Mrad)	(10^{-5} S/cm)	(^{o}C)
7A	0.27	20	0.21	5.14
7B	0.33	20	0.27	16.76
7C	0.38	20	1.03	51.15
7D	0.44	20	2.89	57.93
7E	0.49	20	8.26	69.33
8	0.49	40	11.31	68.66
Nafion 115	0.88	0	2600.82	110.03
Sample	Water Swelling	Pure MeOH Swelling	10% MeOH Swelling	MeOH Crossover
	(%)	(%)	(%)	(10^{-9} cm^2/sec)
7A	33.6	53.8	35.0	2.1
7B	49.9	57.3	47.4	2.5
7C	52.3	67.6	65.5	2.9
7D	69.9	75.7	73.0	3.3
7E	84.1	84.2	89.7	5.3
8	75.3	70.3	74.2	2.7

Nafion 115	15.9	61.3	27.7	498.2

5.3.4. Water swelling behavior

The water uptake values of each membrane were determined by comparison of the dry weight to the fully hydrated weight and are reported in **Tables 5-1** and **5-2**. The numbers obtained from different samples were compared as a function of the IEC value of the polymer membrane, as shown in Figure 5-5. The water swelling of the uncrosslinked materials increased exponentially as the IEC increased. This result suggests that the higher concentrations of sulfonic acid groups definitely induced the formation of aqueous clusters. Thus, increased incorporation of sulfonate groups generates higher hydrophilicity and higher IECs. The distance between the organic polymer backbone and the acidic groups may also affect the water uptake, as shown from earlier studies [42]. Although the degree of water swelling is high, this effect can be reduced by further crosslinking of the membrane because enhanced rigidity of the polymer structure should prevent the expansion of water clusters. Our results show the logical outcome of a drastic decrease of water swelling in the membrane with an increased degree of crosslinking. For example, with an IEC of 0.49mmolg^{-1} the swelling was reduced from 310% (**6E**) to 84% (**7E**) after 20Mrad of radiation treatment, which translates to 1:0.27 in water uptake. However, when the highest radiation dosages were

applied (**7E** to **8**) an increase in radiation dosage did not lead to decrease of water uptake. This may be caused by a saturation of the radical crosslinking reactions.

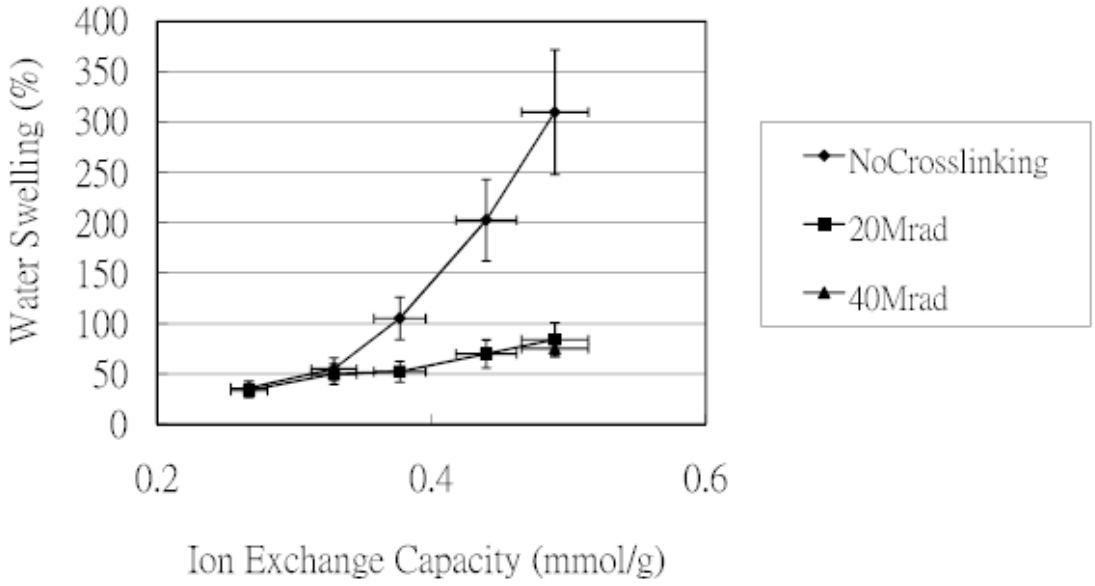

Figure **5-5**: Water swelling versus the IEC value of the uncrosslinked and crosslinked polymer. Error bars are based on average data analysis of at least 6 samples for each data point.

5.3.5. Methanol swelling behavior

Methanol uptake of the samples was determined in a similar way to water uptake, with the weight of membrane fully swelled in pure methanol or in 10% methanol in water, compared with the dry mass. The results are reported in percentages as a function of IEC. As with water uptake, a decrease in methanol uptake was apparent following radiation

crosslinking. An interesting point is that, although the methanol uptake by each sample was slightly higher than the water uptake, the slope for the data points is smaller than for water uptake. And all three values of uptake (water, 10% methanol, pure methanol) became nearly identical as the IEC approached 0.5. This appears to show that the affinity of the material for methanol is higher than that for water, although increases in the degree of sulfonation, and thus the increase in hydrophilicity, gradually cause a decrease in the difference of affinity.

5.3.6. Proton conductivity

The through-plane ionic conductivities of films of the sulfonated polymers were measured by electrochemical impedance spectroscopy. Through-plane conductivity is the most realistic measurement of ionic conductivity in membranes because it corresponds to the proton transmission in an actual fuel cell. The room temperature ionic conductivity data are reported in Table 2.

The ionic conductivities of these polymers at room temperatures were relatively low. This is understandable in terms of the low IECs. The highest measured ionic conductivity was 1.13×10^{-4} Scm^{-1} (polymer **8**), which is approximately two orders of magnitude lower than that of the commercial PEM material Nafion 115. This conductivity, although not a significant breakthrough, is acceptable for small portable devices considering that many other comparable approaches are geared toward operating temperatures much higher than that of our interest [43–45]. We expect the IEC of our materials to improve during future developments. Thus, the polymers described here

remain potentially viable PEM materials, especially for powering small portable devices. For high-temperature applications, further experimental data under different temperature and humidity ranges would be required. In addition, following the trend from polymer **7A** through **7E**, the conductivity increases by nearly one order of magnitude each time the IEC increases by 0.1–0.2 units. An extrapolation of these data suggests that, if the degree of sulfonation can be increased, the conductivity could eventually reach a similar level to that of Nafion when the IEC values of the two materials are equal. It is also interesting to note that the conductivity of polymer **8** increased when the radiation dosage was increased from 20 to 40Mrad. It is suspected that this may be due to radical-induced side reactions, which could potentially induce the formation of additional acidic groups such as POH units. Further discussion of this possibility requires future research focused on radiation effects.

5.3.7. Methanol permeability

The methanol permeability was measured as described above, and was calculated assuming that Fick's first law (steady state diffusion) is applicable **[35]**. This experimental design specifically measures the diffusion coefficient of the membrane under static conditions, which provides a clean test for membrane characteristics. At the same time, it should be noted that the test is different from tests that involved external electric fields where an electrodynamic drag analysis is intended instead **[1, 11]**. The drag experiment is a more realistic approximation of working fuel cell conditions, which will be an interesting direction for future studies. Extreme caution must thus be taken when evaluating

methanol crossover results, as experimental data from two types of experiments cannot be compared side by side.

Fick's law can be simplified to the form shown in **Equation 5-2**, where C_m is the concentration of methanol in the standard solution, C_w is the concentration of methanol in water after diffusion, and x is the thickness of the membrane (see **Figure 5-3**).

$$J_m = -D\frac{dC}{dX} = D\frac{C_m - C_w}{x} \quad \textbf{(Equation 5-2)}$$

Solving this equation with the initial condition of $C_{w(0)} = 0$ this yields **Equation 5-3**, where D is the diffusion coefficient, V is the volume of solution, x is the thickness of the membrane, A is the effective surface area of the membrane, t is the time in minutes, $C_{w(t)}$ is the concentration of methanol in the water after time t, and $C_{m(0)}$ is the concentration of methanol in the standard solution at t=0.

$$C_{w(t)} = \frac{1}{2}C_{m(0)}(1 - e^{-(2ADt/Vx)}) \quad \textbf{(Equation 5-3)}$$

Rearrangement of this equation gives us the diffusion constant D as **Equation 5-4:**

$$D = -\frac{Vx}{2At}\ln\left(1 - \frac{2C_{w(t)}}{C_{m(0)}}\right) \quad \textbf{(Equation 5-4)}$$

In this experimental design, we used 10% methanol in water for the standard methanol solution and performed the experiments at room temperature. The reason for this arrangement is to obtain a close approximation to the actual working conditions in a possible room-temperature methanol fuel cell assembly. The methanol permeability data of polymers **7A**–**8**, as well as the value for Nafion 115 using our method, are reported in **Table 5-2**. The diffusion coefficients of our materials generally follow the trend of the IEC values, as shown in **Figure 5-6**, which is to be expected since it is assumed that the

hydrophilic channels aid methanol diffusion. These data indicate that the methanol permeabilities of these materials are very low—typically two orders of magnitude lower than for Nafion. Finally, the increase in crosslink density brought about by utilizing 40Mrad of gamma radiation reduces the methanol crossover by half, which reflects the enhanced rigidity of the polymer matrix.

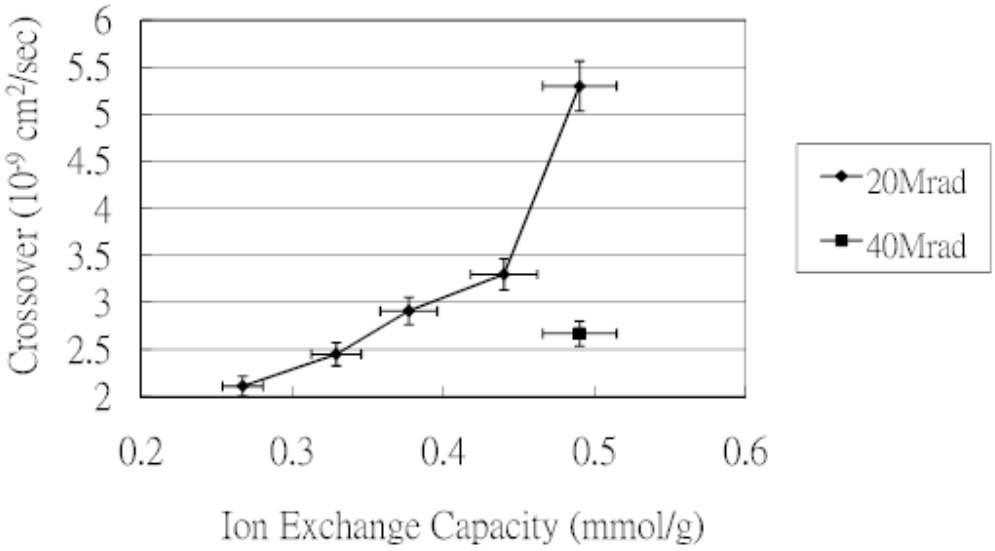

Figure **5-6**: Methanol crossover of membranes relative to the IEC values of the materials. Error bars are based on average data analysis of at least 6 samples for each data point.

5.3.8. Relationship of IEC, swelling, conductivity and permeability

At the same time, the increase in methanol diffusion with increases in conductivity seems to be minor, as shown in **Figure 5-7**. The linear relationship suggests

that the norbornane-phosphazene membrane should still have methanol permeability 10 times less than Nafion at the point where it has the same ionic conductivity.

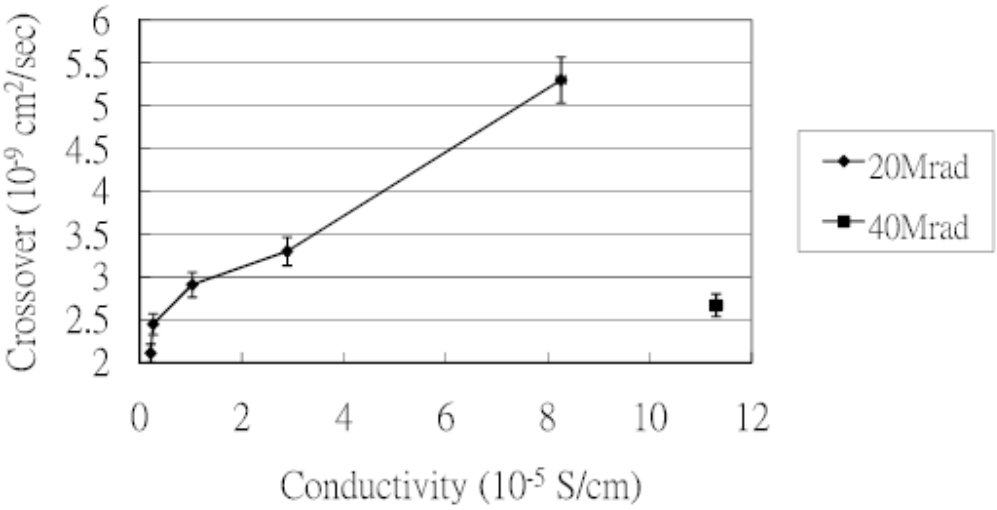

Figure **5-7**: Dependence of methanol crossover on ionic conductivity of the membranes. Error bars are based on average data analysis of at least 6 samples for each data point. Note the standard deviations of ionic conductivity data is too small to show on the figure.

Usually it would be expected that the low methanol crossover, when combined with low ionic conductivity, results from the presence of small amounts of hydrophilic domains that form only small or isolated clusters and thus cannot efficiently transport these water-soluble species. In such a case, there will be no continuous conductive channel in the membrane microstructure for either protons or methanol, and thus the conductivity and crossover will both remain low. However, in our case the assumption of cluster formation cannot fully explain the high water uptake compared with the ionic

conductivity and IEC, because a lack of hydrophilic clusters should lower water affinity [5]. One possibility is the formation of large but isolated hydrophilic clusters in a film structure, since our long spacer groups connecting the sulfonated side groups to the hydrophobic main chain could very well promote enough flexibility to induce large micelle-like isolated structures within the polymer matrix. Nafion, on the other hand, may be generating smaller clusters in greater numbers compared to our material and have a higher chance of forming interconnected channels. It is also possible to contemplate a different mechanism based instead on the chemical structure. Because our results indicate a high degree of hydrophilicity but low ion mobility, it is suspected that sites other than sulfonate groups may contribute to the coordination of cations [46]. These may include the nitrogen atoms on the phosphazene rings. Such immobilized protons, while still within the polymeric structure and causing the material to be more hydrophilic, would not contribute to either our IEC results or the ionic conductivity. If this assumption is correct, it might be expected that higher concentrations of cations would eventually saturate the extra coordination sites and lead to a large increase of ionic conductivity. As shown by **Figure 5-8**, the fact that ionic conductivity increases nonlinearly with the water swelling may be indirect evidence for this effect, although further experiments are required to confirm this assumption as well as an investigation of the actual microstructure of these membranes.

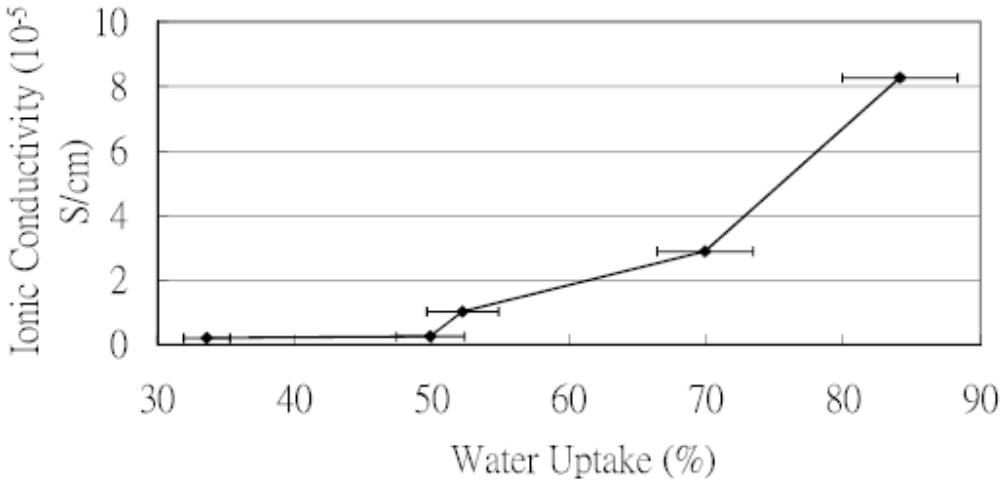

Figure **5-8**: Relationship between ion conductivity and water uptake of 20Mrad crosslinked membranes. Error bars are based on average data analysis of at least 6 samples for each data point. Note the standard deviations of ionic conductivity data is too small to show on the figure.

A similar model can also be used to explain the relatively low methanol crossover values compared to the water and methanol swelling, as shown in **Figure 5-9**. Usually high methanol swelling would indicate high methanol crossover, but in our experiments the samples repeatedly show that the membranes have lower methanol crossover than Nafion under identical experimental conditions, even though Nafion has a lower methanol uptake. Again, it is possible to explain the phenomena through either microstructure or molecular interaction viewpoints: large but isolated hydrophilic clusters are expected to absorb and hold large amounts of methanol given enough time, while diffusion throughout the material will still be restricted by barriers between clusters. On the other hand, because the high methanol uptake probably indicates strong interactions between the polymer and methanol molecules, the movement of methanol molecules

within the polymer matrix could be hindered in a way that is similar to the behavior of species within a chromatography column. Thus, the molecular interactions between the mobile and immobile species may slow the movement of mobile species. This effect is likely to be further enhanced by the radiation crosslinking, because rigidity of the polymer matrix would generate higher levels of steric restriction to methanol molecule movement. Experiments to confirm the actual mechanism will be included in future research.

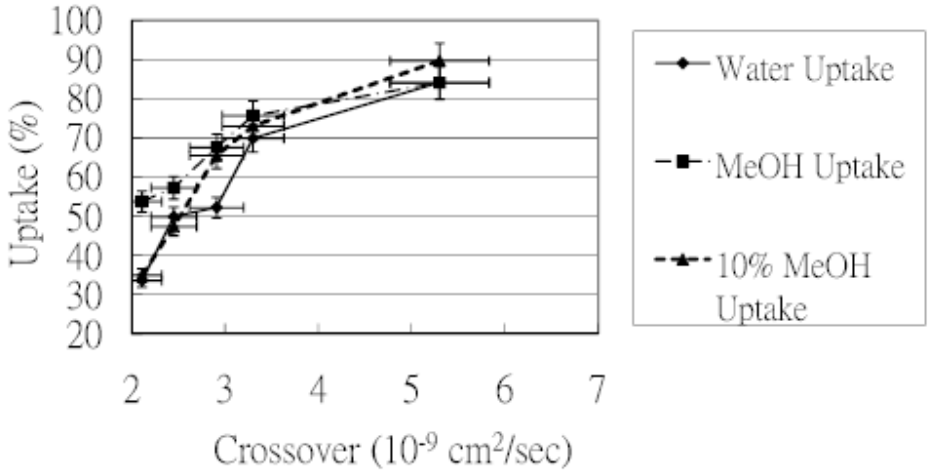

Figure **5-9**: Relationship of methanol crossover to water and methanol uptake of 20Mrad crosslinked membranes. Error bars are based on average data analysis of at least 6 samples for each data point.

5.4. Conclusions

We have synthesized polynorbornanes with pendent cyclic phosphazene groups that bear aryl sulfonic acid units as potential proton conductive membranes material for small, portable DMFCs. The polymers were evaluated by IEC and water swelling to determine their suitability as proton conductive membrane materials in DMFCs. We also fabricated membranes of the polymer with different degrees of sulfonation and crosslinking. The differences in proton conductivity, methanol permeability, and water/methanol uptake between these membranes and that of commercially available Nafion 115 were then compared.

The IEC values of the polymers were controlled accurately through the ratio of SO_3 to repeating units in the polymer. Although the degree of water swelling of the membranes was high, it can be decreased by crosslinking the polymer by gamma radiation. The resultant polymers had lower ion exchange capacities than traditional materials such as Nafion and, as a consequence, lower conductivities. However, the methanol permeabilities of these polymers were low, and were generally of the order of 10^{-9} cm^2/s. This is roughly two orders of magnitude lower than for the commercial polymer Nafion 115. This result can be explained by the low IECs (and hence ionic strengths) of these materials, the microstructure effect, and the affinity effect of the material on cations and methanol.

The ionic conductivities of these materials were not exceedingly high, but their low methanol permeabilities suggest that they may be viable materials for use as proton exchange membranes in direct methanol fuel cells for use in small portable devices. We

plan to further improve these materials by future investigations of alternative sulfonation procedures, as well as possible utilization of double bonds in the original norbornene backbone as reaction sites or crosslink promoters.

5.5. Acknowledgements

This project was supported by the Institute of Nuclear Energy Research Taiwan. We thank Dr. Daniel Welna for his help with the synthesis of the membrane materials and Dr. Toshiki Fushimi for his helpful discussions.

5.6. References

[1] Winter, M.; Brodd, R. J. *Chem. Rev.* **2004,** *104*, 4245–4270.

[2] Deluca, N. W.; Elabd, Y. A. *J. Polym. Sci. Part B: Polym. Phys.* **2006,** *44,* 2201–2225.

[3] Scott, K.; Shukla, A. K. *Rev. Environ. Sci. Biotechnol.* **2004,** *3,* 273–280.

[4] Elabd, Y. A.; Walker, C. W.; Beyer, F. L. *J. Membr. Sci.* **2004,** *231,* 181–188.

[5] Yeager, H. L.; Steck, A. *J. Electrochem. Soc.* **1981,** *128,* 1880–1884.

[6] Mauritz, K. A.; Moore, R. B. *Chem. Rev.* **2004,** *104,* 4535–4585.

[7] Kreuer, K. D. *J. Membr. Sci.* **2001,** *185,* 29–39.

[8] Kreuer, K. D.; Paddison, S. J.; Spohr, E.; Schuster, M. *Chem. Rev.* **2004,** *104,* 4637–4678.

[9] Roziere, J.; Jones, D. *Annu. Rev. Mater. Res.* **2003,** *33,* 503–555.

[10] Schultz, T.; Zhou, S.; Sundmacher, K. *Chem. Eng. Technol*. 2001, 24, 1223–1233.

[11] Heinzel, A.; Barragan, V. M.; J. Power Sources **1999,** *84*, 70–74.

[12] Hickner, M. A.; Ghassemi, H.; Kim, Y. S.; Einsla, B. R.; McGrath, J. E. *Chem. Rev*. **2004,** *104*, 4587–4612.

[13] Allcock, H.R.; Wood, R.M. *J. Polym. Sci. Part B: Polym. Phys.* **2006,** *44*, 2358

[14] Carter, R.; Wycisk, R.; Yoo, H.; Pintauro, P.N. *Electrochem.Solid State Lett.* **2002**, *5*, 195

[15] Zhou, X.; Weston, J.; Chalkova, E.; Hofmann, M.A.; Ambler, C.M.; Allcock, H.R.; Lvov, S.N. *Electrochim. Acta.* **2003**, *48*, 2173

[16] Wycisk, R.; Lee, J.K.; Pintauro, P.N. *J. Electrochem. Soc.* **2005**, *152*, A892

[17] Guo, Q.; Pintauro, P.N.; Tang, H.; O'Connor, S. *J. Membr. Sci.* **1999**, *154*, 175

[18] Allcock, H.R.; Hartle, T.J.; Taylor, J.P.; Sunderland, N.J. *Macromolecules* **2001**, *34*, 3896

[19] Allcock, H.R. *J. Inorg. Organomet. Polym.* **2006,** *17*, 349

[20] Allcock, H.R.; Laredo, W.R.; deDenus, C.R.; Taylor, J.P. *Macromolecules* **1999**, *32*, 7719

[21] Bielawski, C. W.; Grubbs, R. H. *Prog. Polym. Sci.* **2007,** *32*, 1–29.

[22] Randall, M. L.; Snapper, M.L. *J. Mol. Catal. A: Chem.* **1998,** *133*, 29–40.

[23] Allcock, H. R.; Laredo, W.R.; Kellam, E. C.; Morford, R. V. *Macromolecules* **2001,** *34*, 784–794.

[24] Welna, D. T.; Stone, D. A.; Allcock, H. R. *Chem. Mater.* **2006,** *18,* 4486–4492.

[25] Kim, J.; Kim, B.; Jung, B. *J. Membr. Sci.* **2002,** *207,* 129–137.

[26] Xing, P.; Robertson, G. P.; Guiver, M. D.; Mikhailenko, S. D.; Wang, K.; Kaliaguine, S. *J. Membr. Sci.* **2004,** *229,* 95–106.

[27] Genies, C.; Mercier, R.; Sillion, B.; Cornet, N.; Gebel, G.; Pineri, M. *Polymer* **2001,** *42,* 359–373.

[28] Kopitzke, R. W.; Linkous, C. A.; Nelson, G. L. *J. Polym. Sci. Part A: Polym. Chem.* **1998,** *36,* 1197–1199.

[29] Asensio, J. A.; Borros, S.; Gomez-Romero, P. *J. Polym. Sci. Part A: Polym. Chem.* **2002,** *40,* 3703–3710.

[30] Allcock, H. R., Klingenberg, E. H.; Welker, M. F. *Macromolecules* **1993,** *26,* 5512–5519.

[31] A.B. Pangborn, M.A. Giardello, R.H. Grubbs, R.K. Rosen, F.J. Timmers, Safe and convenient procedure for solvent purification, Organometallics 15 (1996) 1518–1520.

[32] J.M. Blanco, F. Fern´ andez, X. Garc´ıa-Mera, J.E. Rodr´ıgues-Borges, Divergent synthesis of two precursors of 3_-homo-2_-deoxy- and 2_-homo-3_-deoxycarbocyclic nucleosides, Tetrahedron 58 (2002) 8843–8849.

[33] Hoogers, G. *Fuel Cell Technology Handbook,* CRC Press, New York, 2003.

[34] Zhou, X.; Weston, J. A.; Chalkova, E.; Hofmann, M. A.; Ambler, C. M.; Allcock, H. R.; Lvov, S. N.; *Electrochim. Acta* **2003,** *48,* 2173–2180.

[35] Fedkin, M.V.; Zhou, X.; Hofmann, M. A.; Chalkova, E.; Weston, J. A.; Allcock, H. R.; Lvov, S. N. *Mater. Lett.* **2002,** *52,* 192–196.

[36] Lapinte, V.; Brosse, J.-C.; Fontaine, L. *Macromol. Chem. Phys.* **2004,** *205,* 824–833.

[37] Seehof, N.; Grutke, S.; Risse, W. *Macromolecules* **1993,** *26,* 695–700.

[38] Sohn, B. H.; Gratt, J. A.; Lee, J. K.; Cohen, R.E. *J. Appl. Polym. Sci.* **1995,** *58,* 1041– 1046.

[39] Allcock, H.R.; Fitzpatrick, R.J. *Chem. Mater.* **1991,** *3,* 1120–1132.

[40] Montoneri, E.; Gleria, M.; Ricca, G.; Pappalardo, G. C. *J. Macromol. Sci. A: Pure Appl. Chem.* **1989,** *26,* 645–661.

[41] Wysick, R.; Pintauro, P. N. *J. Membr. Sci.* **1996,** *119,* 155–160.

[42] Li, Q.; He, R.; Jensen, J. O.; Bjerrum, N. J. *Chem. Mater.* **2003,** *15,* 4896–4915.

[43] Narayanan, S. R.; Yen, S.-P.; Liu, L.; Greenbaum, S. G. *J. Phys. Chem. B* **2006,** *110,* 3942–3948.

[44] Yamada, M.; Honma, I. *Polymer* **2005,** *46,* 2986–2992.

[45] Yamada, M.; Honma, I. *Polymer* **2004,** *45,* 8349–8354.

[46] Roziere, J,; Deborah, J.J.; Marrony, M. *Solid State Ionics* **2001,** *145,* 61–68.

Chapter 6

From electrical energy to mechanical motion: A redox responsive polymeric gel based on ionic crosslinking

6.1. Introduction

Discussions on energy-related materials are often focused on the generation of electrical energy, but efficient transformation of electrical energy in to other types of energy are often just as important and interesting. After all, even when we refer to "generation" of energy we are really discussing transformation of existing energy from one state to another. In the case of batteries and fuel cells, the devices are transforming chemical energy to electrical energy (and in rechargeable battery systems, also the transformation of electrical energy into chemical energy); In the case of solar cells, it is from photon energy to electrical energy. One interesting topic discussed here is the generation of mechanical motion using designed materials – More specifically, the group of materials known as responsive hydrogels.

A number of responsive hydrogel systems have been synthesized recently in our program. These include thermosensitive gels of type **1** derived from MEEP-polyphosphazenes aforementioned (**Figure 6-1**), [1,2] which have LCST temperatures that vary from 30 ^{o}C to 80 ^{o}C depending on the side groups. Related systems, such as polyphosphazene **2** (Figure 6-2), which bear both oligoethylene chains and acidic side groups are sensitive to pH changes.[3] Gels derived from **2** also expand in the presence of

a monovalent cation and contract in the presence of a di- or trivalent cation.[3] We now report responsive behavior in gels from **2** following electrical actuation. The electrochemical conversion of monovalent cations to the di- or trivalent states allows the swelling behavior of the gel to be controlled and reversed.

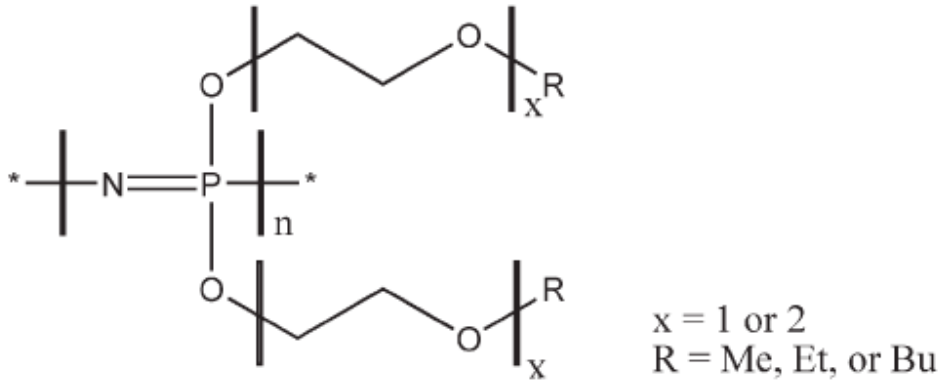

1

Figure **6-1**: Structure of thermosensitive polyphosphazene polymer system.

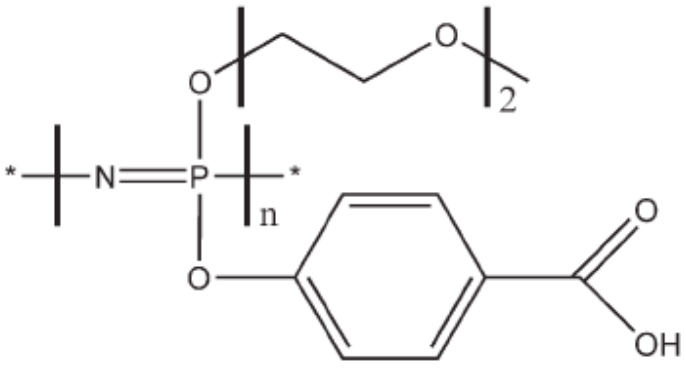

2

Figure **6-2**: Structure of polyphosphazene system with both oligoethylene side chains and acidic side groups. The polymer is named poly（methoxyethoxyethoxy phosphazene) - poly (carboxylatophenoxy phosphazene) and abbreviated as MEEP-PCPP.

Stimulant-sensitive polymer hydrogels have received attention as viable responsive materials due mainly to the large induced geometrical changes that are possible, and their ability to operate in aqueous environments. This has led to robotic and medical implant actuator applications, as well as possible uses in drug delivery, micromanipulators, nanomotors, and lab-on-a-chip devices.[4–6] Although hydrogels can be responsive to a wide variety of stimulants, [3,7] direct electroactivity (response to an applied electric signal) is preferred due to the interface requirements for controls and the extensive use of computer systems in many related applications. [8–10] Most of the successful electroactive hydrogels reported so far are based on an ion-diffusion mechanism [11] where an applied electrical field is used to direct the movement of free ions and, in turn, the adsorbed water molecules. The principal limitation of this approach is the need for external field generation, which restricts the design for practical applications.

Hydrogels crosslinked with metal cation centers that undergo redox reactions could trigger a response in geometry induced by an electrical potential without relying on the migration of counterions. This provides a simple and efficient way for producing electroactive materials as self-contained responsive units. We have established the validity of this concept by a series of prototype experiments.

6.2. Experimental

6.2.1. General synthesis and hydrogel preparation

Polymer **2** was synthesized according to a method described previously. [3] In a typical experiment, a film of the polymer ester was cast from a solution in THF by slow solvent evaporation. The resultant film was subjected to 2.5–20 Mrad gamma radiation (Penn State University Breazeale Reactor) [1,12] to induce a low level of covalent crosslinking via the alkyl ether side groups. It was then cut into square films of 1 cm square, and the ester groups were deprotected to the potassium carboxylate unit with 3 mol equivalents of KOH in 20 ml deionized (DI) water.[13] Alternatively, the polymer can be deprotected by 3 mol equivalents of t-BuOK in THF–H_2O before film casting and radiation crosslinking.

6.2.2. Cationic exchange

Metal ions were doped into the polymer films by soaking each film in a solution of metal ion (0.005 M, 20 mL) for 16 h. The films were washed with deionized (DI) water, with each wash liquid checked with Varian SpectrAA 220FS atomic absorption spectrometer to ensure removal of mobile ions, and each film was then stored in deionized (DI) water.

6.2.3. Cyclic voltammetry

In order to verify the electrochemical behavior of metal-doped gels, films of the same size were first doped with Cu^{+}, Cu^{2+}, Fe^{2+} or Fe^{3+}. The films were allowed to swell in DI water for 16 h for removal of excess ions, and the dimensions were measured. The electrochemical response of the gels was followed by cyclic voltammetry (CV) of the metal-doped films swollen by water. The electrochemical responses of the gels were then compared with those of a standard aqueous solution of the corresponding metal salts, which provided evidence of a redox reaction at the metal centers within the gel. The CV was carried out with use of a BS-100B electrochemical workstation using a silver working electrode, a platinum counter electrode, and a silver choride reference electrode. Recordings were made at a sensitivity of 100 mA and a scan rate of 50 mV s^{-1}. The scan range was 2100–1000 mV with a sample interval of 5 mV.

6.2.4. Electrochemical swelling

To test the electrochemical swelling behavior of bulk gels, 0.5 cm 6 1 cm strips of Cu^{2+} or Fe^{3+} infused film were connected to a 9 V dc source at two ends. The current was maintained for 1 h, the shape and dimensions were measured, and the current was then reversed and maintained for one more hour before being disconnected and the size/shape measured again. The process was repeated six times. The bending test was performed by sandwiching a 1 cm x 1 cm metal-infused film between two 0.5 cm-wide copper plates, followed by the same electrochemical routine while tracking the bending movement and current as a function of time. The passive–active compartment test involved casting the

polymer within multi-well trays made from commercially available poly(dimethylsiloxane) (PDMS) (10–15 wells of identical size, ranging from 0.1 cm x 0.5 cm x 0.3 cm to 0.5 cm x 1.5 cm x 1 cm for each well). After insertion of one pair of gold or silver wires into each well, the tray of polymer was then gamma-ray crosslinked, deprotected and infused with cations as described above. The trays were then tested by passing current through each pair of wires in each well by the same procedure as described above.

6.3. Results and discussion

6.3.1. Cation exchange

The polymer used in the initial experiment, MEEP-PCPP polyphosphazene **2** (**Figures 6-2 and Fig. 6-3**), is a mixed-substituent macromolecule with both water-solubilizing methoxyethoxyethoxy side groups and p-carboxy-phenoxy side groups for both pH-response and cation coordination. The polymer is readily radiation crosslinked through the ethlyeneoxy side groups by gamma-radiation to give hydrogels. These gels are known to be thermally responsive (via the methoxyethoxyethoxy groups [1]) and pH responsive (via the acidic side groups). The gels are also ion responsive: ionic replacement of monovalent cations by multivalent species causes contraction through ionic crosslink formation.[3]

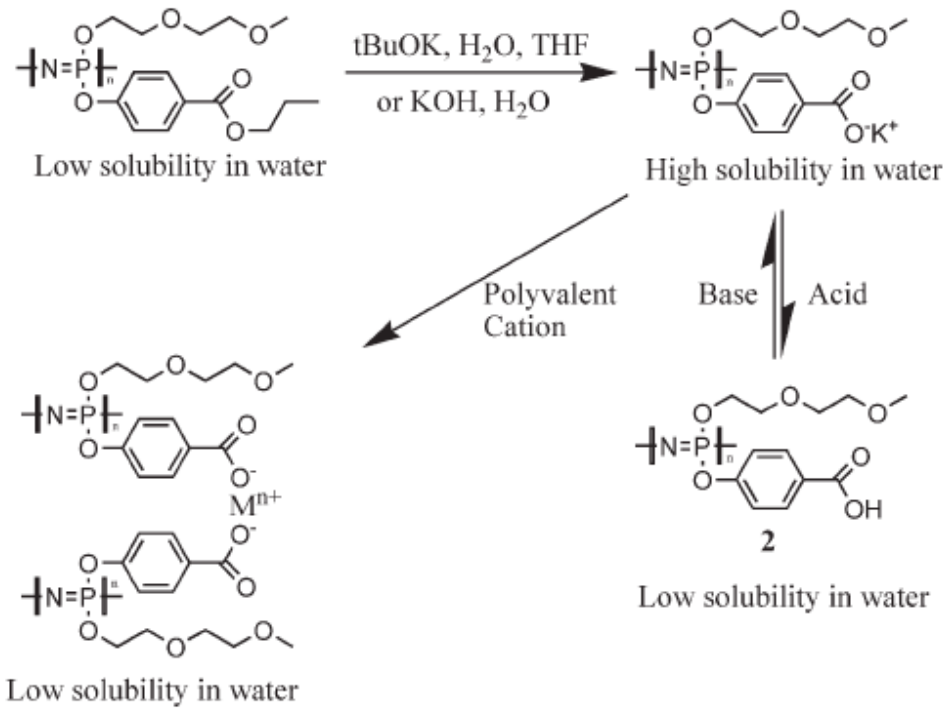

Figure **6-3**: The structure of MEEP-PCPP polyphosphazene ester (upper left) and the deprotected form after base treatment (upper right). The basic form can be then acidified to **2** or crosslinked with polyvalent cations, both of which have a lower solubility in water.

6.3.2. Influence of different cations in the gel

The present work involved two sets of experiments. First, the response of radiation-crosslinked gels from **2** was monitored as a function of different cations introduced into the samples. The results are summarized in **Figure 6-4**. Certain anomalies became evident. Although the K^+ salt showed the most gel expansion, the Ag^+ and Cu^+ systems were among the least expanded. This may reflect the ability of the Ag^+ and Cu^+ ions to coordinatively crosslink polymer chains via the carbonyl groups and/or the

backbone nitrogen atoms. [14,15] The declining degree of swelling along the series Fe^{2+}, Cu^{2+}, Co^{2+}, Fe^{2+}, and Co^{3+} probably reflects the ability of these ions to form ionic intermolecular linkages between carboxylic groups.[16]

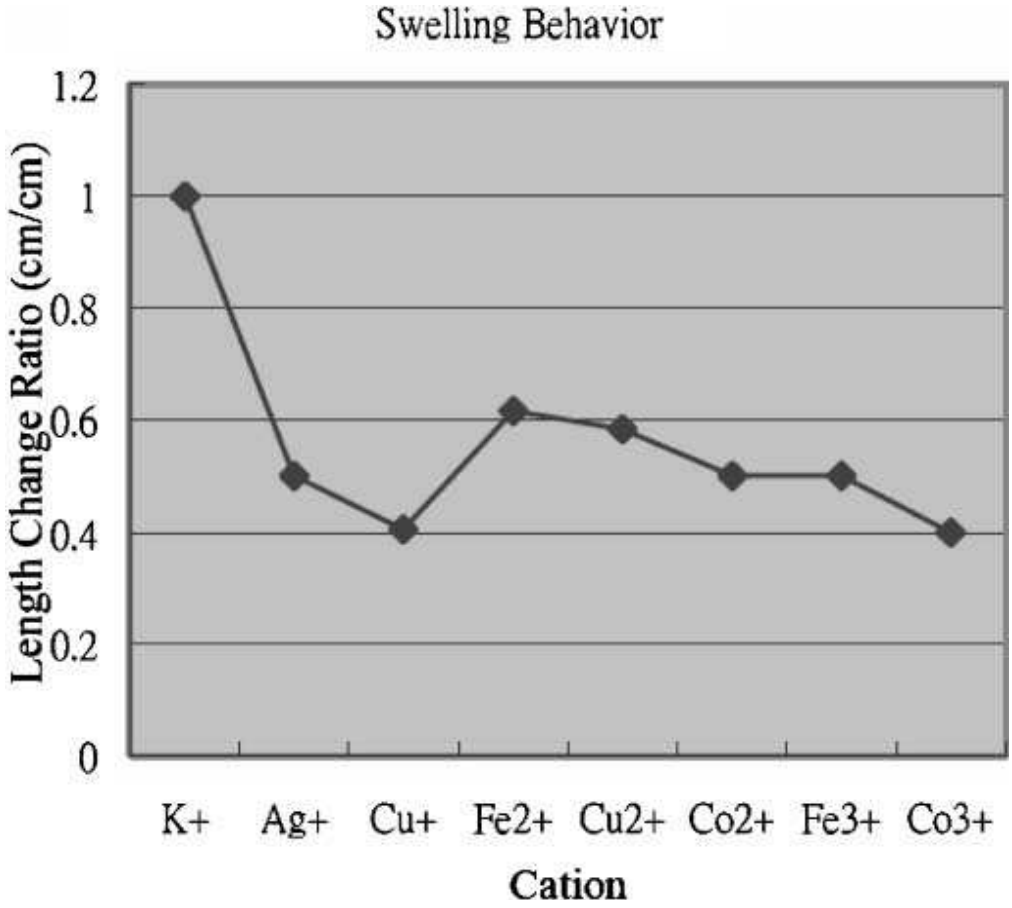

Figure **6-4**: The different swelling behaviour of MEEP-PCPP gel after cation exchange.

6.3.3. Cyclic voltammetry

The second series of experiments involved electrochemical examination of the behavior of gels derived from **2** with different ions. Initially it was shown by cyclic voltammetry (CV) scans for water-swollen gels that contained Cu^{2+} and Fe^{3+} that the cations underwent redox reactions within the gels. These data are summarized in **Figure 6-5** and are compared to the behavior of the same ions in aqueous media in the absence of the gel. The difference in electrochemical behavior between ions in the gel and those in the free solution phase is partially due to overpotential required to overcome the resistance of the insulating MEEP-PCPP layer, but also reflects the coordination role of the carboxylic acid groups. [17] Nevertheless, such differences strongly suggest that the ions are immobilized within the gel.

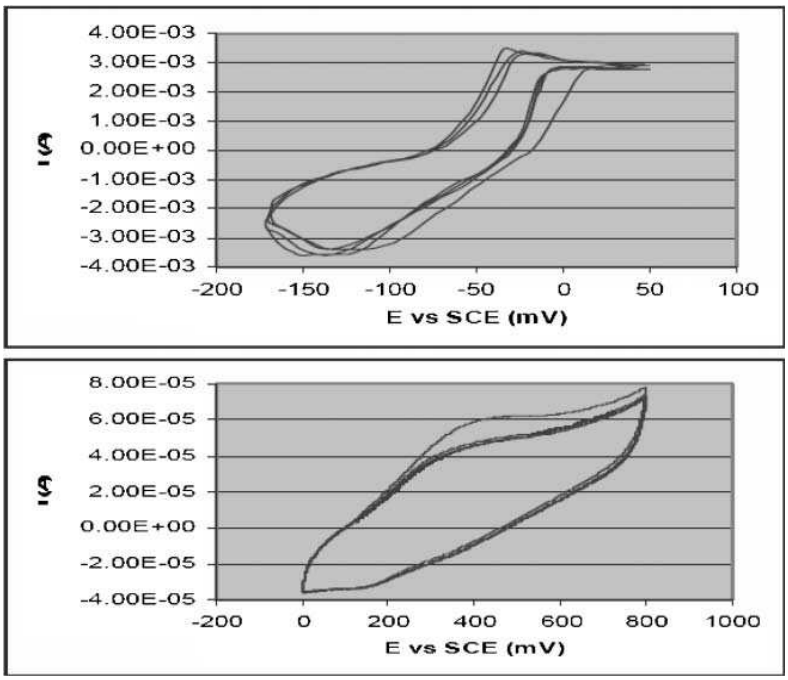

Figure **6-5**: Cyclic voltammetry of Cu^{2+} infused MEEP-PCPP gel (above) and an Fe^{3+} infused gel (below). The different ranges for voltage sweeps of two elements are intended

to highlight the difference in redox potentials – No significant peaks have been found with wide voltage range scans. MEEP-PCPP without metal ions did not show redox behavior within the voltage range investigated and its CV data is thus not reported here.

6.3.4. Electrochemical swelling

The gels that contained Cu and Fe ions expanded during the passage of an electric current and contracted when the current was reversed. The swelling behavior for gel samples connected to a dc source was localized around the cathode, and was found to be reversible when the direction of applied current was reversed, causing expansion at the other electrode. (**Figure 6-6**) When properly aligned, this allows for the construction of a device capable of a bending motion, with the gel bending away from the cathode up to 45^{o}. Again, this bending behavior is fully reversible. (**Figure 6-7**) The bending motion occurred over a period of 1 h, with the most dramatic changes between 5 to 25 min after the application of a direct current source. This also corresponds to the change of current in the device. (**Figure 6-8**)

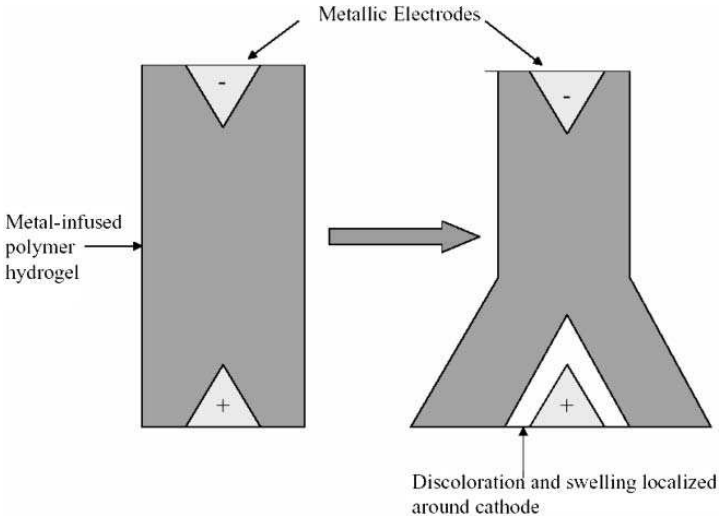

Figure **6-6**: Schematic representation of partial swelling for direct electrochemical redox of Cu-infused gel.

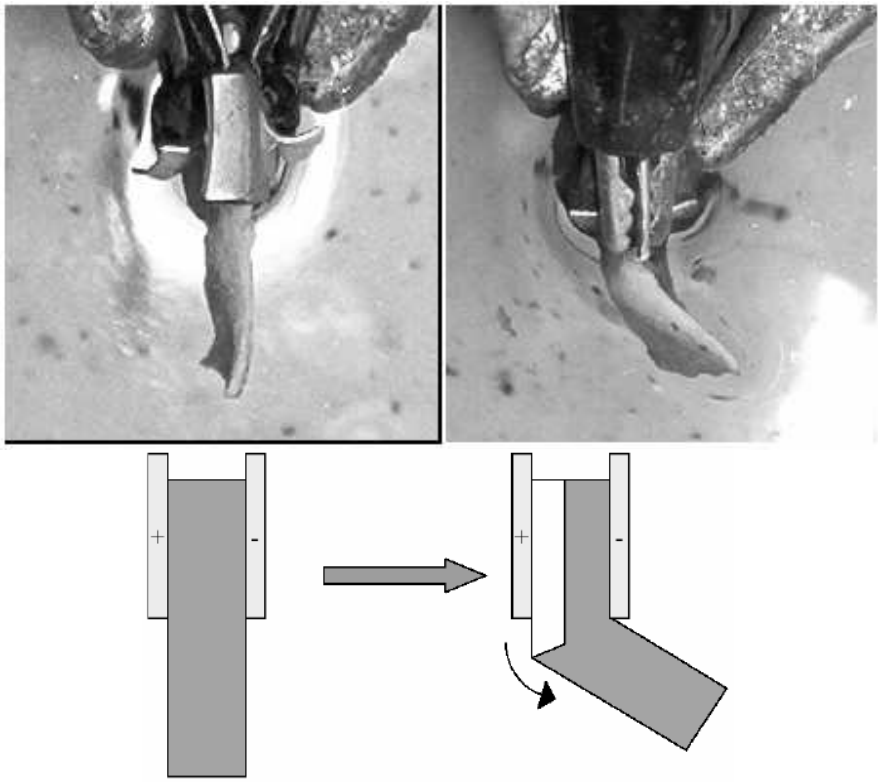

Figure **6-7**: Responsive gel behavior. Upper: actual gel before and after bending. Lower: schematic representation of potential induced bending. The white section indicates expanded gel near cathode.

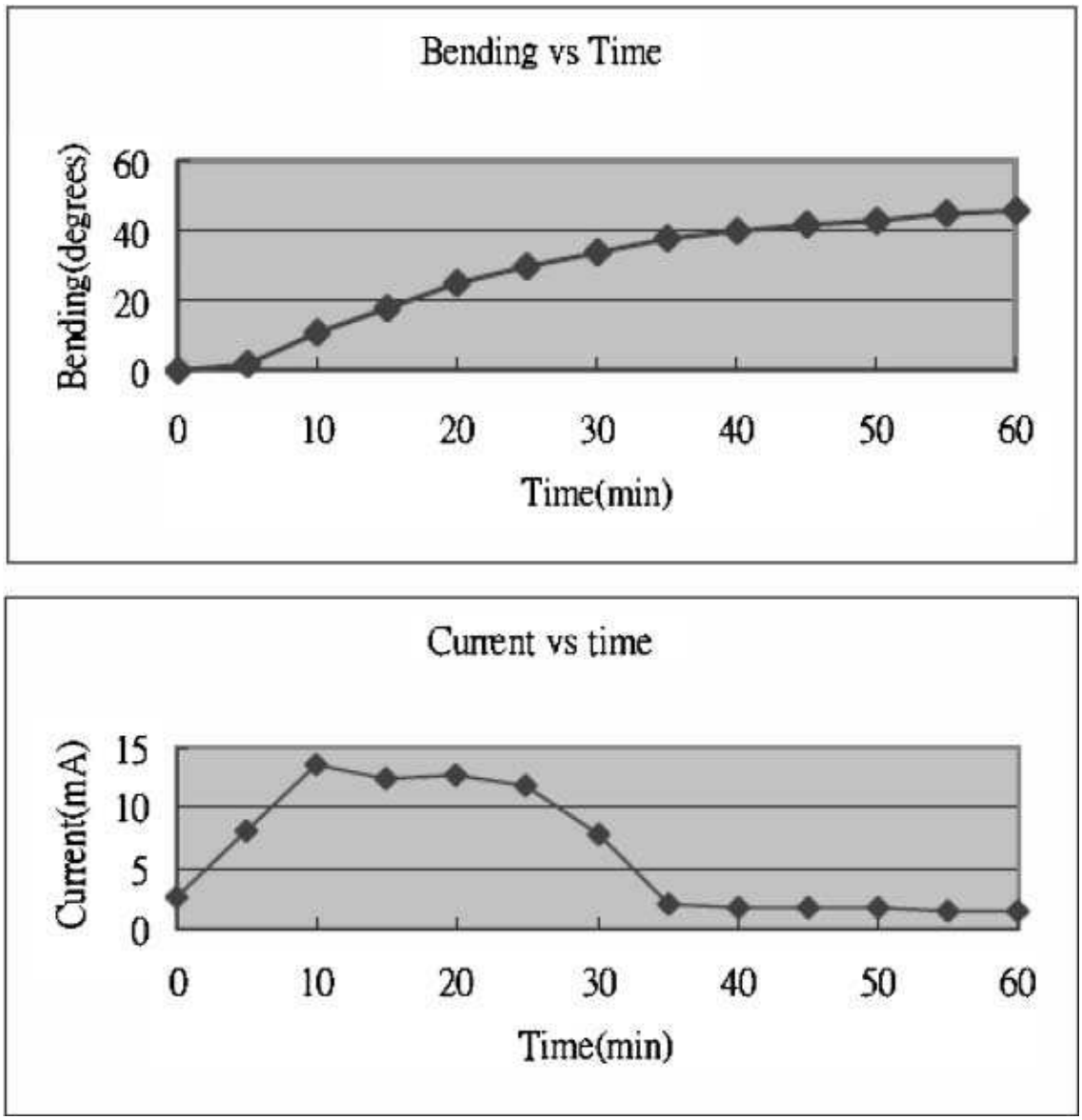

Figure **6-8**: Response of gel bending versus time. Upper: degree of gel bending during a typical electrochemical reaction. Lower: observed change of current during the same experiment.

Finally, we attempted to construct a passive–active actuator system by inserting the polyphosphazene gel samples and electrodes into open-top hydrophobic poly-(dimethylsiloxane) (PDMS) compartments. The system bends with the initial application of current due to the swelling of the polyphosphazene.

The electroactive behavior observed here differs from the classical electroactive gels that are based on ion-mobility. This suggests a response to changes in crosslinks in three aspects: the gel undergoes a net swelling without the existence of mobile counterions (all reactions are in deionized water) during the initial application of a potential, which strongly suggests that the mechanism is not a response to mobile anion movement. For an electroactive gel to be based on counteranion movement, the gel must either (a) exhibit net swelling at a section of the gel where a positive charge is generated (usually via oxidation of the gel) due to the increased ion concentration and thus osmotic pressure, or (b) shrink at one end accompanied by swelling at other end (overall no net change in gel volume) due to the migration of water along the induced electric field. In our case, the swelling is observed at the location where reduction reactions only should occur. On the other hand, for the gel to operate through the electric field induced movement/alignment of the negatively charged side groups, the deformation should be uniform along the field lines as opposed to the highly localized reaction observed.

The swelling is localized around the cathode with no indication of increased cation concentration (the swollen part becomes transparent instead of darker blue in the case of Cu), and the reverse reaction of shrinking also originates from the electrode. For the gel to operate on the alternative mobile cation mechanism, the swelling should either

(a) lead to a similar or deeper shade of blue at the swelling areas due to the concentration effect of copper cations, or (b) show no net size change as explained in the anion argument.

The gel remains in its deformed state for more than 16 h after being disconnected from the power source. Gel electroactive behavior due to field-induced migration of ions should be unstable once the electric field is removed due to the charge separation involved.

These observations lead us to propose a swelling mechanism based on the change in crosslink density due to the redox behavior of metal centers. (**Figure 6-9**) Cations with a lower ability to bind to carboxylic acids (which usually translates to lower charge and thus a lower oxidation state) should give ionic crosslinks that are easier to dissociate in water. This leads to an overall decrease in degree of ionic crosslinking and an increase in the water swelling ability of the gel. Thus, when the metal center changes from a higher oxidation state to a lower oxidation state, ionic crosslinks dissociate and the gel swells.

Similarly, a return to a higher oxidation state promotes the reformation of crosslinks and leads to a contraction of the gel. For gel systems crosslinked by iron cations, this can be achieved though the changes between 2+ and 3+ state. For copper ions, the situation may be more complex: the reduction of Cu(II) to Cu(0) may occur because Cu^{+} is unstable under aqueous conditions and readily forms an insoluble salt. Thus, further mechanistic work on this reversible system is required.

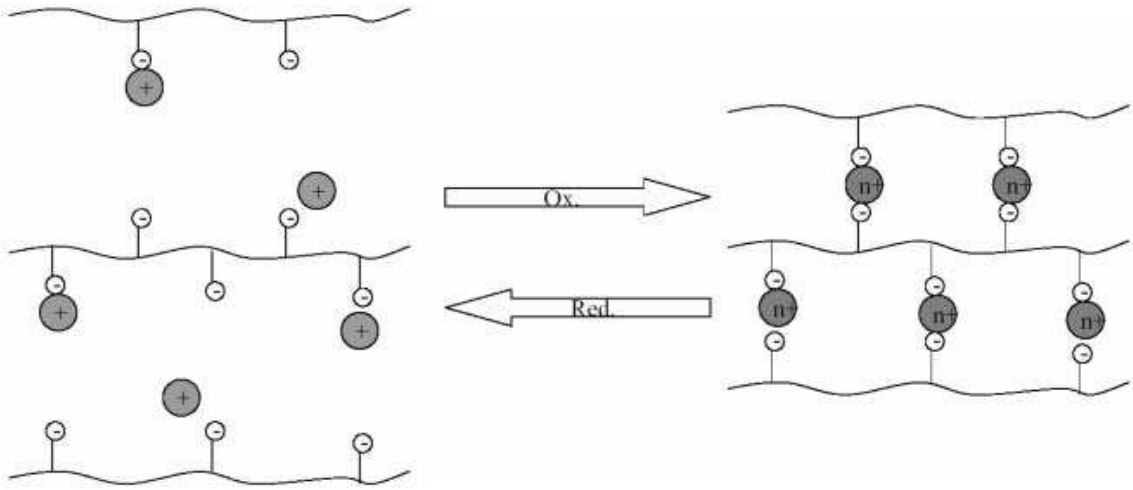

Figure **6-9**: Proposed mechanism for swelling–contraction, with ionic crosslinks dissociating when cations serving as crosslinkers are reduced (left), and reforming crosslinks when oxidized (right).

The low ion mobility and high electrical resistance of the gel contributes to the localized swelling behavior, since in such a situation the electrodes can only extract electrons from metal atoms close to the electrode surface. This phenomenon is further supported by the relationship between the deformation speed and the current: at first, the cations closest to the cathode are reduced, forming a thin conductive layer that helps to reduce the contact resistance between the electrode and the gel.However, as more cations are reduced, the gel areas become depleted of cations and form an insulating barrier, which drives down the current with increases in electrical resistance. The same reasons also explain the stability of the deformed gel, as it is difficult for cations involved in crosslink behavior to diffuse to a lower concentration area and replace the cations that were removed via electrochemical redox.

6.4. Conclusions

We report here an electrochemically responsive polymer hydrogel based on ionic crosslinking. The crosslinking by metal cations and anionic carboxylic acid side groups can be controlled by redox reactions. The crosslinks dissociate when the cation crosslinker is reduced to a lower oxidation state and reform following oxidation, which leads to a reversible and localized swelling–contraction. By choosing biocompatible components and miniaturization designs, the system has the potential to be useful in microrobotic and biomedical applications.

6.5. Acknowledgements

This work was supported by D.A.R.P.A.

6.6. References

[1] Allcock, H. R.; Pucher, S. R.; Turner, M. L.; Fitzpatrick, R. J. *Macromolecules*, **1992,** *25*, 5513–5511.

[2] Allcock, H. R.; Dudley, G. K. *Macromolecules*, **1996,** *29*, 1313–1319.

[3] Allcock H. R.; Ambrosio, A. M. A. *Biomaterials*, **1996,** *17*, 2295–2302.

[4] Bar-Cohen, Y. *Proc. SPIE-Int. Soc. Opt. Eng.*, **1999,** *3669*, 1–414.

[5] Bar-Cohen, Y. *Int. News Micro. MEMS*, **2001,** *3*, 45–46.

[6] Jager, E. W. H.; Smela, E.; Inganas, O. *Science*, **2000,** *290*, 1540–1545.

[7] Zhang, K.; Huang, H.; Yang, G.; Shaw, J.; Yip, C.; Wu, X. Y. *Biomacromolecules,* **2004,** *5,* 1248–1255.

[8] Schreyer, H. B.; Gebhart, N.; Kim, K. J.; Shahinpoor, M. *Biomacromolecules,* **2000,** *1,* 642–647.

[9] Buckley, G. S. ; Roland, C. M.; Casalini, R.; Petchsuk, A.; Chung, T. C. *Chem. Mater.,* **2002,** *14,* 2590–2593.

[10] Bobnar, V.; Vodopivic, B.; Levstik, A.; Kosec, M.; Hilczer, B.; Zhang, Q. M. *Macromolecules,* **2003,** *36,* 4436–4442.

[11] Kudaibergenov, S. E.; Sigitov, V. B. *Langmuir,* **1999,** *15,* 4230–4235.

[12] Allcock, H. R.; Kwon, S.; Riding, G. H.; Fitzpatrick, R. J.; Bennett, J. L. *Biomaterials,* **1988,** *19,* 509–513.

[13] Allcock, H. R.; Morrissey, C. T.; Way, W. K.; Winograd, N. *Chem. Mater.,* **1996,** *8,* 2730–2738.

[14] Konradi, R.; Ruhe, J. *Macromolecules,* **2004,** *37,* 6954–6961.

[15] Richards, P. I.; Steiner, A. *Inorg. Chem.,* **2004,** *43,* 2810–2817.

[16] Allcock, H. R.; Kwon, S. *Macromolecules,* **1989,** *22,* 75–79.

[17] Chidsey, C. E. D.; Murray, R. W. *J. Phys. Chem.,* **1986,** *90,* 1479–1484.

VITA

Shih-To Fei

Education

2003-2010	Ph.D., Chemistry, The Pennsylvania State University, University Park Thesis Title: "INORGANIC-ORGANIC ELECTROLYTE MATERIALS FOR ENERGY APPLICATIONS" Graduate Advisor: Harry R. Allcock, Evan Pugh Professor of Chemistry
1994-1998	B.S., Chemistry, National Taiwan University

Publications

- Shih-To Fei and Harry R. Allcock* *J. Power Sources* **2010,** *195,* 2082-2088
- Shih-To Fei and Harry R. Allcock* *Mater. Res. Soc. Symp. Proc.* 1127-T01-05, **2009**
- Shih-To Fei, Richard M. Wood, David K. Lee, David A. Stone, Hwei-Liang Chang and Harry R. Allcock* *J. Membr. Sci*. **2008,** *320,* 206 - 214
- Shih-To Fei, Mwita V. B. Phelps, Yang Wang, Eric Barrett, Farhan Gandhi and Harry R. Allcock* *Soft Matter*, **2006,** *2*, 397 - 401